

**University of Mosul  
College of Veterinary Medicine**



# **The Effects of Different Biological Materials on the Healing of Surgically Created Mandibular Defect in Dogs Model**

**Ali Ghazi Atiyah Zarraq**

**Ph.D./ Dissertation  
Veterinary Medicine / Veterinary Surgery**

**Supervised By  
Professor Dr.**

**Layth Mahmoud Dawoud Al-Kattan**

# **The Effects of Different Biological Materials on the Healing of Surgically Created Mandibular Defect in Dogs Model**

**A Dissertation Submitted  
By**


**Ali Ghazi Atiyah Zarraq**

**To  
The Council of The College of Veterinary Medicine  
University of Mosul**

**In  
Partial Fulfillment of The Requirements  
For The Degree of Doctor of Philosophy  
In  
Veterinary Medicine / Veterinary Surgery**

**Supervised By  
Professor Dr.**

**Layth Mahmoud Dawoud Al-Kattan**



بِسْمِ اللَّهِ الرَّحْمَنِ الرَّحِيمِ  
(يَرْفَعِ اللَّهُ الَّذِينَ آمَنُوا مِنْكُمْ وَالَّذِينَ  
أُوتُوا الْعِلْمَ دَرَجَاتٍ وَاللَّهُ بِمَا  
تَعْمَلُونَ خَبِيرٌ)

سورة المجادلة، الآية (11)

### **Supervisor Certification**

I certify that this dissertation entitled “ **The Effects of Different Biological Materials on the Healing of Surgically Created Mandibular Defect in Dogs Model**” was prepared under my supervision at the College of Veterinary Medicine / University of Mosul, as a partial fulfillment of the requirements for the degree of Ph.D. in Veterinary Medicine/Veterinary surgery.

Signature:

Name: **Prof. Dr. Layth Mahmoud Dawoud**

Date: / / 2024

### **Linguist Certification**

I certify that this dissertation entitled “ **The Effects of Different Biological Materials on the Healing of Surgically Created Mandibular Defects in Dogs Model**” has been linguistically reviewed and corrected for language and expression mistakes; therefore, it becomes ready for the defense as for as the integrity of the writing and expression.

Signature:

Name: **Assest. Lect. Saffaa R. Mohammed**

Date: / / 2024

### **Statistic Certification**

I certify that this dissertation entitled“ **The Effects of Different Biological Materials on the Healing of Surgically Created Mandibular Defect in Dogs Model**” has been statistically reviewed and corrected for statistic and expression mistakes; therefore, it becomes ready for the defense as for as the integrity of the writing and expression.

Signature:

Name: **Assest. Prof. Muzahem M. Al-Hashimi**

Date: / / 2024

### **Department of Surgery and Theriogenology Head Certification**

Based on the supervisor and linguistcian recommendations, I forward this thesis for the defense.

Signature:

Name: **Prof. Dr. Mohammed Abdalelah Aziz**

Date: / / 2024

### **Postgraduate Committee Director Certification**

Based on the supervisor, linguist, and the Head of the Department of Surgery and Theriogenology recommendations, I am forwarding this thesis for defense.

Signature:

Name: **Prof. Dr. Raad Abdulghany Alsanjary**

Date: / / 2024



### **Examination Committee Decision**

We, the members of the Evaluation and Discussion Committee, have reviewed this dissertation and discussed the student **Ali Ghazi Atiyah Zarraq** in its contents on 30/5/2024, and certify that he deserves the degree of Ph.D. in Veterinary Medicine/ Veterinary Surgery.

Signature Professor <b>Dr. Osama Hazim Ismail</b> Member	Signature Assistant Professor <b>Dr. Rayan Salim Hamed</b> Member	Signature Assistant Professor <b>Dr. Hadeel Basim Thannon</b> Member
---	--	---

Signature  
Assistant Professor  
**Dr. Nazhad Hussein Qader**  
Member

Signature  
Professor  
**Dr. Layth Mahmoud Dawoud**  
Member and Supervisor

Signature  
Professor  
**Dr. Abdul-Haleem Mawlood Saleh**  
Chairman

### **College Council Decision**

The College of Veterinary Medicine Council was met, the meeting , on 30/5/2024, and decided to award him a degree of Ph.D. in Veterinary surgery.

Signature  
Professor  
**Dr. Raad Abdulghany Alsanjary**  
Assistant Dean for Scientific Affairs

Signature  
Professor  
**Dr. Dhafer Mohammad Aziz**  
Dean

# Acknowledgement

I thank **God Almighty** for His protection in my life and for allowing me to succeed in all periods of my studies.

I express my thanks and gratitude to the **staff of the College of Veterinary Medicine/University of Mosul** for providing me with unlimited support to complete this study.

I am very indebted and grateful to my supervisor, **Professor Dr. Layth Mahmoud Dawoud AL-Kattan**, for his great help, support, endless advice, patience, and suggestions for presenting this work in the most comprehensive, clear, and accurate way.

Last but not least, I want to express my appreciation to all the academic and technical staff of the **Department of Surgery and Theriogenology** and the **Animal House Center** at the College of Veterinary Medicine / University of Mosul for their tremendous support and patience that contributed to the success of this work.

*Ali Ghazi Atiyah Zarraq*

## Abstract

The study aimed to reconstitute surgically induced large mandibular bone defects by using different types of biomaterials in a dog's model. In this study, forty-eight healthy stray male dogs, with a weight of  $(20 \pm 0.5)$  kg and age of  $(2 \pm 0.6)$  years, were included. All animals were divided equally into four groups. A circular mandibular bone defect of (14) mm in diameter was created in the body of the mandible of all animals. In the first group (control group), the defect was left without any treatment. In the second group (QESCH group), the bone defect was filled with fabricated calcium hydroxide powder of quail egg shells. In the third group (OSHA group), the bone defect was filled with fabricated hydroxyapatite powder of oyster shells. In the fourth group (PRF group), the bone defect was filled with a prepared autologous platelets rich fibrin gel. Depending on the post-operative evaluations like clinical signs, macroscopic, field emission scanning electron microscopy (FESEM) radiological, histopathological, and immunohistochemical at the different periods of the study to evaluate the obtained results.

The clinical evaluation showed that all animals recovered well after surgical correction without any complications. However, all animals in treated groups showed normal signs of eating, chewing, and barking during the first-week post-surgical operations. While the animals of the first group showed varying degrees of ability to eat normally during the same periods. Grossly, in all groups, the site of surgical wounds was healed normally by first intention after surgical correction. In addition, the macroscopical results in the treated groups during all the periods of the study appeared to show a progressive reduction in the size of the mandibular bone defect through new connective tissue formation, especially in the fourth group. In

contrast to the control group, the mandibular bone defect was still open relatively at the end of the this study.

The radiological results of the mandibular bone defect in the control group revealed little bone tissue formation with less or absent trabecular bridging where the bone defect stilled open and radiolucent on day 60 post-operation. While in the treated groups, the radiographic examination revealed progressive disappearance in the size of the mandibular bone defect through new bone tissue formation and trabecular bridging where the bone defect appeared radiopaque and disappeared relatively and at the end of the study restrictedly in the fourth group also. Additionally, the field emission scanning electron microscopy revealed the closure of the mandibular bone defect relatively with new connective tissue in a treated group, especially in a fourth group, in contrast to the first group, where the defect remained open.

The histopathological sections after filling the mandibular bone defect with different biomaterials in all experimental animals showed various degrees of new bone and granulation tissue formation. In addition to the angiogenesis and infiltration of inflammatory cells. Generally, the histopathological results in the treated groups showed a significant increase with varying percentages in the proliferation of osteoblasts and osteocyte formation with priority to the fourth group at ( $P \leq 0.05$ ) when compared with the first group during the periods of the study after surgical operations. Furthermore, the immunohistochemical results in the first group showed weakly expressed alkaline phosphatase (ALP) in both cartilaginous and ossification zones. In the second group, the expression of ALP appeared mildly in the ossification zone and moderately in the cartilaginous zone. In the third group, the ALP expression appeared mildly in the newly formed bone trabeculae surface and moderate in the cartilaginous zone. In the fourth group, the expression of ALP appeared highly in the center of the



bone defective area and moderately expressed in the surface of the newly formed lamellar bone.

In conclusion, the filling of mandibular bone defects with fabricated calcium hydroxide powder of quail egg shells, fabricated hydroxyapatite powder of oyster shells, and platelets rich fibrin improved the healing process of bone defect. It enhanced the closure of it, especially in the fourth group when compared with the first group.

## Contents

<b>Chapter one</b>	<b>Introduction</b>	<b>1-3</b>
<b>Chapter two</b>	<b>Review of literature</b>	<b>4-34</b>
2-1	Anatomy of the bone	4-6
2-2	Cellular Components of the bone	6-8
2-3	Anatomy of the mandible in dogs	8-9
2-4	Blood Supply and Nerves	9-10
2-5	Muscular attachment to the mandible	10-12
2-6	Bone Healing of Mandible	13
2-6-1	Primary Bone Healing	13-14
2-6-2	Secondary Bone Healing	14-15
2-7	Alkaline phosphatase	15-16
2-8	Mandibular Defect	16-17
2-9	Etiology of Mandibular Defect	17
2-10	Complications of mandibular defect	18
2-11	large Size Bone Defect	18-19
2-12	Surgical Approaches to the Mandible	19-20
2-13	Biomaterials	20-21
2-14-1	Natural Sources Biomaterials	21-22
2-14-2	Synthetic Sources Biomaterials	22-24
2-15	Properties of the Bone Substitutes Biomaterials	24-25
2-16	Types of bone substitute biomaterial	25-26
2-17	Bioceramic in Orthopedic Field	26-28
2-17-1	Oyster Hydroxyapatite	28-31
2-17-2	Quail Eggshell Calcium Hydroxide	31-32
2-18	Platelets Rich fibrin	32-34
<b>Chapter Three</b>	<b>Materials and Methods</b>	<b>35-51</b>
3-1	Experimental animals	35
3-2	Experimental design	35-36
3-3	Laboratory preparation of autologous PRF	37-38
3-4	Preparation of quail eggshell calcium hydroxide powder	38-39
3-5	Preparation of oyster shell hydroxyapatite powder	39-40
3-6	Evaluations of bone substitute biomaterials	40
3-6-1	X-ray diffractometer (XRD) analysis	41

3-6-2	Field emission scanning electron microscopy (FESEM)	41
3-6-3	Energy dispersive X-ray (EDS) Spectrometer	41
3-7	Surgical procedure	42-43
3-8	Post operative care	43
3-9	Animal Sacrifices	46
3-10	Animals' evaluations	47
3-10-1	Clinical evaluations	47
3-10-2	Macroscopical evaluation	47
3-10-3	Radiographical evaluation	47
3-10-4	Histopathological evaluation	47-48
3-10-5	Immunohistochemistry (IHC) evaluation	50
3-11	Statistical analysis	51
<b>Chapter four</b>	<b>Results</b>	<b>52-84</b>
4-1	Evaluation of quail eggshell calcium hydroxide powder	52
4-1-1	X-ray diffraction	52
4-1-2	Felid emission trance electron microscope (FESEM).	52-53
4-1-3	Energy Dispersive X-ray (EDS) Spectrometer	53-54
4-2	Evaluations of oyster shell hydroxyapatite	55
4-2-1	X-ray diffraction	55
4-2-2	Felid emission trance electron microscope (FESEM).	55-56
4-2-3	Energy Dispersive X-ray (EDS) Spectrometer	56-57
4-3	FESEM of autologous PRF sample.	58
4-4	FESEM of mandibular bone defect samples after 30 days post-surgery.	58-59
4-5	Clinical evaluations	60
4-6	Macroscopical evaluations	60-62
4-7	Radiographical evaluations	62
4-7-1	Radiography of the first group	62-64
4-7-2	Radiography of the second group.	64-66
4-7-3	Radiography of the third group.	66-68
4-7-4	Radiography of the fourth group.	68-70
4-8	Histopathological evaluations	70

4-8-1	Histopathological evaluation of the first group	70
4-8-2	Histopathological evaluation of the second group	71
4-8-3	Histopathological evaluation in the third group	71
4-8-4	Histopathological evaluation in the fourth group	71-72
4-9	Immunohistochemistry	80-84
<b>Chapter five</b>	<b>Discussion</b>	<b>85-109</b>
5-1	large size mandibular bone defect in dog models	85-86
5-2	Clinical evaluations	86-87
5-3	X-ray Diffraction (XRD)	87-88
5-4	Energy dispersive X-ray spectroscopy	88-90
5-5	Field Emission Scanning Electron Microscopy (FESEM)	90-92
5-6	Field Emission Scanning Electron Microscopy (FESEM) at 30 days after surgery	92-97
5-7	Macroscopical evaluations	97-98
5-8	Radiographical evaluations	98-101
5-9	Histopathological evaluations	101-107
5-10	Immunohistochemistry	107-109
	<b>Conclusions</b>	<b>110</b>
	<b>Recommendations</b>	<b>111</b>
	<b>References</b>	<b>112-153</b>

## List of Figures

<b>Figure No.</b>	<b>Title</b>	<b>Page</b>
Figure 2-1	Superficial muscle connection to the jaw, side view, lateral aspect.	12
Figure 2-2	Deep muscle connection to the jaw, lateral aspect.	12
Figure 3-1	The Diagram of experimental design.	37
Figure 3-2	Preparation of autologous PRF gel.	39
Figure 3-3	A, the quail eggshell before fabrication. B, the fabricated calcium hydroxide powder from the quail eggshell.	40
Figure 3-4	A, the oyster's shells before fabrication. B, the fabricated oyster shell hydroxyapatite powder	41
Figure 3-5	The site of surgical operation under aseptic surgical technique.	45
Figure 3-6	The body of the mandibular bone is covered with periosteum.	45
Figure 3-7	A bone defect was surgically created in the body of the mandibular bone using a bone drill square under continuous irrigation of saline solution.	46
Figure 3-8	The lateral plain radiographic image of the mandibular bone defect immediately after surgery.	46
Figure 3-9	The bone defect of the mandibular bone. (A), first group (control). (B), second group (QESCH) powder. (C), third group (OSHA) powder. (D), fourth group (PRF) gel.	47
Figure 4-1	The XRD patterns of blue color indicate the fabricated quail eggshell $\text{Ca}(\text{OH})_2$ sample, matching with ICDD reference card number: (00-100-0045) red color.	53
Figure 4-2	The FESEM image of the fabricated quail eggshell $\text{Ca}(\text{OH})_2$ powder obtained at the calcination temperature $1200^\circ\text{C}$ for 2hr, used magnification 15000X and 6000X.	54
Figure 4-3	The EDS spectrum peaks of the fabricated quail eggshell $\text{Ca}(\text{OH})_2$ powder sample showed the elemental compositions of the prepared powder sample.	55
Figure 4-4	The EDS elemental mapping analysis of the fabricated quail eggshell $\text{Ca}(\text{OH})_2$ powder sample.	55
Figure 4-5	The XRD peaks patterns, in blue color, indicate that the fabricated oyster shell hydroxyapatite	56

<b>Figure No.</b>	<b>Title</b>	<b>Page</b>
	powder sample matches with the ICDD reference card number (09-0432) green in color.	
Figure 4-6	FESEM images of the fabricated oyster shell hydroxyapatite were obtained at the calcination temperature of 1200°C for 2h at magnification 130X and 1000X.	57
Figure 4-7	The EDS spectrum analysis of fabricated oyster shell hydroxyapatite powder sample.	58
Figure 4-8	The EDS elemental mapping analysis of the fabricated oyster shell hydroxyapatite powder sample.	58
Figure 4-9	The FESEM images of the prepared autologous PRF gel sample at magnification 80X and 150X.	59
Figure 4-10	The FESEM images show the defective area of mandibular bone defects obtained at 30 days post-surgery, using magnification 50X. A, control group. B, second group. C, third group. D, fourth group.	60
Figure 4-11	The macroscopical findings of the mandibular bone defect defects in different groups at seven days post-surgery.	62
Figure 4-12	The macroscopical findings of the mandibular bone defect defects in different groups at 15 days post-surgery.	62
Figure 4-13	The macroscopical findings of the mandibular bone defect defects in different groups at 30 days post-surgery.	62
Figure 4-14	A lateral radiographical image of the first group at 15 days PS.	63
Figure 4-15	A lateral radiographical image of the first group at 30 days PS.	64
Figure 4-16	A lateral radiographical image of the first group at 60 days PS.	64
Figure 4-17	A lateral radiographical image of the second group at 15 days PS.	65
Figure 4-18	A lateral radiographical image of the second group at 30 days PS.	66
Figure 4-19	A lateral radiographical image of the second group at 60 days PS.	66
Figure 4-20	A lateral radiographical image of the third group at 15 days PS.	67



<b>Figure No.</b>	<b>Title</b>	<b>Page</b>
Figure 4-21	A lateral radiographical image of the third group at 30 days PS.	68
Figure 4-22	A lateral radiographical image of the third group at 60 days PS.	68
Figure 4-23	A lateral radiographical image of the fourth group at 15 days PS.	69
Figure 4-24	A lateral radiographical image of the fourth group at 30 days PS.	70
Figure 4-25	A lateral radiographical image of the fourth group at 60 days PS.	70
Figure 4-26	Histological section of the mandible bone of the first group (7 days).	73
Figure 4-27	Histological section of the mandible bone of the first group (15 days).	73
Figure 4-28	Histological section of the mandible bone of the first group (30 days).	74
Figure 4-29	Histological section of the mandible bone of the second group (7 days).	74
Figure 4-30	Histological section of the mandible bone of the second group (15 days).	75
Figure 4-31	Histological section of the mandible bone of the second group (30 days).	75
Figure 4-32	Histological section of the mandible bone of the third group (7 days).	76
Figure 4-33	Histological section of the mandible bone of the third group (15 days).	76
Figure 4-34	Histological section of the mandible bone of the third group (30 days).	77
Figure 4-35	Histological section of the mandible bone of the fourth group (7 days).	77
Figure 4-36	Histological section of the mandible bone of the fourth group (15 days).	78
Figure 4-37	Histological section of the mandible bone of the fourth group (30 days).	78
Figure 4-38	Immunohistochemical staining for expression of the ALP activity under the light microscope in the mandible bone defect area in the first group at 30 days PS.	81
Figure 4-39	Immunohistochemical staining for expression of the ALP activity under the light microscope in the	82

<b>Figure No.</b>	<b>Title</b>	<b>Page</b>
	mandible bone defect area in the second group at 30 days PS.	
Figure 4-40	Immunohistochemical staining for expression of the ALP activity under the light microscope in the mandible bone defect area in the third group at 30 days PS.	83
Figure 4-41	Immunohistochemical staining for expression of the ALP activity under the light microscope in the mandible bone defect area in the fourth group at 30 days PS.	84

## List of tables

<b>Number</b>	<b>Title</b>	<b>Page</b>
Table 2-1	The most frequent etiologies of mandibular defects	17
Table 3-1	The histopathological indices and scores according to modify (Lucaciu et al., 2015).	49
Table 4-1	The contents values of the prepared quail eggshell $\text{Ca(OH)}_2$ powder sample.	54
Table 4-2	The content values of the prepared oyster shell hydroxyapatite powder sample.	57
Table 4-3	The mean values of the histopathological score used Duncan's test.	79

## List of Abbreviations and Symbols

<b>Abbreviation</b>	<b>Name</b>
HA	Hydroxyapatite
XRD	X-ray diffractometer
EDX	Energy-dispersive X-ray spectroscopy
FESEM	Field emission scanning electron microscopy
PRF	Platelets Rich Fibrin
IHC	Immunohistochemistry
Mm	Micron

Abbreviation	Name
Mm	Millimeter
Cm	Centimeter
MSC	mesenchymal stem cell
TNF- $\alpha$	include tumor necrosis factor- $\alpha$
TCP	Tricalcium phosphate
IL-1	interleukin-1
LSBD	Large-Size Bone Defect
ECM	extracellular matrix
CaP	Calcium phosphate
FDA	Food and Drug Administration
CaO	Calcium oxide
CaCO <sub>3</sub>	Calcium carbonate
CHA	coralline hydroxyapatite
Ca(OH) <sub>2</sub>	Calcium hydroxide
Rpm	Revolutions per minute
QESCH	Quail eggshell calcium hydroxide
OSHA	oyster shell hydroxyapatite
2 $\theta$	two theta
ICDD	International Centre for Diffraction Data
IU	International Unit
IM	Intramuscular
B.W.	Body weight
kV	Kilovolt
mAs	Milliampere-seconds
F.F.D.	Focal film distance
EDTA	ethylenediamine tetraacetate acid
PBS	Phosphate buffer saline

<b>Abbreviation</b>	<b>Name</b>
CRD	complete random design test
ALP	Alkaline phosphatase
PS	post-surgery
BMPs	Bone morphogenetic proteins
M	Mollari

# Chapter One

## Introduction

The mandibular bone plays an important role in supporting the lower teeth and muscles, maintaining the structural integrity of the face, providing masticatory forces during biting and animal eating, permitting regular inhalation of air by keeping the mouth cavity open, and permitting the tongue to move. A mandibular bone defect is the absence of normal bone tissue in the mandible caused by many factors such as direct trauma, infection, tumor, disease, surgery, or congenital abnormalities. If the bone defect in the mandible is a large size, it can lead to difficulty in mastication, salivation, barking, and even breathing (Balanta-Melo *et al.*, 2019). Normal bones can repair and regenerate, but in cases of large size defects, which can be brought on by several circumstances, including advanced age, car accidents, nonunion fractures, and removal of bone tumors, the healing process cannot be accomplished independently (Alonzo *et al.*, 2021).

Large size bone defects refer to defects that cannot be healed spontaneously and require further surgical intervention. The surgical interventions aim to reconstruct the defective tissue, prevent any amputation, provide sufficient functional outcomes, and control the healing process of defective bones (Migliorini *et al.*, 2021). In general, large size bone defects remain a clinical challenge in orthopedic surgeries, especially in the craniofacial surgery of animals, because there is limited evidence for the treatment of large bone defects. Also, the constant movement of the mandible during mastication, biting, and barking makes the bone healing process difficult to achieve. Recently, bone grafts or substitute biomaterials have been used as bone substitute materials to fill bone defects, reconstruct large-size bone defects, and control the healing process of defective

bones(Al Maruf *et al.*, 2023). The ideal properties of bone substitute biomaterial should be osteogenesis, osteoconduction, osteoinduction, and biocompatibility, as well as being readily available and ready to use without any risk of inflammatory or immunological reactions (Baldwin *et al.*, 2019).

The reconstructions for mandibular bone defects typically involve bone grafting or bone regeneration procedures, which aim to induce new bone tissue growth to fill the defect. The treatment recommendations are based on several factors, including the defect's size, location, the animal's general condition, and medical history. The gold standard for treating bone defects is still autologous grafts, which are biocompatible and have osteoconductive and osteoinductive properties. Unfortunately, they require a second surgical procedure to harvest the tissue, which might be risky due to potential consequences like donor site damage, a high rate of morbidity, deformity, and the formation of fibrous tissue at the implanted site (Haugen *et al.*, 2019). Furthermore, it takes into account a costly operation that carries a high risk of bleeding, inflammations, infections, and persistent discomfort during surgery. Allografts have a more extended history of failure and a greater potential for immunoreactions and infections spread than autografts. When it comes to bone transplantation, allografts involve the harvesting bone tissue from one individual and transplanting it to a genetically different individual within the same species (Winkler *et al.*, 2018). The platelets rich plasma (PRF) is considered as an autologous biomaterial product with a gelatinous matrix to promote osteogenic cellular migration and proliferation, a greater leukocyte count and fibrin mesh both have an antibacterial impact during tissue regeneration. (Caruana *et al.*, 2019). Because of its biological and clinical characteristics, PRF is frequently used in medicine to treat skin ulcers and necrosis, as well as in



cosmetic and reconstructive surgery to serve as reinforced material during hernioplasty procedures (Zedan *et al.*, 2022), as well as in the regeneration of a large bone defect in the skeletal system (Pinto *et al.*, 2018; Soares *et al.*, 2023).

The biological characteristics of bone substitute biomaterials include the absence of the possibility of disease transmission and the host tissue's immunological reactions following implantation (Knöfler *et al.*, 2016). Also, they are capable of controlled biodegradability, bioactivity, and biocompatibility (Haugen *et al.*, 2019). Furthermore, bone biomaterials need to not only bridge bone defects but also facilitate faster bone healing and less tissue response (Gao *et al.*, 2017). Therefore, many recent studies have been interested in studying new bone substitute biomaterials made from naturally derived and synthetic derived materials similar to the organic or inorganic components of bone tissue (Sharifianjazi *et al.*, 2021; Barbeck *et al.*, 2023).

### **Aimes of this study**

1. Preparation of oyster shell hydroxyapatite powder and quail eggshell calcium hydroxide powder as bone substitutes through modification in the fabrication process.
2. Reconstruction the induced large mandibular bone defects in dogs by filling the defect with oyster shell hydroxyapatite powder, quail eggshell calcium hydroxide powder, and platelets rich fibrin gel.
3. Comparison between the effect of these biomaterials on the healing of mandibular bone defect through study the clinical signs postoperatively with gross and histopathological changes, in addition to the study the radiographic, immunohistochemical and field emission scanning electron microscopy results

## **Chapter Two**

### **Review of literature**

#### **2-1: Anatomy of the bone**

The bone tissue forms approximately 15% of the total weight of the living body. The histology of bone tissue consists of two types of bone: compact and spongy bone. The outer layer, which is the cortical or compact layer, is characterized by high mechanical resistance, and the inner layer is spongy or cancellous bone, which has high porosity.

The inorganic components of the bone consist mainly of calcium and phosphate molecules, and these components make up approximately 65 to 70% of the dry weight of the bone (Dec and Pawlik., 2023). The organic portion of the bone, about 30% of the total weight of the bone, consists of proteins mainly of collagen (type I), proteoglycans, glycoproteins (osteonectin and osteocalcin), and various cellular constituents. The organic components of the bone give the bone flexibility and aid in the bone healing process (Luo and Amromanoh, 2021).

The structure of bone is formed by dense connective tissue, it acts as a framework of body structure and also plays a main role in the protection of the internal body structures and serves as the mineral preserver of the body (Florencio *et al.*, 2015). There are numerous ways to classify bones, including size, consistency, shape, and placement (Safadi *et al.*, 2009). Bones that are tubular include the clavicles, the long bones of the limbs, and the little tubular bones of the fingers and toes (metacarpals, metatarsals, and phalanges). The diaphysis, a hollow shaft mainly composed of dense cortical bone; the paired metaphyses, with their flared ends, and the epiphyses, an area that holds the articular surface close to the

metaphysis, are the three separate parts that make up their creation (Buck and Dumanian, 2012).

The morphological characteristic of a bone comprises the cortex, medulla, and periosteum. The outer layer of bones, except the articular cartilage region, is covered by the periosteum. The periosteum is composed of two layers: the dense, uneven connective tissue that makes up the thick outer layer, often known as the "fibrous layer", and the is the inner layer, called the "osteogenic layer", which is composed of osteogenic cells. (Duchamp *et al.*, 2018).

The endosteum, which consists only of bone lining cells, coats the inside surfaces of bones. Although its function is unclear, the endosteum is believed to act as a barrier between the bone marrow and the bone (Kalfas, 2001). The osteoprogenitor cells and vasculature are present in the comparatively cellular endosteum, which is in direct contact with the marrow cavity (Buck and Dumanian, 2012).

The cortex, composed of osteons, is thicker along surfaces and is located beneath the periosteum, particularly at the epiphyses, the interior part of these bones is trabecular, which means beam-like and resembling a meshwork. Additionally, it is occasionally called cancellous bone or, somewhat inaccurately, "spongy" bone (Tzelepi *et al.*, 2009).

Histologically, there are three main types of bone tissue: woven bone, cortical bone, and cancellous bone. The woven bone is present both during embryonic development and after fracture healing (callus formation). It is composed of unevenly shaped vascular regions, collagen bundles scattered randomly, and osteoblasts bordering it, usually, a new layer of cancellous or cortical bone is laid over the rebuilt woven bone. The vascular matrix infiltrates the periosteal and endosteal surfaces of the bone

throughout embryonic development, reshaping it from woven bone into the cortical, compact, or lamellar bone. It creates the external surfaces of long bones and the internal and external surfaces of flat bones. characterized by uniformly distributed osteocytes and bone matrix and densely packed collagen fibrils in sheets. During the bone growth and the final phase of bone development, the woven bone is entirely replaced by the lamellar or compact bone. Lamellar bone becomes strong and inflexible because of its consistency (Buck and Dumanian, 2012). Osteons, which are sometimes called haversian systems, are the primary building blocks of compact bone. The compact bone and most of the diaphysis are constituted of osteon, which is a type of lamellar bone with a cylindrical shape that encircles haversian canals that are aligned longitudinally around the vascular channels. Volkmann canals are horizontally oriented channels that connect adjacent osteons. The mechanical strength of cortical bone is determined by the closely packed osteons (Lin *et al.*, 2020).

The cancellous bone also called trabecular bone or spongy bone, it located at the ends of long bones and within the vertebral bodies. Trabecular bone has a higher porosity surface. It contains trabeculae called spicules which consist of mineralized tissue. In mammalian animals, these spaces between the spicules are filled with bone marrow (Reece and Rowe, 2017). Cancellous bone is thought to exhibit increased metabolic and remodeling activity, as well as a rapid response to mechanical stress. This is because the main bone cells are located on the surface of the bone, beneath the circulating growth factors and cytokines. (Hart *et al.*, 2020).

## **2-2: Cellular Components of the bone**

There are three distinct cell types can be seen in the bone: osteocytes, osteoblasts, and osteoclasts. The surface of the bone is considered the home to these cells, which are derived from local mesenchymal progenitor cells

(Lin *et al.*, 2020). Mesenchymal cells differentiate into osteoprogenitor cells during the formation of bone tissue, and these cells then proliferate to differentiate into osteoblasts, these cells eventually develop into osteocytes by depositing organic elements of the bone matrix (Shang *et al.*, 2021). Osteoblasts are cuboidal cells that can create new bone. They constitute 4-6% of all resident bone cells. They run along the surface of the bone (Henry and Bordoni, 2022). The two main steps in the process of osteoblasts synthesizing bone matrix are the deposition of organic matrix and its subsequent mineralization. The organic matrix is formed by the proteoglycans, such as biglycan, and noncollagenous proteins, such as osteonectin and osteopontin, which are secreted by the osteoblasts in the first stage (Florencio *et al.*, 2015).

The cells that make up the majority of bones (90–95%) are called osteocytes, and they have a life span of up to 25 years. Their shape varies depending on the tissue, and they are trapped in the calcified matrix within lacunae, the shape of osteocytes from cortical bone is longer than that of those from trabecular bone. (Riquelme *et al.*, 2020). The morphology of embedded osteocytes differs depending on the bone type. For example, cortical bone osteocytes have an extended form, whereas trabecular bone osteocytes are more rounded. A subset of osteoblasts turns into osteocytes at the end of a bone formation, and these cells are integrated into the bone matrix (Burr, 2019).

However, the osteoclasts are derived from hemopoietic stem cells and are massive, multinucleated giant cells that belong to the monocyte-macrophage lineage. The function of the osteoclast is to break down the bone matrix, which is found on the periosteal surface under the periosteum and on endosteal surfaces within the Haversian system. It has two to 100 nuclei per cell, but it typically has between 10 and 20 nuclei per cell. Its

diameter can reach up to 100  $\mu\text{m}$ . It can also be found in deep resorption spaces known as cutting cones, and it is essential to the remodeling and repair of bone (Arnett and Orriss, 2018).

### **2-3: Anatomy of the mandible in dogs**

The mandible mainly consists of two parts, the mandibular body and the mandibular ramus. The right and left sides of the mandible joint together anteriorly by fibrocartilaginous connective tissue joint called intermandibular articulation (Voss *et al.*, 2009). The body of the mandible faces laterally the cheek, and is called the buccal surface, and faces anteriorly by the lower lips and is called the labial surface. It faces medially with the tongue and is called the lingual surface. The lingual surface of the mandible has a wide, smooth, longitudinal ridge, which represents the mylohyoid line which supports the mylohyoid muscle. The lateral surface of the mandible is long, smooth, and of an equal width caudal to the mandibular symphysis. Rostrally, it rotates medially and has a mental foramen, which is two foramina in a dog, it is located between the first two cheek teeth. A small mental foramen present caudal to the middle mental foramen. The mental blood vessels and nerves emerge from these foramina (Hermanson and DeLahunta, 2020).

Each mandible of the dog bears three processes at the proximal portion: the condylar process, the coronoid process, and the angular process. The condylar process articulates with the mandibular fossa of the temporal bone at the temporomandibular articulation. The coronoid process positioned between the zygomatic arch and the medial osseous wall of the orbit, provides a surface area for the insertion of the powerful temporalis muscle. The mandibular notch lies between the coronoid and the condyloid processes. The angular process forming the caudoventral portion of the mandible provides a point of insertion for another muscle of



the mandible near the base of the coronoid process in the masseteric fossa which acts as an area for the masseteric muscle insertion (Adams, 2004).

## **2-4: Blood Supply and Nerves**

Some authors suggested that the mandibular bone in dogs was supplied by periosteal vessels and supporting nutrient arteries enter the cortex of the bone by a small accessory foramen at the lower edge of the mandible (Kuwabara *et al.*, 2018). Other authors showed that the inferior alveolar artery was the major nutrient artery of the body of the mandibular (Hellem and Östrup, 1981). It is commonly known that the mandibular alveolar artery, which enters the mandibular canal at the medial surface of the mandible and supplies blood to the mandible's body as well as a portion of the ramus, is the primary source of blood supply to the mandible. The mandibular alveolar nerve and the mandibular vein are also transmitted through the mandibular canal. The mandibular nerve innervates the muscles involved in biting and feeding, giving the mouth motor function. The sensation is supplied to the cheeks, tongue, mandibular teeth, lower lip, and head skin by the mandibular nerve and its branches (Mills, 2013).

In addition, the mandibular nerve plays a vital role in the motor function of the mastication muscles, particularly the masseter, digastric, and temporal muscles. It forms several nerves such as the pterygoid nerves. The buccal nerve supplies motor innervation to the temporal and masseter muscles. The temporal nerve supplies motor innervation to the temporal muscle. The masseter nerve supplies motor innervation to the masseter muscle. The auriculotemporal nerve supplies motor innervation to the ear, parotid gland, and temporomandibular joint. The mylohyoid nerve supplies motor innervation to the mylohyoid muscle and digastric muscle. Finally, the lower alveolar nerve that enters through the mandibular canal in the

mandibular foramen gives branches to the mental nerves, which innervate the nerves of the lower lips (Singh, 2018).

## **2-5: Muscular attachment of mandible**

The muscles of the mandible serve to open, close, or move the jaw, the muscles that are attached to the mandible include platysma, buccinator, mentalis, masseter, temporalis, digastricus, mylohyoideus, and genioglossus muscles (Hermanson and De Lahunta, 2018).

The platysma is a well-developed muscle sheet. It originates from the mid-dorsal tendinous raphe present in the neck. In its longitudinal fibers, it extends over the parotid and masseter regions toward the cheek and commissure of the lips and inserted into the anterior border of the mandible which it is radiates into the Orbicularis Oris muscle. the platysma muscle acts to pull the commissure of lips cranially.

The buccinator muscle lies deep in the zygomaticus muscle between the rostral margin of the masseter muscle and the caudal margin of the Orbicularis Oris muscle it originates from the inner part of the Orbicularis Oris. It functions to make the cheek taut. It is divided into two parts; the buccal and molar parts. The buccal part which is the greater portion originates from the mandible ventrally and maxilla dorsally deep to the Orbicularis Oris. The molar part lies under the buccal part and is composed of longitudinal fibers that originate from the ramus of the mandible and extend rostrally to cover the cheek and blend with the buccal part as well as the Orbicularis Oris (Hermanson and DeLahunta, 2020).

The mentalis muscle originates from the alveolar border and the body of the mandible about the third incisor. The fibers connect with those of the opposite side and radiate into the inferior lip. The function of this muscle is to stiffen the lower lip in the apical region.

Masseter muscle is a larger muscular mass located along the lateral border of the ramus of the mandible ventral to the zygomatic arch. It appears slightly beside the ventral and caudal surface of the mandible.

The Temporalis muscle originates from the temporal fossa of the skull and inserts on the medial border of the coronoid process of the mandible. Both the temporalis and the masseter muscle act to close the mouth by elevating the lower jaw.

Digastricus muscle is located along the cauda-ventral surface of the mandible, arises from the jugular process of the occipital bone, and inserts on the caudoventral portion of the body of the mandible. The function of this muscle is to open the jaw.

The mylohyoideus muscles are a thin sheet of transversely directed fibers situated superficially between the body of the right and left mandibles, and these muscles act as a sling ventral to the tongue.

The genioglossus muscle is a smooth, triangular muscle that is located in the intermandibular space originating from the medial side of the mandible, and insert into the body and root of the tongue (Evans and De Lahunta, 2012). (Fig. 2-1 and 2-2).

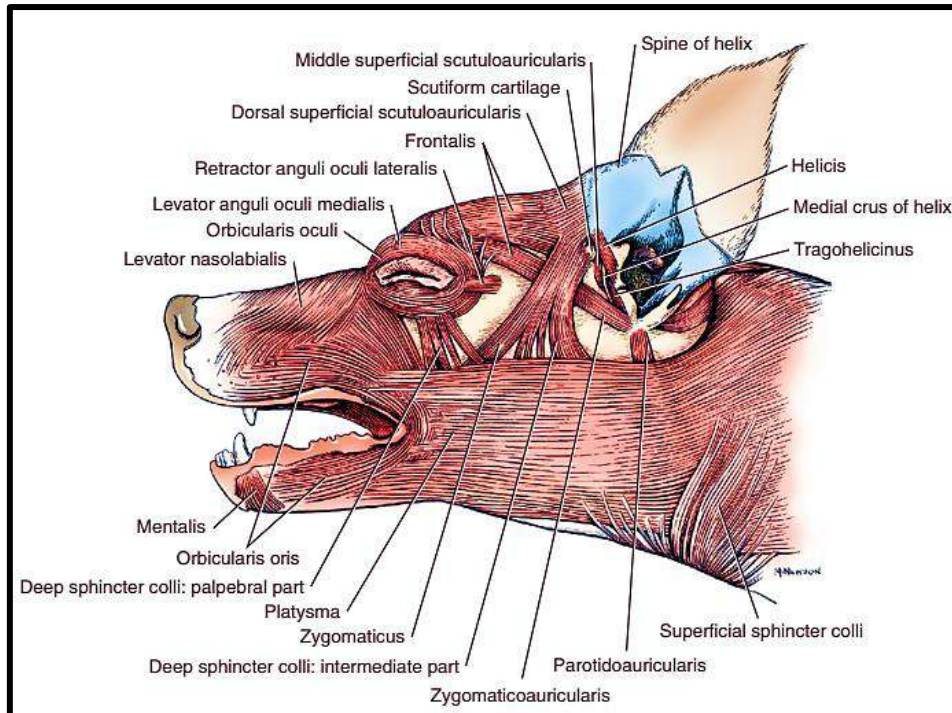


Figure 2-1: Superficial muscles connection to the jaw, side view, lateral aspect (Hermanson and De Lahunta, 2018).

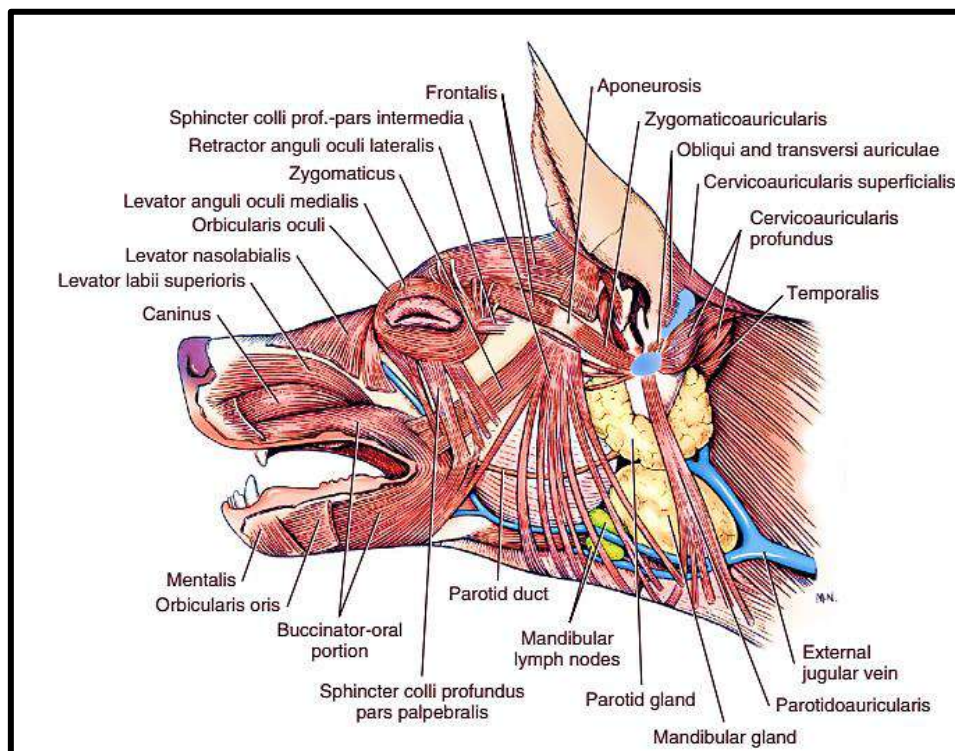


Figure 2-2: Deep muscles connection to the jaw, lateral aspect (Hermanson and De Lahunta, 2018).

## **2-6: Bone Healing of Mandible**

The mandible is considered the main portable bone of the facial skeleton. Mandibular bone healing is considered a challenge for orthopedic surgeons. Various components affect the healing process and are involved in delaying this process, such as the mechanical stress during the animal's mastication, the complex anatomical structure of the mandible, the less appropriate soft tissue mass, the less blood supply, and the higher incidence of inflammatory periodontal diseases, all these factors may decrease the healing times of the mandible (Brown *et al.*, 2016; Tatara *et al.*, 2019). Canine mandibles are different from long bones in that they don't have a marrow cavity, and the mandibular cortex covers the mandibular canal, which contains the inferior alveolar blood vessel structures but without hematopoietic cells (Wilson, 2002). In the canine, the roots of the tooth obtain a large volume of the mandible which directly affects the consequence of the bone healing (Härle and Boudrieau, 2012). In general, bone defect repair is a difficult process to restoration of the normal functional anatomy of the bone after fracture. These repairing events can be categorized into two types; primary and secondary healing (Calcei and Rodeo, 2019).

### **2-6-1: Primary (Direct) Bone Healing**

Primary bone healing is the restoration of normal bone continuity without callus formation. It happens if a fracture defect is strongly fixed through reduction and rigid fixation without micromotion (Sheen and Garla, 2022). The Primary healing of bone is also called direct bone healing, which is determined by intramembranous ossification. Furthermore, this form of bone healing takes place on a very small bone defect size between (10-100  $\mu\text{m}$ ). In contrast to intramembranous ossification, where bone tissue is directly synthesized by osteoblasts

generated by mesenchymal stem cell differentiation (MSC), endochondral ossification involves the formation, calcification, and eventual replacement of cartilage by bone. Bone abnormalities are frequent and come with a heavy emotional cost. The treatment for these injuries is still debatable, especially for those deformities that are large in size. (Schemitsch, 2017). Based on the defects between the fracture fragments, there are two distinct forms of direct (primary) bone healing: gap healing and contact healing (Marsell and Einhorn, 2010).

### **2-6-2: Secondary (Indirect) Bone Healing**

The most prevalent type of bone healing is secondary bone healing, which is very similar to normal endochondral ossification during development. This type of healing involves creating a cartilage template and then having it entirely replaced by bone (Affshana and Priya, 2015). Secondary bone healing is divided into three phases: inflammation, reparative, and remodeling phase. The inflammatory phase starts immediately after the fracture and forms a hematoma resulting from damaged blood vessels in the medullary canal of the broken bone forming the temporary frame for the subsequent healing process. Afterwards, inflammatory cells such as polymorphonuclear leukocytes, macrophages, and lymphocytes infiltrate the area and trigger angiogenesis through the production of cytokines (Parvizi and Kim, 2010). Several growth factors and cytokines, including tumor necrosis factor- $\alpha$  (TNF- $\alpha$ ), IL-1, IL-6, IL-11, and IL-18, are generated through the initial phase of inflammation. These substances encourage the formation of new blood vessels (Marsell and Einhorn, 2011). The release of cytokines and various growth factors control the migration of mesenchymal stem cells from the periosteum and endosteum to the defect site (Hak *et al.*, 2014). The reparative phase involves steps of chondrogenesis through chondroblast cell differentiation,



and the development of a soft callus, a cartilaginous covering that connects the two fragments of bone (Cheng and Shoback, 2019). The remodeling phase involves the mineralization and expansion of the soft callus by osteoclast cells through the process called endochondral ossification, which involves replacing the woven bone with stronger lamellar bone (Einhorn and Gerstenfeld, 2015).

## **2-7: Alkaline phosphatase**

Alkaline phosphatase (ALP) or tissue nonspecific alkaline phosphatase (TNAP) is a membrane-bound glycoproteins metalloenzyme composed of several isoenzymes. It is a crucial inducer of mineralization in bone and catalyses the dephosphorylation of pyrophosphate resulting in the inactivation of this calcification inhibitor and providing phosphate ions for hydroxyapatite crystal formation (Furmanik and Shanahan, 2018). The importance of ALP in bone formation and mineralization was first recognized by (Robison, 1923). ALP has been demonstrated immunohistochemically in decalcified, paraffin-embedded bone and cartilage sections (Tulli *et al.*, 1992). Also, it is highly expressed in the cells of mineralized tissue and plays a critical function in the formation of hard tissue. There are four different varieties of alkaline phosphatase identified by the tissues in which they are expressed: intestine, placental, germ cell, and tissue nonspecific (Liver, Bone, Kidney) (Sharma *et al.*, 2014). Tissue-nonspecific alkaline phosphatase (TNAP) is found in hypertrophic chondrocytes and osteoblasts cell membranes and often concentrates in those cells on the membranes of matrix vesicles (Vimalraj, 2020).

The mechanisms through which ALP expression is regulated are complex (Sterner *et al.*, 2018). ALP is produced early in growth and is

easily found on the cell's surface and in matrix vesicles of bones and calcifying cartilages. Also, ALP was highly articulated in the extracellular space, while cytoskeleton, mitochondria, peroxisomas, nuclei, endoplasms, and lysosomes were moderately expressive. It starts with the formation of hydroxyapatite crystals in the matrix of vesicles and then with the distribution of hydroxyapatite to the extracellular matrix of the bone tissues (Vimalraj, 2020).

## **2-8: Mandibular Defect**

The mandibular defect is defined as the loss of a part of the lower jaw. It includes the second most common facial mammalian fracture skeleton (Akinbami, 2016). The defect of the mandibular body from the canine teeth to the angle of the mandible is the most commonly reported mandibular defect in the dog (Guzu and Hennet, 2017). Mandibular defects are clinically defaulted for reconstitute due to the complex anatomy of the jaw and defaulted for soft tissue repair (Tatara *et al.*, 2019). It accounts for nearly 59% of all facial defects, and its repair is complicated by postoperative infections due to risk from oral flora ( Abdullaev *et al.*, 2021).

Other studies describe the mandibular defect by classification, such as the (Jewer) classification (Jewer *et al.*, 1989), that can be used to better categorize mandibular abnormalities: The grade of a defect is (C) for the central section, (L) for the lateral area that does not include the condyle, and (H) for the condyle and lateral mandible combined. Because it is the most common site of fracture in dogs, the mandibular body and particularly the premolar region can sustain a broad range of injuries ( Castejón-González *et al.*, 2022).

Also, other various research classified bone defects into three types. The first one is a segmental defect, where a part of the bone is missed, causing the fractured bone end to be disconnected and unsupportive. In the second kind, known as a penetrating defect, the whole thickness of the bone tissue is torn away from the cortical bone while the adjacent tissue stays linked and undamaged. The third kind of bone defect is called a burr hole defect. In this type, the bone tissue is continuous on one side and forms an incomplete hole on the other. Nonpenetration and non-segmentation are the hallmarks of this defect type (Kumar *et al.*, 2016; Xian *et al.*, 2016; Buchbender *et al.*, 2018).

## 2-9: Etiology of Mandibular Defect

The most defects of mandible are caused by automobile or bite wound trauma, loss secondary to severe periodontal or endodontic disease (Paré *et al.*, 2019), these causes shown in (Table1). Causes such as cysts, benign and malignant tumors, trauma, chronic osteomyelitis, tooth loss, and abnormalities in the alveolar and basal jawbone can lead to impaired chewing ability, the congenital causes are uncommon. (Lim *et al.*, 2022).

Table 2-1: The most frequent etiologies of mandibular defects.

No.	Causes	Origin
1.	Tumors	of cases are squamous cell carcinoma, 95% .sarcoma, or cancer of the salivary glands Ameloblastoma is a benign tumor
2.	Trauma	Road accidents, and Gunshot
3.	Osteonecrosis of mandible	Osteoradionecrosis, medication-related Osteonecrosis
4.	Osteomyelitis	Dental infection, autoimmune disease

## **2-10: Complications of mandibular defect**

Complications of the mandibular defect healing process derived from mandibular fractures include malunion or nonunion, malocclusion, infections, and periodontal and/or endodontic disease. In addition, the other most common complication related to the surgical approach is trauma and damage to the trigeminal nerve and mental nerve but most injuries to these nerves can be healed and animal restore their sensation without complications (Castejón-González *et al.*, 2022).

## **2-11: large Size Bone Defect**

A Large-Size Bone Defect (LSBD) is the smallest type of bone defect that cannot be repaired on its own within an animal's lifetime or with conventional therapies (Haines *et al.*, 2016). Generally, many studies have been illustrated that the defect size length ranges from (5–20) mm. and more than 30-50% loss of the circumference of the bone which considered a large in size (Huh *et al.*, 2005; Culla *et al.*, 2022). Also, researchers have used defects of (8) mm, and direct healing does not normally occur with the natural process of bone healing (Meeson *et al.*, 2019). There are many factors that determine the size of large size bone defects depending on the pattern of the bone loss, morphological, and anatomical location of the defect (diaphyseal/metaphyseal/articular), infection, tumor resection, the associated soft tissue losses including damage to the periosteum and surrounding muscles, age, and presence of chronic diseases (Schemitsch, 2017). large sized defect also called large segmental bone defect directly affects bone vascularization and tissue differentiation, which leads to the development of non-union if it left without any interventions (Sela and Bab, 2012).

A recently created biomaterial's efficacy has been experimentally used to evaluate the large size defect as a model. Research on bone regeneration in various anatomical locations has made use of many animal models of bone abnormalities, including those of the tibia, radius, mandible, and skull (Liu *et al.*, 2020; André *et al.*, 2022).

## **2-12: Surgical Approaches to the Mandible**

Different approaches have been reported to access to the mandibular bone, including a ventral paramedian approach, ventral approach, and a lateral approach (Cinti *et al.*, 2021). The most preferable approach for access to the mandibular defect and fracture is a ventral paramedian approach (Rudy and Boudrieau, 1992). In this approach, the digastricus (caudal), platysma (lateral), and mylohyoid (medial) muscles are seen. The digastricus is a point of entry for a facial vein branch. Compared to clamp fixation, this method allows for easier implant insertion and the capacity to fix several tiny fragments from different angles using pins or screws with smaller diameters. This is of utmost importance when it comes to smaller dogs that have complicated fractures (Brinker *et al.*, 1983). To expose the mandible by this approach, the Orbicularis Oris and buccinator muscles are bluntly separated from the ventral surface of the mandibular and retracted laterally, and the mylohyoideus with genioglossus muscles are separated from the medial border of the mandible and retracted medially. It is recommended to preserve the attachment of the digastricus muscle to the ventral border of the mandibular body because it is the only muscle that serves to open the lower jaw (Johnson *et al.*, 2005).

In the ventral approach, the patient is placed at dorsal recumbency with the forelimbs extended caudally. The surgical preparation is performed in the area between the mandibular rami and the cranial portion of the neck. The neck is extended and elevated by placing a towel

underneath. A ventral incision is made in the area between the midline of the mandible and the mandibular ramus on the affected side, in the body of the mandibular horizontal ramus. A blunt dissection through the subcutaneous tissues and platysma muscle reveals the digastricus muscle, which is followed by further cranial dissection along the sublingual salivary gland to expose the body of the mandible (Johnson, 2013).

In the lateral approach, the patient is positioned in a dorsal recumbent with extended forelimbs caudally, and bluntly dissected the platysma muscle to reveal the digastricus muscle, then elevate the masseter muscle from the ramus to present its lateral mandibular surface and angular and coronoid processes (Fossum, 2018). This approach is commonly used for exposure to the vertical ramus and temporomandibular joint (Risselada, 2020).

## **2-13: Biomaterials**

During the consensus development conference in Chester, UK, in the 1980s, the first definition of biomaterial was established. (David, 1986), where biomaterials are substances (not including drugs) that can be used alone or in combination with other materials to treat, augment, replace, or restore the function of any organ, tissue, or system in the living body for an extended period (Ratner *et al.*, 2020). During the international consensus conference in 2018, the term biomaterials was redefined as “a material designed to take a form that can direct, through direct interactions with living systems (Zhang and Williams, 2019).

Biomaterials have a wide range of medical applications, especially in tissue engineering, drug delivery, medical devices, and the treatment of numerous diseases (Wang, 2013). The therapeutic outcomes of the biomaterials have been established in the tissue regeneration by stimulants healing process, promoting proliferation and differentiation of cells

through incorporation within the cellular activities of the damaged tissues (Moukbil *et al.*, 2020). After implantation, the host responds in a variety of ways to both natural and synthetic biomaterials. These reactions include the construction of a provisional matrix, inflammation (both acute and chronic), interactions between blood and the material, and the development of granulation or fibrous tissues (Sarkar *et al.*, 2017).

### **2-14-1: Natural Sources Biomaterials**

Because of their incredible diversity, biomaterials derived from plants, animals, and microbes are abundant and exhibit a wide range of desirable characteristics (Insuasti *et al.*, 2022). To be considered a natural biomaterial, a substance must be not only renewable but also nonimmunogenic, biocompatible, biodegradable, readily available, inexpensive, and sterilizable. Many researchers still know very little about biomaterials found in nature, but finding new ones from marine animals that have surprising qualities could lead to improved healthcare options (Khrunyk *et al.*, 2020).

In general, natural biomaterials are prepared from natural biopolymers, while synthetic biomaterials are made up of synthetic polymers. The three main categories of biomaterials generated from natural sources are proteins, polysaccharides, and decellularized tissue matrices (Ige *et al.*, 2012). The polysaccharides, that can be obtained from living organisms. Natural polymers derived from polysaccharides, such as fibrin, alginate, hyaluronic acid, and chitosan, have found widespread application in tissue regeneration (Abbasian *et al.*, 2019). Collagen, fibrin, gelatin, and silk are all proteins that belong to a class of polymers derived from natural sources (Klimek and Ginalska, 2020).

On the other hand, the process of extracting cells from natural tissues or organs allows for the creation of decellularized tissue matrices, which are used as a source for the host extracellular matrix to stimulate healing potentials when implanted in vivo (Sarkar *et al.*, 2017). In tissue engineering, natural biomaterials play a significant role due to their bioactivity which mimics of natural extracellular matrix (ECM), supporting cell infiltration, and differentiation (Ullah and Chen, 2020). Moreover, the limitation of using natural biomaterials in the medical field is related to their low mechanical properties, especially when used in hard tissue regeneration (Haugen *et al.*, 2019). According to recent research, hybrid biomaterials, which combine natural and synthetic polymers, have the potential to enhance the mechanical properties of natural biomaterials while also supporting their physiochemical and biological functions (Lei *et al.*, 2019).

## **2-14-2: Synthetic Sources Biomaterials**

Synthetic materials are known for their exceptional processing properties, which make them readily available for purchase. On the other hand, they have issues such as being "foreign" to cells, causing inflammatory reactions, and not being able to integrate with host tissues or comply with regulations (Ravi and Chaikof, 2010). Over the past century, researchers have utilized synthetic materials to repair many organs and tissues. At first, there were implanted materials that were mostly inert and used for mechanical function replacement (Nardo *et al.*, 2017). Synthetic biomaterials are more predictable and controllable in terms of their physicochemical, mechanical, and degrading properties; they are also easy and cheap to make in large batches. In addition, synthetic materials are known for their exceptional processing properties, which guarantee their readily available stock. But they're not without their flaws, such as being



"foreign" to cells, causing inflammatory reactions, and either not complying with host tissues' requirements or not being able to integrate with them (Sarkar *et al.*, 2017).

Synthetic biomaterials primarily encompass polymers, metals or a combination of both (Lam and Wu, 2012). Historically, surgical methods have made use of metals dating back to the seventeenth century. Metals have found widespread use in load-bearing applications because of their superior mechanical qualities compared to other biomaterials (Samavedi *et al.*, 2014). Because of its superior mechanical qualities, metal implants have long been the material of choice in orthopedics. The three most common metals used for implants are stainless steel, titanium, and chromium. The risks associated with metallic implants include allergic reactions, metal discoloration, and implant failure (Prakasam *et al.*, 2017). Furthermore, erosion and toxicity are of most common problems uses of the metals, which can release potentially harmful byproducts of degradation into the body (Krishnakumar and Senthilvelan, 2021).

Among the many readily accessible synthetic biomaterials used in bone tissue engineering are highly porous biological scaffolds. These scaffolds can enhance cell adhesion, proliferation, and the creation of new tissues and fluids with respect to bone defects. Surface erosion and bulk erosion are two distinct pathways by which this scaffold degradation might take place, named surface erosion and bulk erosion. The erosion that occurs on a device's surface is known as surface erosion. In bulk erosion, the pace at which body fluid penetrates the device surpasses the rate at which the scaffold is transformed into water-soluble components, causing erosion throughout the device. This causes the scaffold device to become thinner over time while maintaining its bulk integrity (Doppalapudi *et al.*, 2014). The advantages of these scaffolds include their biodegradability, which

allows them to break down alongside bone repair, and their biocompatibility, which prevents unpleasant reactions. This process continues until new tissue entirely replaces the scaffold (Idumah, 2021).

In addition, other synthetic sources of biomaterials were polymers like Polyhydroxyalkanoates, polyetheretherketone, polycaprolactone, polyurethane, polyethylene, and polysulfone are among the most typically utilised biocompatible polymeric materials in orthopaedic surgery (Dziadek *et al.*, 2018). These polymers have advantages, including high shear strength, elasticity and transparency, ideal bacterial resistance, and the material's prolonged shelf-life, low cost, flexibility, and easy manipulation (Rey-Vinolas *et al.*, 2019). In general, one of the main disadvantages of synthetic biomaterials is that they require chemical treatment to improve cell attachment, and they also do not have any cell-binding sites (Ye *et al.*, 2022), also the by-products of their breakdown can cause acid buildup and induce tissue inflammation (Terzopoulou *et al.*, 2022). There are only a few significant uses for polymers in bone replacement, and those include the articulating bearing surfaces of knee and hip replacements and the interposition cementing substance that seals the implant surface to the bone. In general, when choosing a polymer to use as a biomaterial, it's important to make sure that its mechanical qualities and degradation time are suitable for the purpose (Krishnakumar and Senthilvelan, 2021).

## **2-15: Properties of the Bone Substitutes Biomaterials**

Biomaterials used as bone substitutes have three main goals: preserving the morphologic contour, restoring mechanical strength and function, and eliminating dead space to decrease infection after surgery and improve the healing process. (Ausenda *et al.*, 2019). Because they improve cell activity and function and provide a matrix for cell adhesion,

proliferation, and differentiation, bone biomaterials are crucial in the repair of bone fractures (Gao *et al.*, 2017). Bone biomaterials, sometimes known as bone graft alternatives, have seen a surge in popularity during the past decade (Shadjou and Hasanzadeh, 2015). In an ideal world, biomaterials used as bone substitutes wouldn't cause any harm, have no inflammatory or immunological rejection effects, and cause very little fibrosis (Abdulghani and Mitchell, 2019). In addition to being biodegradable under control, they should be biocompatible and bioactive (Haugen *et al.*, 2019).

Bone biomaterials should also enhance bone healing processes with little tissue reactivity and minimal time required to fill bone deficiencies (Gao *et al.*, 2017). Bone substitute biomaterials mainly act as a mechanical support and osteogenic function, which may involve the most important biological elements of grafting: osteoconduction, osteoinduction, or osteogenesis properties (Wang and Yeung, 2017; Kazimierczak and Przekora, 2020).

Osteoconduction refers to a biomaterial's ability to facilitate the migration and adherence of bone cells inside the graft's three-dimensional structure. The term "osteoinduction" describes the process by which a bone transplant can encourage bone stem cells to become bone-forming cells. The process of osteogenesis involves transforming stem cells from the host or transplants into osteoblasts, which then differentiate into new bone (Albrektsson and Johansson, 2001; Roberts and Rosenbaum, 2012).

## **2-16: Types of bone substitute biomaterial**

Once implanted, bone biomaterials provide contact and interaction between the biomaterials and the cells and tissues in the immediate vicinity. Thus, a crucial step in preparing for optimum bone implants is the selection of bone biomaterials. Bone biomaterials are typically chosen for

their mechanical qualities, biodegradability, and biocompatibility (Shamsoddin *et al.*, 2019).

There is the development of large numbers of natural and synthetic bone substitute biomaterials, such as demineralized bone matrix (DBX), hydroxyapatite (HA) and its products such as tricalcium phosphate (TCP) ceramics, and oyster-based substitutes, calcium-based biomaterials, calcium phosphate (CaP) cement, bioactive glass (BG), and polymer, all these bone biomaterials are approved by FDA biological bone substitutes (Fernandez de Grado *et al.*, 2018).

## **2-17: Bioceramic in Orthopedic Field**

Bioceramics means biocompatible materials that can be used in the medical or clinical fields. Calcium phosphates (CaP) are one type of bioceramic, although there are other crystalline and amorphous varieties, and the process of sintering moulded powders at high temperatures is typically used to create crystalline bioceramic products (Best *et al.*, 2008). In 1892, Dressman published the first report on using plaster of Paris to treat bone defects, marking the first usage of bioceramics. (Peltier, 1961; Shaffer and App, 1971). In 1920, the first reliable application of tricalcium phosphate was documented. In the 1960s, Hulbert and colleagues laid the groundwork for what would become an interest in bioceramics. However, between 1970 and the early 1980s, interest levels plateaued (Hench, 1991). In 1963, Smith created the concept of bioceramics with his research on Cerosium, a ceramic bone substitute. (Smith, 1963), their work demonstrated that a porous ceramic made through a high-temperature reaction may be as strong as bone while remaining in rabbit tissues. However, bioceramic-coated implants were first found on the market in the 1980s, marking the beginning of bioceramics' usage in human surgery (Muthutantri, 2009).

The alumina, zirconia, bioactive glass, glass ceramics, hydroxyapatite, and calcium phosphates are among the bioceramic materials that can be categorized as either bioactive or bioinert, according to their interaction with the surrounding bodily tissue (Cirstea *et al.*, 2020). The term "bioinert ceramics" refers to materials that are either not biologically active or that when implanted in living tissue, do not cause the desired physiological or biological reactions (Udduttula *et al.*, 2019). Alumina, zirconia, and titania are the three most common types of bioinert ceramics, and they have found widespread use in orthopedics, maxillofacial surgery, and dental implant procedures (Best *et al.*, 2008).

The orthopedic surgery frequently employs bioactive ceramic materials, categorized as resorbable or non-resorbable based on their stability. These materials are utilized for joint or tissue replacements and cover metal implants to enhance biocompatibility. The porous bioactive ceramics, especially those containing calcium phosphate, have also found extensive application as alternatives to traditional bone grafts (Xiao *et al.*, 2022). Bioactive ceramics which can form a direct chemical bond with bone or even with the soft tissue of a living body.

In 1988, LeGeros was the first to use calcium phosphate as a bioceramic restorative dental cement (LeGeros, 1988). Calcium phosphates-based materials have been frequently used in medicine as scaffolds to replace or regenerate damaged tissues, to control and synchronize material resorption and stimulate bone formation. Numerous studies have demonstrated that composition and textural property manipulation, including nano-, micro-, and macro-surface porosity, is an effective strategy (Ali *et al.*, 2013; Islam *et al.*, 2017; Sekar *et al.*, 2021). The bioactive calcium phosphates-based materials closely resemble the composition and structure of the inorganic phase of the bone mineral and

can be produced using low or high-temperature processing pathways (Ginebra *et al.*, 2018).

In addition, bioceramic materials containing calcium phosphate have two primary benefits. First, the fact that they are biocompatible means that the body's tissues won't reject them. Secondly, bioceramic materials can improve bioceramics' setting qualities and produce an inorganic phase-like crystalline structure and chemical composition, much like natural tooth and bone (Kucko *et al.*, 2019). Biologically, the calcium phosphate compounds are ideal for use as a bone replacement material in orthopaedic procedures because they contain the ions  $\text{H}_2\text{PO}_4^{3-}$  and  $\text{PO}_4^{3-}$ , which are naturally present in the inorganic mineral phase of bones and teeth (Kucko *et al.*, 2019). The most widely used calcium phosphate-based material is calcium hydroxide and its precipitation of hydroxyapatite (HA) bioceramics (Malhotra *et al.*, 2014; Chaikina *et al.*, 2019), which is used mainly in many applications such as bone defects in dogs for repairing tibial defects.

### **2-17-1:. Oyster Hydroxyapatite**

Hydroxyapatite (HA) has a typical formula of  $\text{Ca}_{10}(\text{PO}_4)_6(\text{OH})_2$  and is structurally very similar to inorganic phases seen in both healthy bone and teeth. Several studies involving HA as bone substitute materials with a Ca/P ratio of 1.67 are underway due to this near closeness. The HA powder is a white crystalline powder (Lopes *et al.*, 2018). Because it is composed only of calcium and phosphate ions, hydroxyapatite poses no risk of local or systemic toxicity when implanted within bone defects. The Ca/P ratio ranges from (1-1.67) considered nontoxic and not induce any foreign body reaction which allows a newly formed bone to directly bind to the bone-implant interface (Prathap *et al.*, 2022). In addition, the trace elements found in natural HA, such as  $\text{Na}^+$ ,  $\text{Zn}^{3+}$ ,  $\text{Mg}^{3+}$ ,  $\text{K}^+$ ,  $\text{Si}^{3+}$ ,  $\text{Ba}^{3+}$ , and  $\text{F}^-$ ,  $\text{CO}_3^{3-}$ , these ions can accelerate the process of bone healing (Naredla

*et al.*, 2022). A recent studies have highlighted the possibility of  $\text{Zn}^{+3}$  and  $\text{F}^-$  ions having antibacterial properties against various bacterial pathogens, including *Streptococcus pneumonia*, *Bacillus subtilis*, *Escherichia coli*, *Klebsiella pneumonia*, *Staphylococcus aureus*, and *Pseudomonas aeruginosa*. This property is particularly important in orthopaedics and dentistry, where infections are common (Raji *et al.*, 2022; Ressler *et al.*, 2022).

As an alternative, hydroxyapatite surfaces can promote osteoblastic cell adhesion, development, and proliferation, facilitating the gradual replacement of dead bone with newly grown bone. Additional functions of hydroxyapatite include the transport of cytokines and growth factors (Sun *et al.*, 2017). Natural hydroxyapatite can be sourced from a variety of biological materials, including animal bones (e.g., those of horses, camels, and bovines), shells (e.g., those of clams, eggs, and seashells), plants, algae, and minerals (e.g., limestone). Many authors have focused on obtaining hydroxyapatite from marine waste and on its use for biomedical applications because the conversion of oyster shells into this product which considered as environmentally friendly and allows for the reduction, reuse, and recycling of large quantities of these readily available materials (Kattimani *et al.*, 2016; Borciani *et al.*, 2022).

An oyster shell is made of marine invertebrates from the sea that are rich in calcium, phosphorus, and other trace elements. Seashells, also known as coral shells, are the tough outer covering of the bodies of marine mollusks, scallops, clams, snails, and cockles, among others. These shells make materials based-hydroxyapatite (Yao *et al.*, 2013). The majority of oyster shell elements reported the presence of calcium oxide (CaO) rather than  $\text{CaCO}_3$  contents, this suggests that the oyster shell has a small amount of organic materials (Yoon *et al.*, 2003). Because of the macroscopic

similarities of these structures to the inorganic phase of bone, these structures can be appropriate for orthopaedic application. In addition, natural oyster-based materials have considerable success in bone healing due to their porous structure (porosity ranges from 100 to 500 $\mu$ m), which is similar to that present in the cancellous bone in morphology, which is considered an essential factor that facilitates the ingrowth of fibrovascular tissue within the bone defect area (Akyol *et al.*, 2019). One unique feature of coral skeletons is the synchronization of in situ resorption with endogenous bone growth. Chemically, coral skeletons are in the apatite family; mechanically, structurally, and crystallinity-wise, they are comparable to normal living bone. One way to improve osteoconduction is to hydrothermally convert oysters to calcium phosphate, which is chemically similar to mammalian bone (Green *et al.*, 2017).

The first coralline implant studied was reported by (Chiroff *et al.*, 1975), from the exoskeleton of the genus *Porites* called coralline hydroxyapatite Porites (CHAP). After that, this material was developed by Holmes (1979), who appeared with parallel interconnecting channels with 190 microns in size, which is similar to the microstructure of the bone and then this material was applied in dog mandibles with a (2)mm defect (Holmes, 1979). Recent research has shown that hydrothermal methods can transform oyster shells into hydroxyapatite. This process involves converting the calcium carbonate skeleton to calcium phosphate (Rocha *et al.*, 2005; Prathap *et al.*, 2022). In general, oyster structures contain both magnesium and strontium, which have a role in bone growth (Chou *et al.*, 2014). Also, many coral genera have already been used as bone graft substitutes, such as *Pocillopora*, *Acropora*, *Montipora*, *Porites*, *Goniopora*, *Fungia*, *Polyphyllia*, *Favites*, *Acanthastrea*, *Lobophyllia* and *Turbinaria* (Cestari *et al.*, 2020; Naredla *et al.*, 2022). Other researchers have looked



at oysters for potential medical uses due to their high carbonate content; however, oysters are not readily available everywhere, and many oyster or coral species are in danger of extinction. (Puspitasari *et al.*, 2021).

### **2-17-2: Quail Eggshell Calcium Hydroxide**

Bird waste is considered an important source of biomaterials, among which the most common ones include collagen, gelatin, keratin, beak bones, hyaluronic acid, chondroitin sulfate, and bioceramics. All bird species share a common mineral composition in their eggshells: calcite, the most common calcium carbonate mineral (Gautron *et al.*, 2021). Research on renewable materials that are both affordable and readily available has already begun. Hence, it was determined that quail eggshells mimic oysters regarding mineral content (Puspitasari *et al.*, 2021). Due to its low protein content, the eggshell of the quail (*Coturnix coturnix*) bird has a higher calcium content than that of the hen or duck (Syafaat and Yusuf, 2018). Also, the solubility of quail eggshell powder is higher than that of other sources of calcium, like limestone, indicating higher bioavailability. Thus, recently the quail shell became a renewable calcium source (Moura *et al.*, 2020).

Calcium carbonate ( $\text{CaCO}_3$ ), magnesium carbonate ( $\text{MgCO}_3$ ), and calcium phosphate ( $\text{Ca}_3(\text{PO}_4)_2$ ) make up the majority of the inorganic components found in eggshells, which are seen as a potential natural source for medical applications (Opris *et al.*, 2020). One of the many benefits of using eggshells as a source of calcium is the low level of toxic substances they contain. Another advantage is that they are an excellent source of calcium carbonate, an amorphous crystal that occurs naturally as calcite (Cestari *et al.*, 2021). Calcinating eggshells at high temperatures produces a number of calcium precursors, including calcium oxide ( $\text{CaO}$ ) and

calcium hydroxide ( $\text{Ca}(\text{OH})_2$ ), from calcium carbonate (Goloshchapov *et al.*, 2013).

Calcium hydroxide has been used in endodontic surgery since 1920 by B. W. Hermann (Hawkins *et al.*, 2015). Calcium hydroxide is white in color with odorless powder with the formula  $\text{Ca}(\text{OH})_2$  and a molecular weight of 74.08m. It has low solubility in water, and it has a high pH level (about 12.5-12.8) (Da Rosa *et al.*, 2019). The highly alkaline nature of the calcium hydroxide, which is bactericidal, especially against bacterial affects the root canals through the hydroxyl ions that destroy the phospholipid structure, which is the major component of the cellular membrane of the bacteria (Vatankhah *et al.*, 2022). Recently, calcium hydroxide was used in root canal filling in cases of root resorption and for the treatment of avulsed teeth (Al-Hiyasat *et al.*, 2021). The ability of  $\text{Ca}(\text{OH})_2$  to enhance bone defect regeneration is related to the rise of alkalization in the tissue in which the pH value of calcium hydroxide is around 10.5. This alkaline environment has favorable differentiation and osteoblast growth, stimulating bone regeneration in the defective area (Kahler *et al.*, 2018; Khosropanah *et al.*, 2018).

## **2-18: Platelets Rich fibrin**

Platelets rich fibrin (PRF), a platelet concentrate of the second generation, is made by drawing blood samples through centrifugation and removing anticoagulants from the process. (Dohan *et al.*, 2006a; Kumar *et al.*, 2016). The methods for second-generation platelet concentrates are easy, inexpensive, and quick (Giannini *et al.*, 2015). Without the use of a coagulation factor either during or after blood collection, the PRF preparation is simply obtained by activating intrinsic coagulation pathways on the inner surface of plan tubes (Yamaguchi *et al.*, 2020). There is a short turnaround time between blood sample collection and centrifugation

because fibrinogen is concentrated in the tube's upper layer and is directly transformed into fibrin upon contact with thrombin, which entraps the platelets (Caruana *et al.*, 2019).

A greater leukocyte count and fibrin mesh in PRF make it an autologous biomaterial that can promote tissue regeneration by increasing the migration and proliferation of osteogenic cells and by acting as an antibacterial (Caruana *et al.*, 2019). Due to its useful biological and clinical properties, PRF finds extensive medical application in the treatment of skin ulcers and necrosis, as well as in plastic and reconstructive surgery as a reinforcing material for hernioplasty (Zedan *et al.*, 2022), Particularly in musculoskeletal lesions, particularly those involving orthopedic surgery, where abnormalities encountered during bone regeneration (Pinto *et al.*, 2018; Soares *et al.*, 2023). In the last years, various procedures in oral and maxillofacial surgery have made use of these autologous biomaterials, including procedures for gingival recession, bone defects, post-extraction filling of alveoli, and sinus elevation, and improving the quality of bone regeneration (Hsu *et al.*, 2013; Gollapudi *et al.*, 2022).

The using of a glass stander tube instead of a plastic one allows for the extraction of PRF since the silica in glass acts as a natural coagulation inducer. Centrifugation at 2700 rpm for 12 minutes yields the final product (Jianpeampoolpol *et al.*, 2016). Also, there was another method for obtaining PRF named advanced PRF, in which sterile plain glass-based vacuum tubes (A-PRF) tube (10 mL; 1500 rpm for 14 minutes) were used (Ghanaati *et al.*, 2014). Another study illustrated that PRF protocol was taken without anticoagulant in (10) ml tubes with centrifugation at 3000 rpm for 10 minutes (Dohan *et al.*, 2006a). A recent study indicated that the PRF tube produces approximately 200–250% smaller PRF clots than the traditional glass tubes (Miron *et al.*, 2020). On the other hand, research by

(Miron *et al.*, 2021) has shown that PRF tubes (silica-coated tubes) can lessen clot size creation compared to plain glass tubes. The PRF tube coated with silica microparticles is easily and quickly removed from the inner surface of the tube and suspended in blood samples as blood is aspirated into the tubes then the silica microparticles exist ubiquitously in blood samples and quickly trigger the coagulation cascade, and the fibrin fiber matrix is uniformly formed in the upper part of the tube (Yamaguchi *et al.*, 2020). Similarly, many previous studies confirmed that the silica-coated tubes were recommended for PRF sample preparations (Dohan *et al.*, 2006a; Dohan *et al.*, 2012).

Recently, many surgical procedures involving fractures, particularly those involving the mandible, have highly used PRF as a biological additive to speed up the healing process and encourage early bone regeneration and soft tissue regeneration owing to the growth factors they contain. (Elhamshary *et al.*, 2023). Thus, the implantation process for filling bone defect abnormalities can be enhanced by employing autologous PRF in oral and maxillofacial surgery to promote bone healing (Naik *et al.*, 2013). A further finding was that PRF showed promise as a new method of root covering for the treatment of gingival recession in the front teeth of the mandible (Panda *et al.*, 2020). Chemically, the PRF gel is associated with small molecules, such as various cytokines and leukocytes. These molecules have a direct ability to mesenchymal stem cell migration and differentiations, promote fibroblast proliferation, increase tissue vascularity, increase the rate of collagen synthesis, increase mitosis of osteoblasts, induce the expression of phosphorylated extracellular-related kinase along with enmeshes glycosaminoglycans resulting in great support of bone healing process (Simonpieri *et al.*, 2012; Faot *et al.*, 2017).

## **Chapter Three**

### **Materials and methods**

#### **3-1: Experimental animals**

The experimental design received approval from the institutional animal care and use committee at the College of Veterinary Medicine, Mosul University, under the registration number (UM.VET.2022.050). In the current experimental study, 48 clinically healthy stray adult male dogs, their weight and age were ( $20 \pm 0.5$ ) kg and age were ( $2 \pm 0.6$ ) years, respectively. To be sure of being healthy, each animal was clinically examined for any suspected diseases, and then all animals were vaccinated against rabies (Zoetis Inc., Kalamazoo, MI49007, USA), then subcutaneously injected with Ivermectin 1% (Promectin, Spanish) of (0.3mg/kg) as a preventive drug for an external and internal parasite. During the duration of the experiment, each animal was housed separately in the animal house center, which is part of the College of Veterinary Medicine at Mosul University. Each animal was housed, fed, and visited according to the same institutional protocol and given unique cage numbers.

#### **3-2: Experimental design**

The experimental animals were randomly divided into four equal experimental groups (n=12):

I. In the first group (Control group) : A circular mandibular bone defect of (14) mm in diameter was created in the body of the mandible using a low-speed bone drill under continuous irrigation with 0.9% sterile saline solution and left empty without any treatment.

II. In the second group (QESCH group): The same mandibular bone defects were created, and filled with four grams of prepared quail eggshell calcium hydroxide powder.

III. In the third group (OSHA group): The induced mandibular bone defects were created, and also filled with four grams of prepared oyster shell hydroxyapatite powder.

IV. In the fourth group (PRF group) : The same mandibular bone defects were created and filled with a previously prepared autologous PRF gel. The experimental design mentioned in (Fig.3-1).

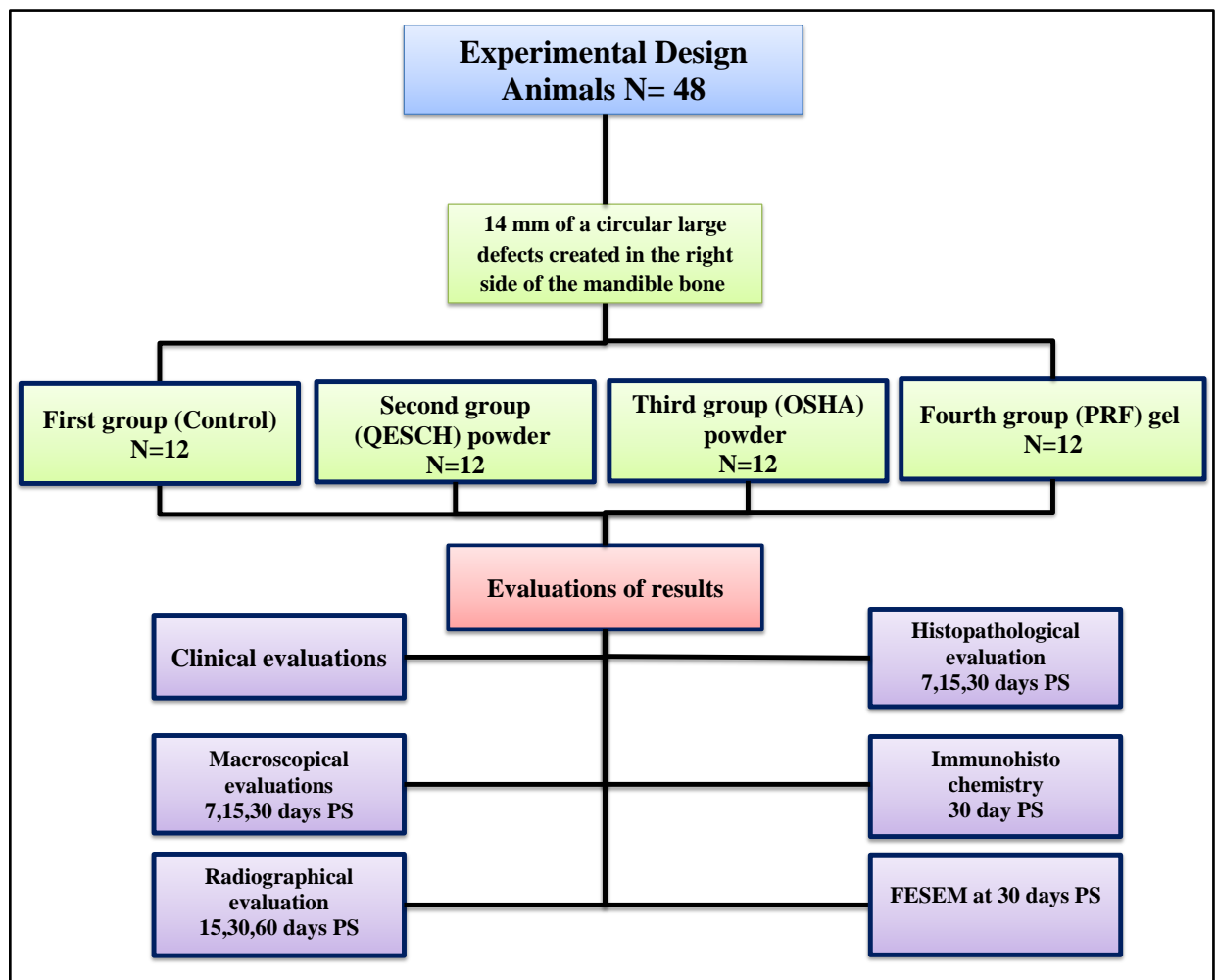


Figure 3-1: The diagram of experimental design.

### **3-3: Laboratory preparation of autologous PRF**

The animals in the fourth group were restrained and sedated with 2% xylazine (Interchemie, Holland) at doses (15 mg/kg), and the collection site was shaved with an electric clipper that started distally at the base of the neck and moved towards the head along the jugular groove and then disinfected with 70% alcohol. The vein is raised by the application of finger compression. About 10 ml of blood was withdrawn from the dog's jugular vein of each animal used a 21-gauge needle syringe. The blood flow from the vein was stopped by applying pressure with sterile gauze to achieve hemostasis. The blood sample was then collected in a sterile PRF tube (Bio-PRF, USA) and immediately centrifuged at 3000 rpm for 10 minutes used (80-1, electric centrifuge, China) (Dohan *et al.*,2006a). After centrifugation, the middle homogenous layer was carefully detached from the inner surface of the PRF tube using a sterile stainless steel (double-ended micro) spatula (Fig.3-2), and then directly applied to the previously created mandibular bone defect.

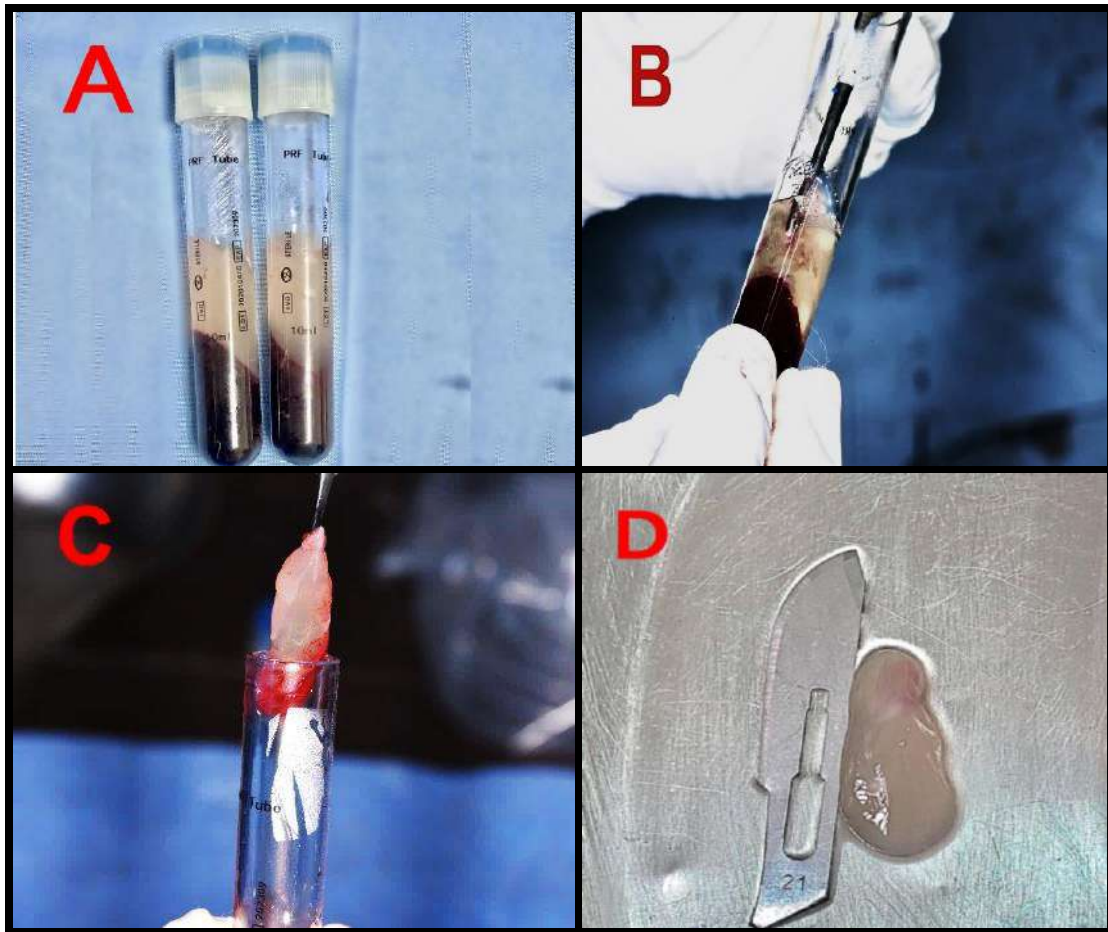


Figure 3-2: Preparation of autologous PRF gel. (A) After centrifugation of the blood sample, the PRF tube. (B) The PRF gel was detached from the inner surface of the PRF tube. (C) Elevated the PRF gel with a stainless-steel spatula. (D) PRF gel before use.

### 3-4: Preparation of quail eggshell calcium hydroxide powder

The calcium hydroxide powder was prepared according to a modified technique described by (Chen *et al.*, 2022). The uncrushed quail eggs were collected from the local farmer in Tikrit City, Iraq. The quail eggshell was cleaned with deionized water and boiled in water for about 30 minutes to remove any debris that may attach to it. The quail shells were ground into a fine powder using an electrical mortar grinder (Retsch, RM200, China), then calcined in a muffled furnace (Prothrom- Turkey) at 1200 °C for 2 hours. In this phase, the quail eggshell's calcium carbonate ( $\text{CaCO}_3$ ) was converted into calcium oxide ( $\text{CaO}$ ), as shown in the



following equation. After that, the (CaO) powder was taken in a beaker and directly dispersed in distilled water. The result of this reaction was a very high liberated temperature with the formation of a white powder (Fig. 3-3), which was a calcium hydroxide  $\text{Ca}(\text{OH})_2$ , as shown in the following equations:

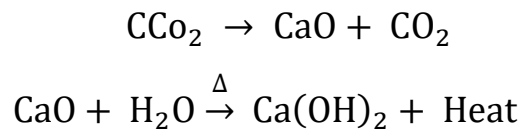


Figure 3-3: A, the quail eggshell before fabrication. B, the fabricated calcium hydroxide powder from the quail eggshell.

### 3-5: Preparation of oyster shell hydroxyapatite powder

The preparation and synthesis method of oyster shell hydroxyapatite powder was done by using a modified procedure described by *Ismail et al.*, 2021). Firstly, the oyster shells (Pectinidae) were purchased from the local market in Basra City, Iraq, and then washed using distilled water. Later, the shells were boiled in a mixture of distilled water and ethanol to remove organic residues and then dried in the oven at 100 °C for 30 h. The dried shells were then ground to a fine powder using an electrical mortar grinder (Retsch, RM200, China). The powder was calcined in a muffled furnace (Prothrom- Turkey) at 1200 C for 2 hours to produce calcium hydroxide powder. Later, an orthophosphoric acid solution (Ridel- Turkey)

with 0.6 M was added to the  $\text{Ca}(\text{OH})_2$  solution to justify the pH of the solution at (8.5) used a pH meter (AD1000-Germany). The white homogenous precipitate was observed at this point. The product was kept at ambient temperature for 48 hours in order to aging, which allowed the complete chemical reaction. The dried precipitation was calcined again at 1200 C for 2 hours in a muffled furnace. The white crystalline powder was produced, indicating the presence of HA crystal powder (Fig.3-4) All the chemical equations were mentioned below:

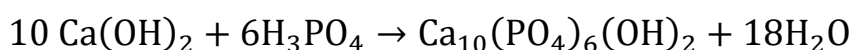
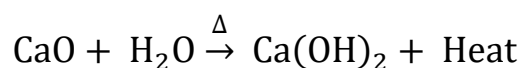


Figure 3-4: A, the oyster's shells before fabrication. B, the fabricated oyster shell hydroxyapatite powder

### 3-6: Evaluations of bone substitute biomaterials

The evaluations of bone substitute biomaterials were done in the nanotechnology laboratories at the Ministry of Science and Technology in Baghdad, Iraq, using the following parameters.

### **3-6-1: X-ray diffractometer (XRD) analysis**

The XRD analyses were performed to determine the crystal phase and purity of quail eggshell calcium hydroxide  $\text{Ca(OH)}_2$  and oyster shell hydroxyapatite powders samples. The XRD data were recorded within the two theta ( $2\theta$ ) range from zero<sup>o</sup> to 80<sup>o</sup>, and intensity counts range from zero to 900<sup>o</sup> used (Malvern Panalytical, Aeris, UK). The XRD data were matched with the standard International Centre for Diffraction Data (ICDD) databases, used Qualx software version (2.24, build data:22.11.18, Italy).

### **3-6-2: Field emission scanning electron microscopy (FESEM)**

The surface morphology is an important characteristic that determines the biological properties of the samples. The surface morphology, crystal size, and porosity of the quail eggshell calcium hydroxide samples, the oyster shell hydroxyapatite, and the autologous PRF samples were detected by the field emission scanning electron microscope (FESEM) model (inspect f 50, fei, Holland). Before electron microscopy, the samples were subjected to a gold covering to give the necessary conductivity.

### **3-6-3: Energy dispersive X-ray Spectrometer (EDS)**

The EDS analysis was used to determine the element's compositions and the relative concentrations of the main trace elements, such as calcium, phosphor, and oxygen, within quail eggshell calcium hydroxide and oyster shell hydroxyapatite powder samples. It is also used to determine the elements distribution mapping to reveal the surface topography of these elements through the use of an energy-dispersive X-ray microanalysis system model (inspect f50, fei, Holland) with an acceleration energy voltage range from zero to 20 keV.

### **3-7: Surgical procedure.**

All dogs were operated under general anaesthesia using a protocol of a mixture containing 10 % ketamine HCL (Alfasan, Holland) and 2% xylazine (Interchemie, Holland) at doses (15 mg/kg) and (5 mg/kg) respectively, through intramuscular injection (Mohammed *et al.*, 2022). Anesthetized animals were restrained on the lateral recumbency with an extension of the neck. The operative region was aseptically prepared, clipping hair with a delicate clipper, and vigorous disinfection was achieved by applying 10% of povidone-iodine solution (Fig3-5). The mouth gag was introduced between the upper and lower canine teeth, and a skin incision approximately five cm in length was performed along the premolar/molar region using surgical scalpels blade size (20), followed by blunt dissection of the deep fascia between the masseter and digastric muscle to expose the mandibular bone (Fig. 3-6). A circular mandibular bone defect experimentally induced with a diameter of (14) mm in diameter made in the of the mandibular body in all experimental animals, through a full-thickness of bone tissue without perforation of the underlying buccal mucosa, using a slow-speed electrical bone drill combined with a cylindrical diamond hole saw (Juster, j3901, China) with continuous irrigation with saline solution to prevent heat damage to the bone tissue (Fig. 3-7).

In the control group, the bone defect was left empty without treatment. In the second group, the defect was filled with fabricated quail eggshell calcium hydroxide  $\text{Ca}(\text{OH})_2$  powder. In the third group, the bone defect was filled with fabricated oyster shell hydroxyapatite powder. In the fourth group, the bone defect was filled with the PRF gel. After that, the muscles were closed by a continuous suture pattern using polyglycolic acid suture materials size 0. The skin was closed by a simple interrupted suture

pattern using silk suture materials size 1. Then, the animals were transferred to an X-ray room to identify the induced mandibular defects' shape and location (Fig.3-8 and 3-9). Finally, during the immediate postoperative period, the animals were transferred to a clean, warm cage for smooth recovery.

### **3-8: Post operative care**

All dogs immediately received postoperative analgesia of Metalgen at a dose of (20mg/kg) through intramuscular injection for five days to relieve the pain. Also, a broad-spectrum systemic antibiotic consisting of a combination of Pencilline-Streptomycine (Penstrep, Alfasan, Holland) intramuscularly injected at the dose of (10,000 IU-15 mg/kg) for seven days, to prevent any postoperative infections. The surgical skin wounds were treated with local wound spray oxytetracycline 2.5% from a distance of (15 – 20) cm, one time a day for seven days following surgery to prevent wound infection. All animals were investigated twice daily during the period of the current study.





Figure 3-5: The site of surgical operation under aseptic surgical technique.

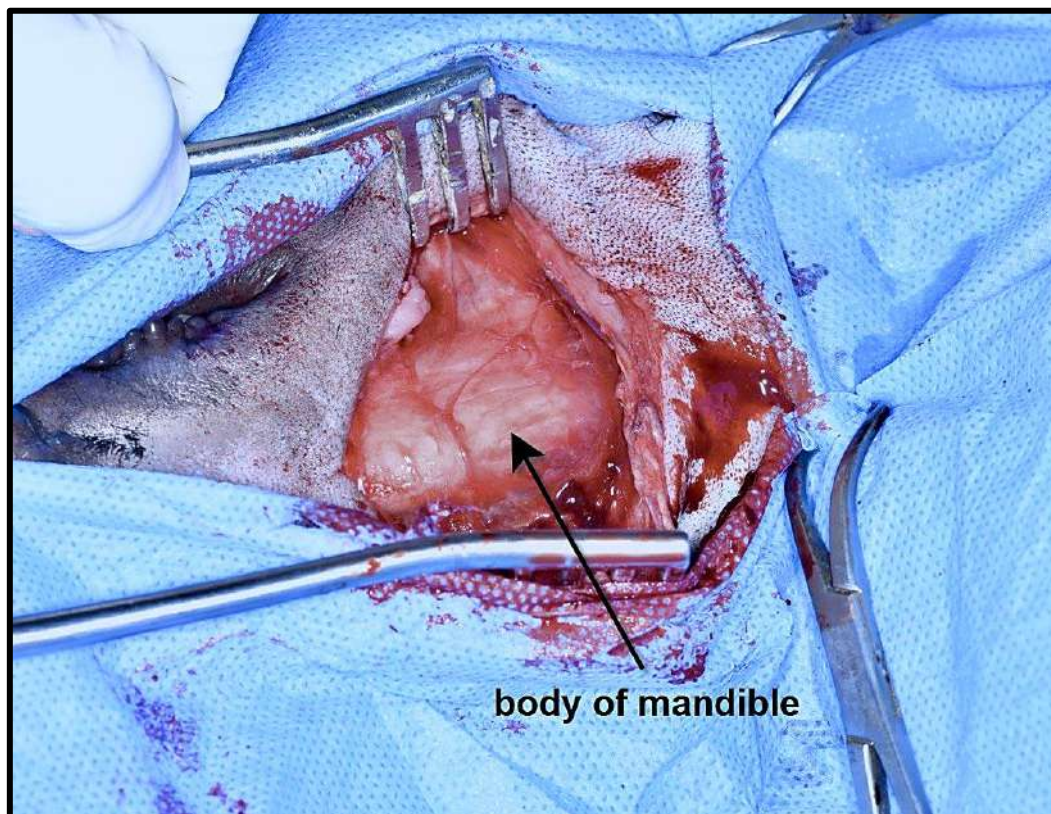


Figure 3-6: The body of the mandibular bone.



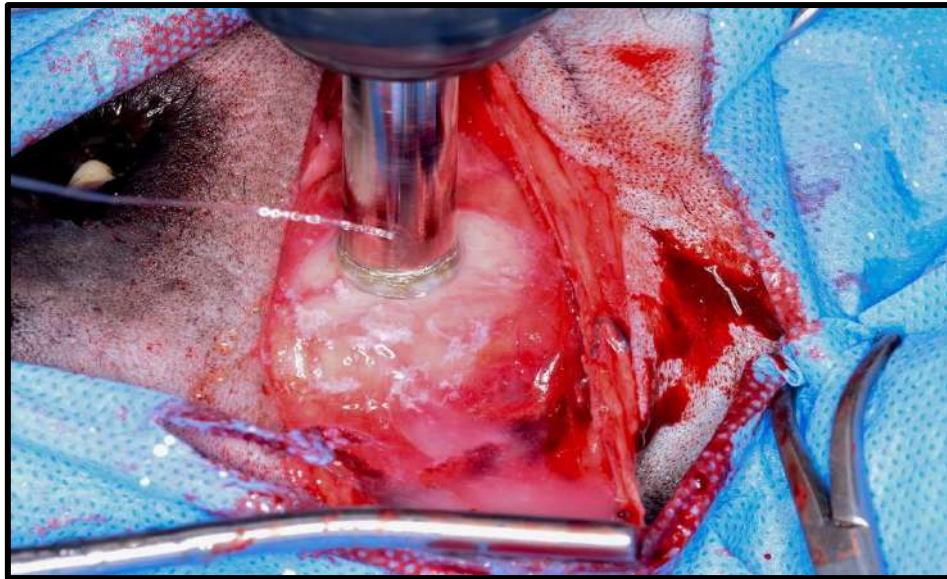


Figure 3-7: A bone defect was surgically created in the body of the mandibular bone using a bone drill square under continuous irrigation of saline solution.



Figure 3-8: the lateral plain radiographic image of the mandibular bone defect immediately after surgery

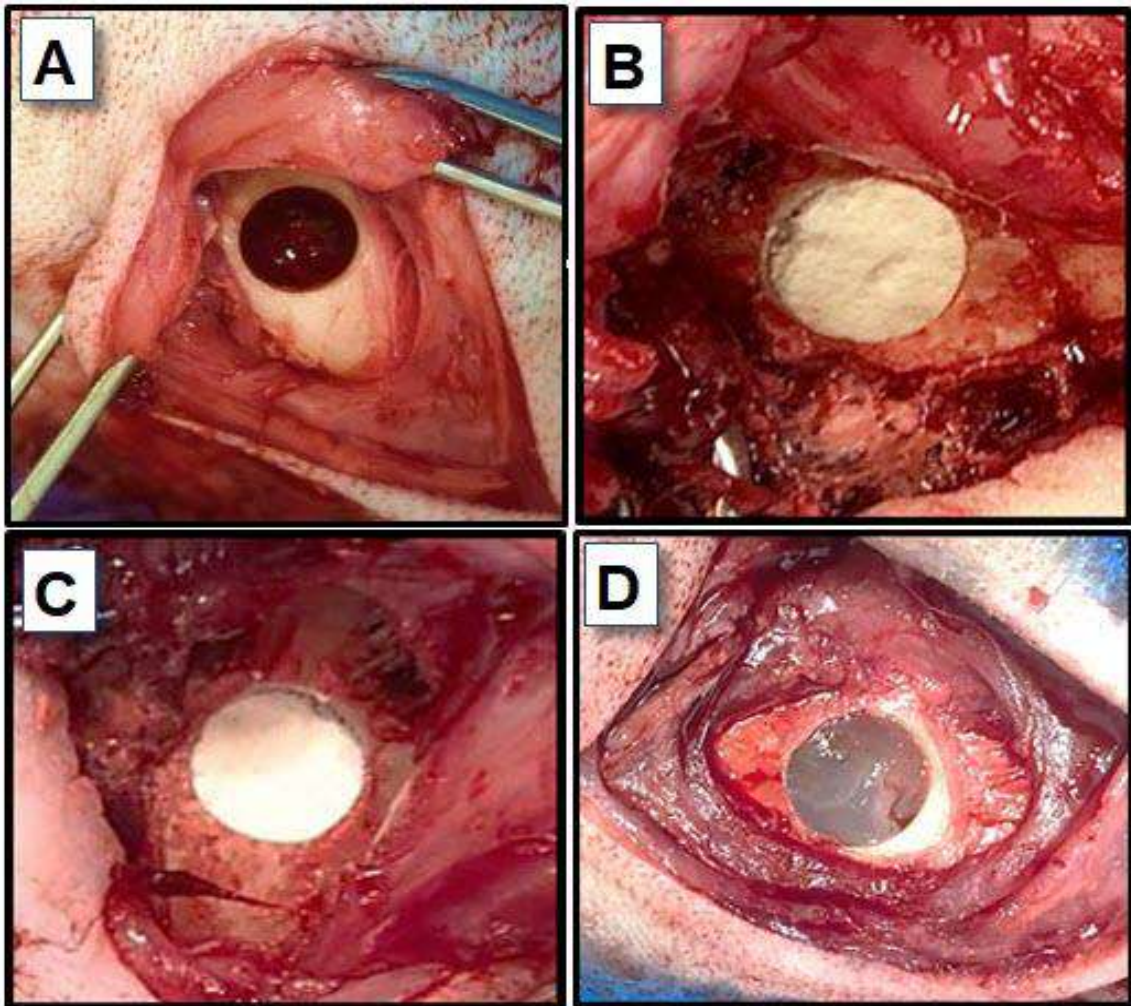


Figure 3-9: The bone defect of the mandibular bone. (A), first group (control). (B), second group (QESCH) powder. (C), third group (OSHA) powder. (D), fourth group (PRF) gel.

### 3-9: Animal Sacrifices

The bone defect biopsies were obtained from the animals at (7,15,30) interval days Ps. The biopsies were obtained by giving the animal general anesthesia. After the skin incision, the subcutaneous tissues muscles were bluntly dissected, followed by applying a bone drill accompanied by a cylindrical diamond hole saw size (4) mm in diameter from the normal and defective area.



### **3-10: Evaluations of the results**

The results of the study were evaluated clinically, macroscopically, radiologically, histopathologically, and immunohistochemically with field emission scanning electron microscopy during the experiment period.

#### **3-10-1: Clinical evaluations**

In all experimental animal groups, the animals were examined twice daily during the first week after surgery for any signs of pain and the presence of abnormal eating habits or excessive salivation.

#### **3-10-2: Macroscopical evaluation**

The biopsy samples of the mandibular bone defect were macroscopically evaluated in all experimental animals at (7,15 and 30) days PS used a Canon digital camera (EOS,70D, China) to inspect the reduction in the size of the mandibular bone defect. In addition, inspect the site of operation after repair by filling it with biomaterials.

#### **3-10-3: Radiographical evaluation**

The lateral view of the skull was taken in the radiological room at the veterinary university hospital immediately post operation, and then at (15,30,60) intervals days post-surgery used a plain X-ray machine (Shimadzu, Japan) accompanied by the digital wireless detector (Italray, Italia) with exposure factors seated at 65 kV and 2.5 mAs, and 90 cm F.F.D. to investigate the bone defects.

#### **3-10-4: Histopathological evaluation**

Bone biopsies were collected aseptically at (7, 15, 30) days after surgeries from all groups. The samples were fixed in a fixing agent with 10% neutral buffer formalin (NBF) for 48 hr. to preserve the tissue. Later, decalcification was done to remove calcium salt and minerals from the bone tissue using ethylenediamine tetraacetate acid (EDTA) solution for 12 weeks, which was refreshed every week. In this stage, EDTA was used

at a concentration of 10% by dissolving 10 grams of this substance in 100 milliliters of distilled water. The final solution was added to the bone sample, and this solution was replaced daily until the calcium removal process was completed (Yang *et al.*, 2021). Once the tissue becomes easily perforated or cut with a needle, it was deemed that the decalcification process was complete. Dehydration, clearing, infiltration, and embedding were the additional steps in processing the decalcified tissue until a firm paraffin block containing the tissue was achieved.

Then, the samples were cut into 5  $\mu\text{m}$  thick sections using a standard rotary microtome from (Leica Microsystems, Germany). After that, they were stained using standard stains of hematoxylin and eosin. Finally, the slide was examined under a light microscope from (AX80T, Olympus, Japan). Also, the bone healing process and new bone formation at the site of bone defects were evaluated as a semiquantitative analysis through the use of histopathological healing score according to the modify (Lucaciu *et al.*, 2015) score that is shown in (Table 3-1).

Table 3-1: The histopathological indices and scores according to modify (Lucaciu *et al.*, 2015).

Index Name	Score level	Description	Index Name	Score level	Description
<b>1.Osteoblasts</b>	0	Absent	<b>7.Bone trabeculae</b>	0	Absent
	1	Present at periphery		1	Present at periphery
	2	Present centrally		2	Present centrally
	3	Present centrally and at the periphery		3	Present centrally and at the periphery
<b>2.Osteocytes</b>	0	Absent	<b>8. Inflammation</b>	0	Present
	1	Present at periphery		1	Absent
	2	Present centrally			
	3	Present centrally and at the periphery			
<b>3.Osteoclasts</b>	0	Absent	<b>9. Granulation tissue</b>	0	Present
	1	Present at periphery		1	Absent
	2	Present centrally			
	3	Present centrally and at the periphery			
<b>5.Mature bone</b>	0	Absent	<b>10. New formation of blood vessels</b>	1	Absent
	1	Present at periphery		2	Present at periphery
	2	Present centrally		3	Present centrally
	3	Present centrally and at the periphery		4	Present centrally and at the periphery
<b>6.Bone bridge</b>	0	Absent			
	1	Narrow			
	2	Thick			

### **3-10-5: Immunohistochemistry (IHC) evaluation**

Immunohistochemistry was achieved at 30 days after surgeries using a modified avidin-biotin immunoperoxidase technique (Hsu *et al.*, 1981). The tissue sections underwent deparaffinization, rehydration, and deactivation, then introduced into the immunohistochemistry protocol. Endogenous peroxidase was blocked by a mixture of 3% hydrogen peroxide-methanol solution for 7 minutes at ambient temperature. After washing with PBS containing 0.01% thiomersal and 50% glycerol at pH 7.3, the sample was blocked with 10% normal goat serum for 30 minutes at ambient temperature. Then, the slides were incubated with primary antibodies for Alkaline Phosphatase (E-AB-93077, Elabscience, USA) which is a rabbit Polyclonal antibody at dilution equal to 1:100 at 4 C° for 24 hr. followed by double times washing of slides with PBS for three minutes., then incubated with polyperoxidase anti-rabbit IgG as a secondary antibody with a dilution of 1:400 (Wuhan Fine Biotech, China) for 30 minutes at room temperature, and finally rewashed with PBS.

Then, the stain was performed using the DAB substrate. Later, all slides were allowed to be counterstained the nuclei with hematoxylin for 30 seconds at room temperature, rinsed with distal water, then dehydrated, and covered with a cover slide. All slides were observed using a light microscope (Leica, USA) and photographed with a digital video camera (Leica ICC50, Leica, USA) in a standardized light condition. The results of ALK expression were classified into four categories based on the intensity of staining. The interpretation was made by the expert pathologist who used the modified method described by (Cha *et al.* 2021). The categories of expression were weak positive, mild positive, moderate positive, and high positive.

### **3-11: Statistical analysis**

Statistical analysis was performed through the complete random design (CRD) used SAS software version 9.4 (2002). All quantitative data are expressed as the mean  $\pm$  standard error ( $M \pm SE$ ). Statistical comparison between the experimental groups was performed using Duncan's test. A probability of 0.05 or less ( $p \leq 0.05$ ) was considered significant.

## Chapter four

### Results

#### 4-1: Evaluation of quail eggshell calcium hydroxide powder.

##### 4-1-1: X-ray diffraction (XRD).

The results of XRD patterns of the prepared quail eggshell  $\text{Ca}(\text{OH})_2$  powder sample revealed that the typical intense peaks were in the two theta ( $2\theta$ ) range from zero to 80. The main diffraction peaks that contain the calcium hydroxide phase observed at ( $7.88^\circ$ ,  $18.08^\circ$ ,  $18.15^\circ$ ,  $28.78^\circ$ ,  $34.21^\circ$ ,  $47.26^\circ$ ,  $50.90^\circ$ ,  $54.47^\circ$ , and  $62.70^\circ$ ) respectively, and associated with the hexagonal crystalline shape of the calcium hydroxide powder fabricated from the quail eggshell. All these peaks were matched with the standard International Center for Diffraction Data (ICDD) database card number (00-100-0045) (Fig.4-1).

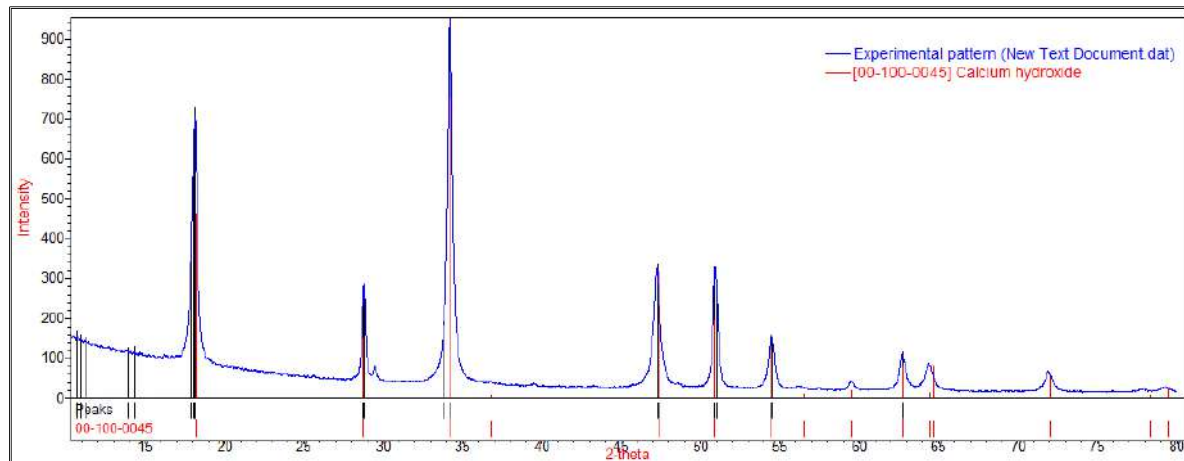


Figure 4-1: The XRD patterns of blue color indicate the fabricated quail eggshell  $\text{Ca}(\text{OH})_2$  sample, matching with ICDD reference card number: (00-100-0045) red color.

##### 4-1-2: Field emission scanning electron microscope (FESEM).

The FESEM images of the quail eggshell  $\text{Ca}(\text{OH})_2$  powder sample indicated that the surface morphology appears as spongy morphology with particles appearing as polygons but with no uniform shape, and these

particles are observed to be agglomerated. Some crystals grow as flower petals around the central point and sometimes appear in a hexagonal shape (Fig. 4-2).

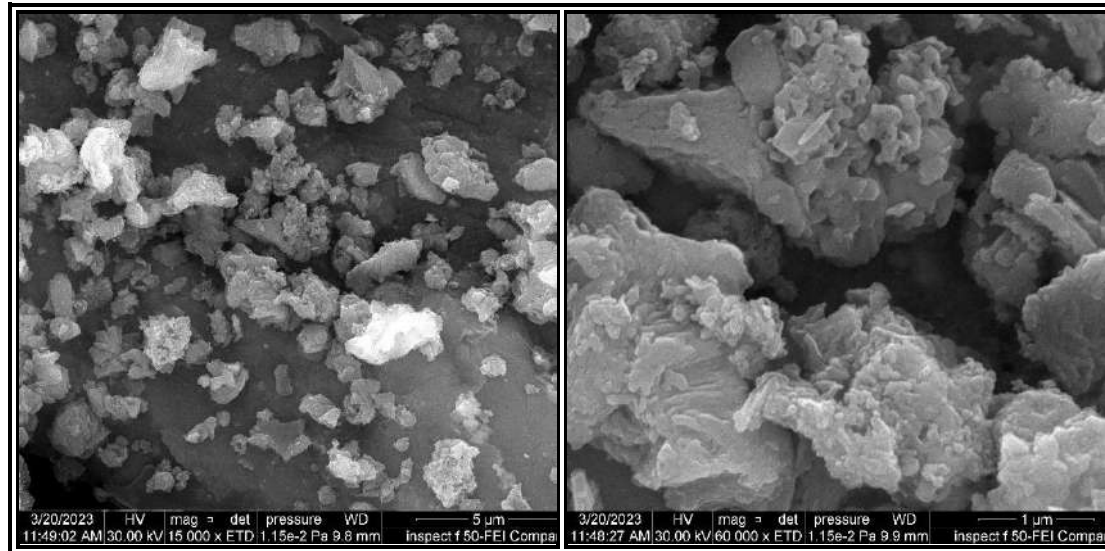


Figure 4-2: The FESEM image of the fabricated quail eggshell  $\text{Ca(OH)}_2$  powder obtained at the calcination temperature  $1200^\circ\text{C}$  for 2hr, used magnification 15000X and 6000X.

#### 4-1-3: Energy Dispersive X-ray (EDS) Spectrometer

The EDS spectrum of the fabricated quail eggshell  $\text{Ca(OH)}_2$  powder sample shown in (Fig.4-3). The main peak values reveal the presence of calcium (Ca) and oxygen (O) elements. The quantity values of these elements measured in atomic and weight (%) were listed in (Table 4-1). The EDS elemental mapping indicated that the particles contained calcium, carbon, and oxygen, as shown in (Fig. 4-4). The EDS mapping analysis appeared green, yellow, purple, and blue, indicating the distribution of calcium, oxygen, carbon, and aluminium particles, respectively.

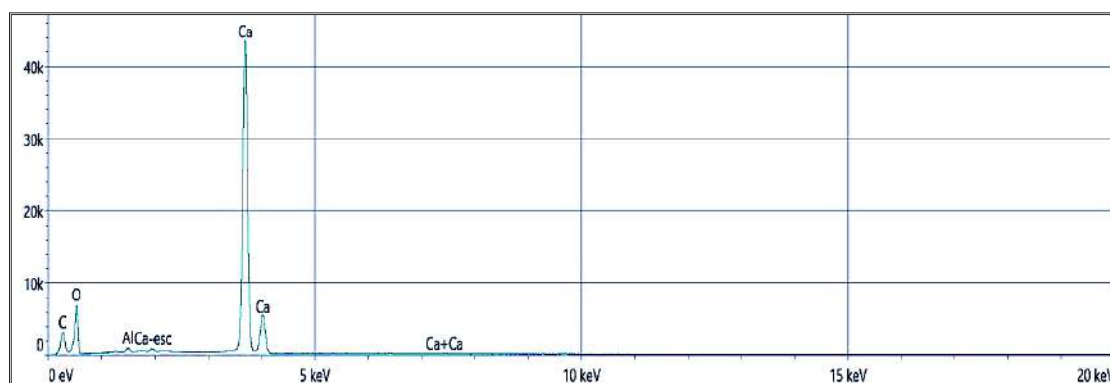


Figure 4-3: The EDS spectrum peaks of the fabricated quail eggshell  $\text{Ca(OH)}_2$  powder sample showed the elemental compositions of the prepared powder sample.

Table 4-1: The contents values of the prepared quail eggshell  $\text{Ca(OH)}_2$  powder sample.

Elements	Weight %	Atomic %
Ca	44.5	23.4
O	46.4	61.2
C	8.5	15.0
Al	0.5	0.4

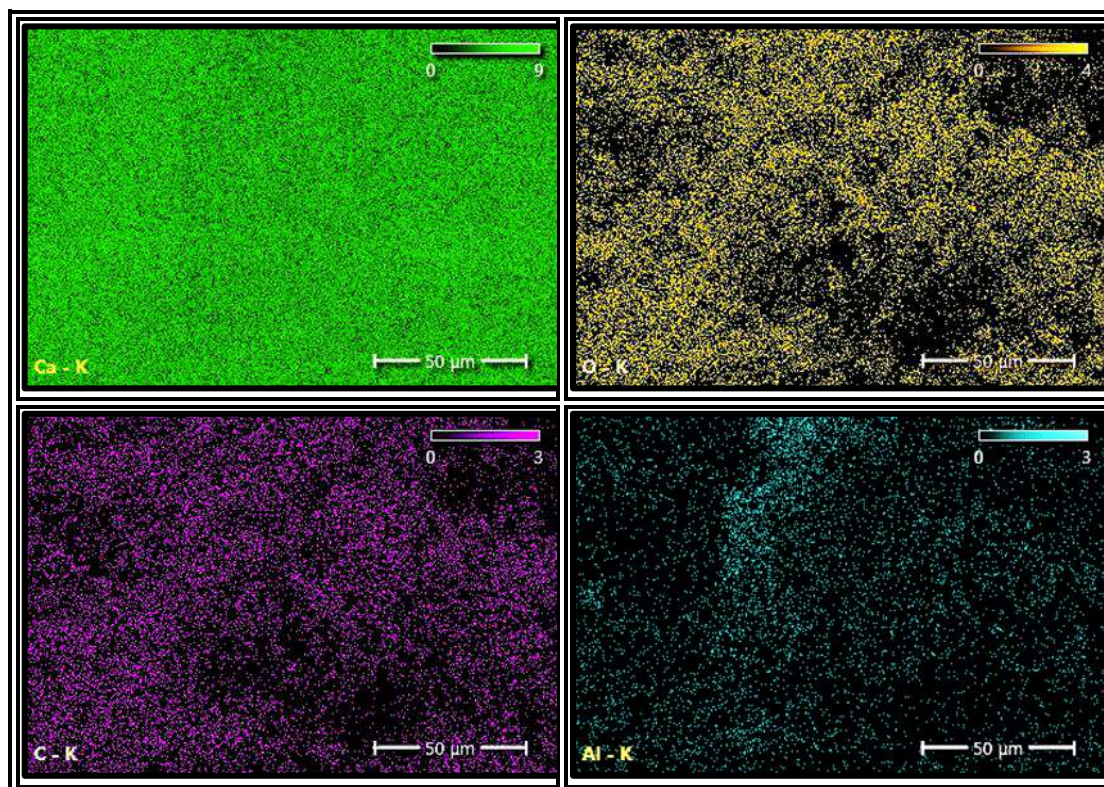


Figure 4-4: The EDS elemental mapping analysis of the fabricated quail eggshell  $\text{Ca(OH)}_2$  powder sample.



## 4-2: Evaluations of oyster shell hydroxyapatite.

### 4-2-1: X-ray diffraction (XRD).

The results of XRD patterns of the fabricated oyster shell hydroxyapatite powder sample revealed that the typical intense peaks of the hydroxyapatite were detected with high crystallinity at two theta ( $2\theta$ ) range from zero to 90. The main diffraction peaks that represented the HA phase were observed at ( $25.46^\circ$ ,  $28.85^\circ$ ,  $31.74^\circ$ ,  $32.75^\circ$ ,  $39.80^\circ$ ,  $46.44^\circ$ ,  $49.11^\circ$ ,  $52.98^\circ$ , and  $76.51^\circ$ ) respectively associated with the hexagonal crystalline shape of hydroxyapatite. All these peaks were matched with the standard ICDD database card number (09-0432) (Fig. 4-5).

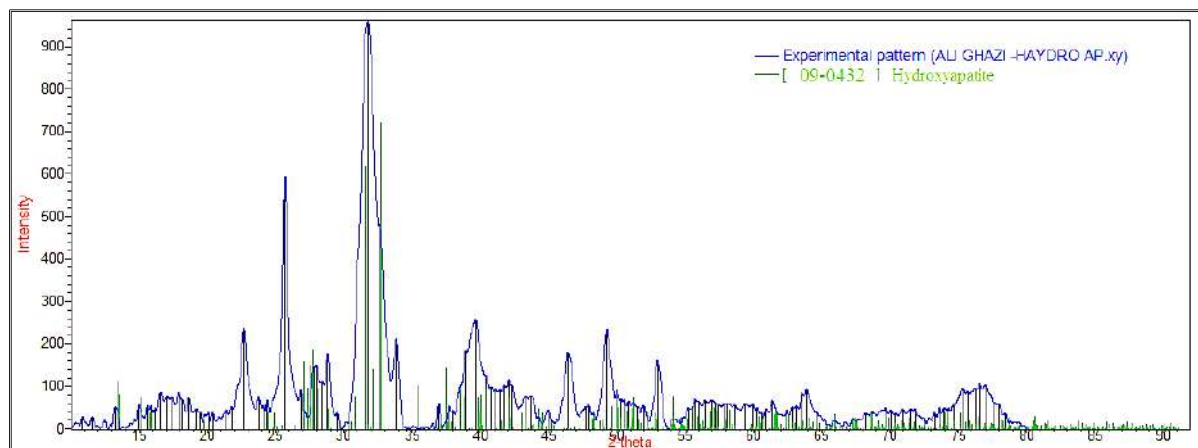


Figure 4-5: The XRD peaks patterns, in blue color, indicate that the fabricated oyster shell hydroxyapatite powder sample matches with the ICDD reference card number (09-0432) green in color.

### 4-2-2: Field emission scanning electron microscope (FESEM).

The surface morphology of oyster shell hydroxyapatite powder sample heated at  $1200^\circ\text{C}$  for 2h. appear as a spherical particle shape that was regularly distributed within the sample with an average diameter of  $(140)\mu\text{m}$  (Fig. 4-6).

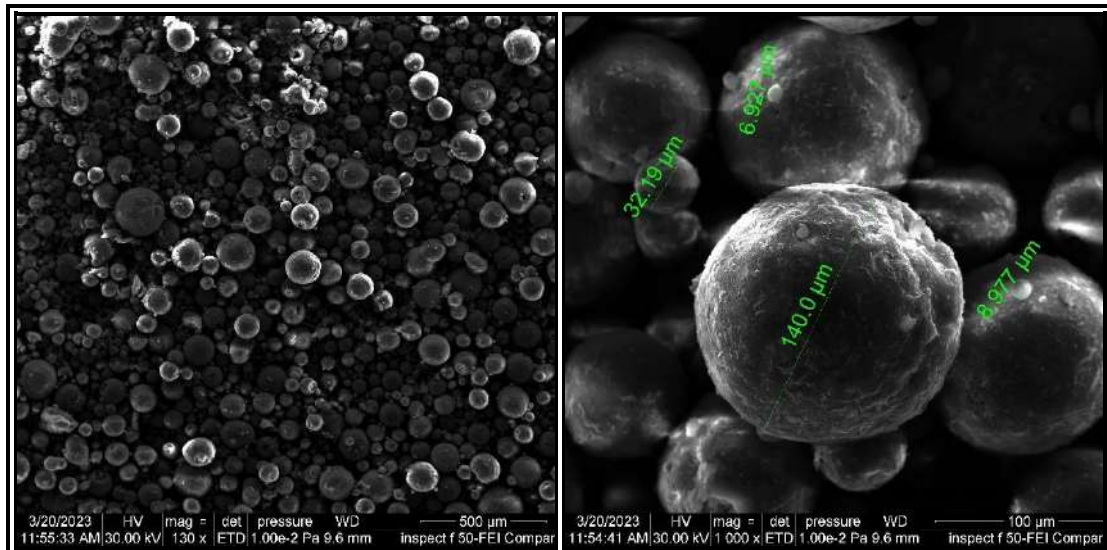


Figure 4-6: FESEM images of the fabricated oyster shell hydroxyapatite were obtained at the calcination temperature of 1200°C for 2h at magnification 130X and 1000X.

#### 4-2-3: Energy Dispersive X-ray (EDS) Spectrometer

The EDS spectrum of the fabricated oyster shell powder shown in (Fig. 4-7) the main peak values reveal the presence of calcium (Ca), phosphor (P), oxygen (O), carbon (C), and potassium (K) elements. The quantity values of these elements measured in atomic and weight (%) were listed in (Table 4-2). The EDS elemental mapping of fabricated oyster shell hydroxyapatite powder sample shown in (Fig. 4-8) were green, blue, purple, and yellow colors, indicating the surface morphology of distributed particles of the calcium, phosphor, carbon, and oxygen, respectively.

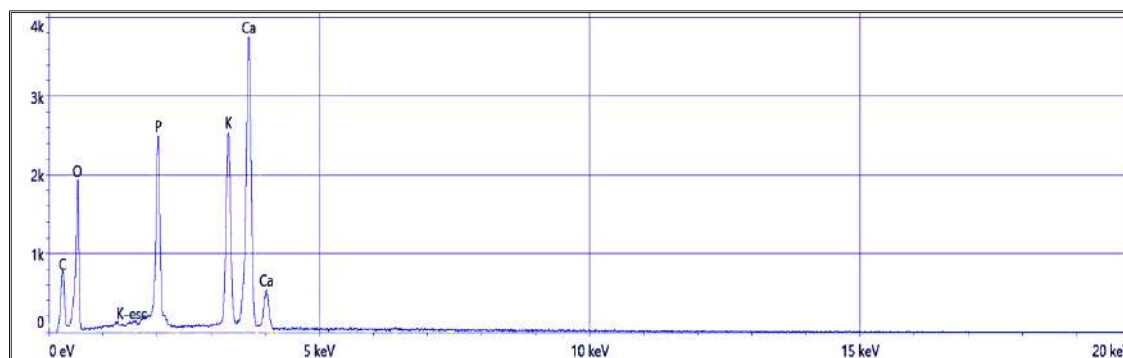


Figure 4-7: The EDS spectrum analysis of fabricated oyster shell hydroxyapatite powder sample.

Table 4-2: The content values of the prepared oyster shell hydroxyapatite powder sample.

Element	Weight %	Atomic %
C	13.4	21.5
O	49.2	59.3
P	8.0	5.0
K	10.2	5.0
Ca	19.2	9.2

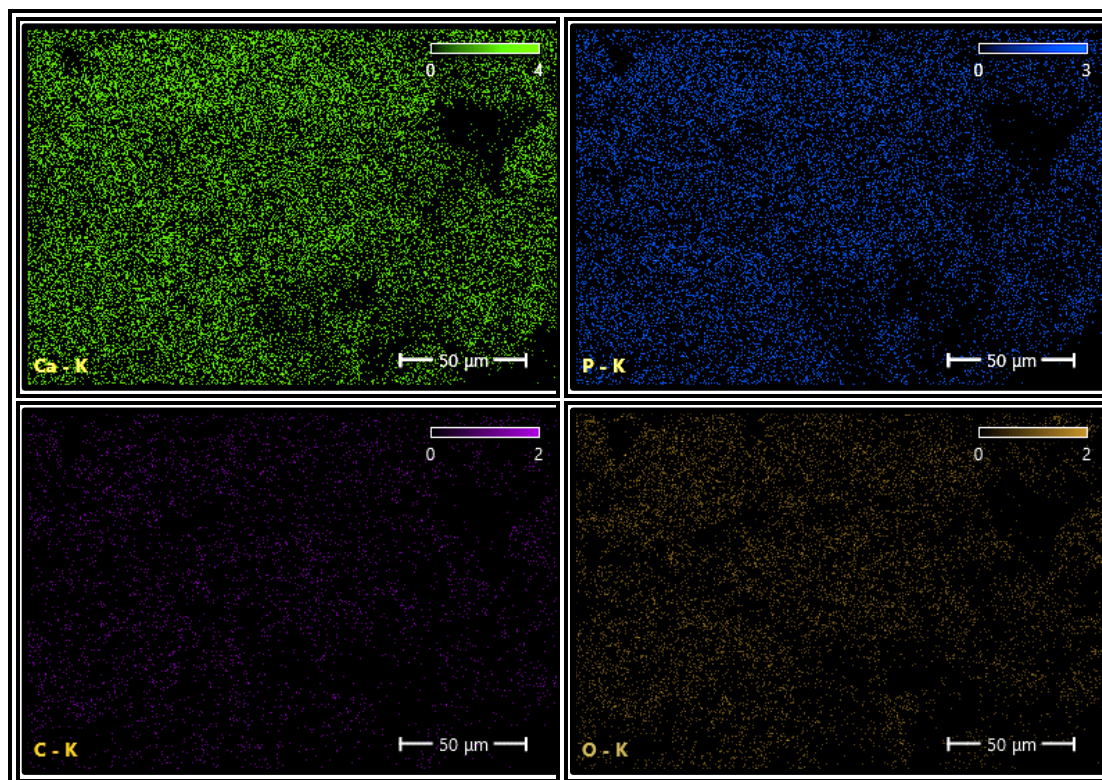


Figure 4-8: The EDS elemental mapping analysis of the fabricated oyster shell hydroxyapatite powder sample.

### **4-3: FESEM of autologous PRF sample.**

The FESEM image of the autologous PRF sample showed the surface morphology of the sample, which appears as acellular dense, smooth, homogenous surface morphology with a swirl-like appearance and without any porosity (Fig. 4-9).

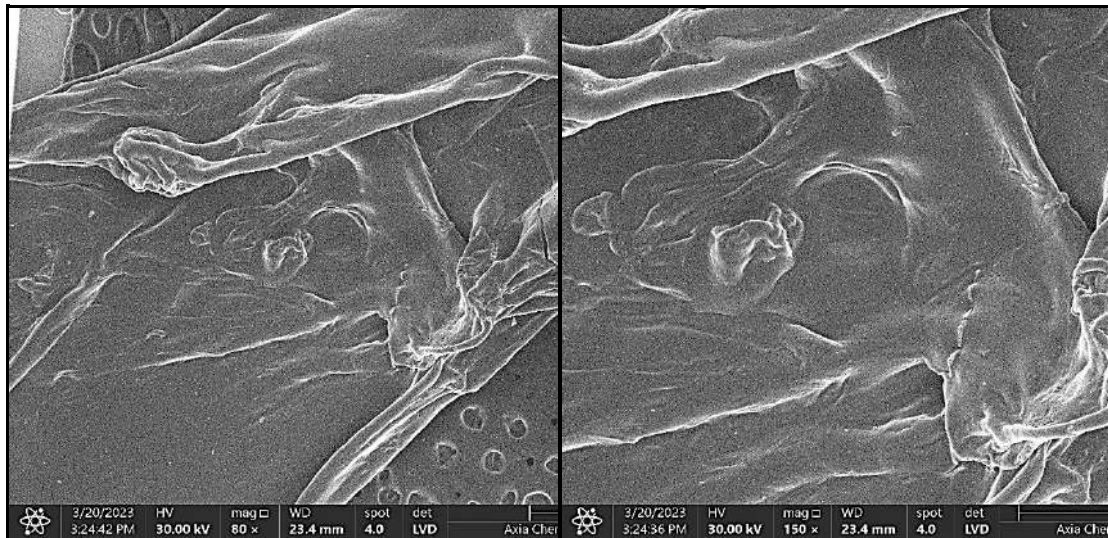


Figure 4-9: The FESEM images of the prepared autologous PRF gel sample at magnification 80X and 150X.

### **4-4: FESEM of mandibular bone defect samples after 30 days post-surgery.**

The FESEM images of the bone defect of the mandible bone samples were obtained at 30 days post-surgery, as shown in (Fig. 4-10). In the control group, the bone defect appeared partially open. The center of the bone defect was filled with a homogenous, smooth matrix surrounded by multiple aggregates of fibrous tissues, which was the predominant tissue (Fig. 4-10, A).

In the second group, the bone defect was filled with an unmineralized matrix surrounded by a thin layer of a mineralized matrix that appeared to be light in appearance (Fig. 4-10, B).



In the third group, the bone defect appears filled with a thick layer of osteoid matrix, which appears as a light region beyond many excavations of bone trabeculae that faces toward the center of the bone defect (Fig. 4-10, C).

In the fourth group, the bone defect appears completely closed and the center of the defect was filled with a thick layer of osteoid matrix, which appears brighter in color. The bone defect was surrounded by thin layers of newly formed bone crystal plates (Fig. 4-10, D).

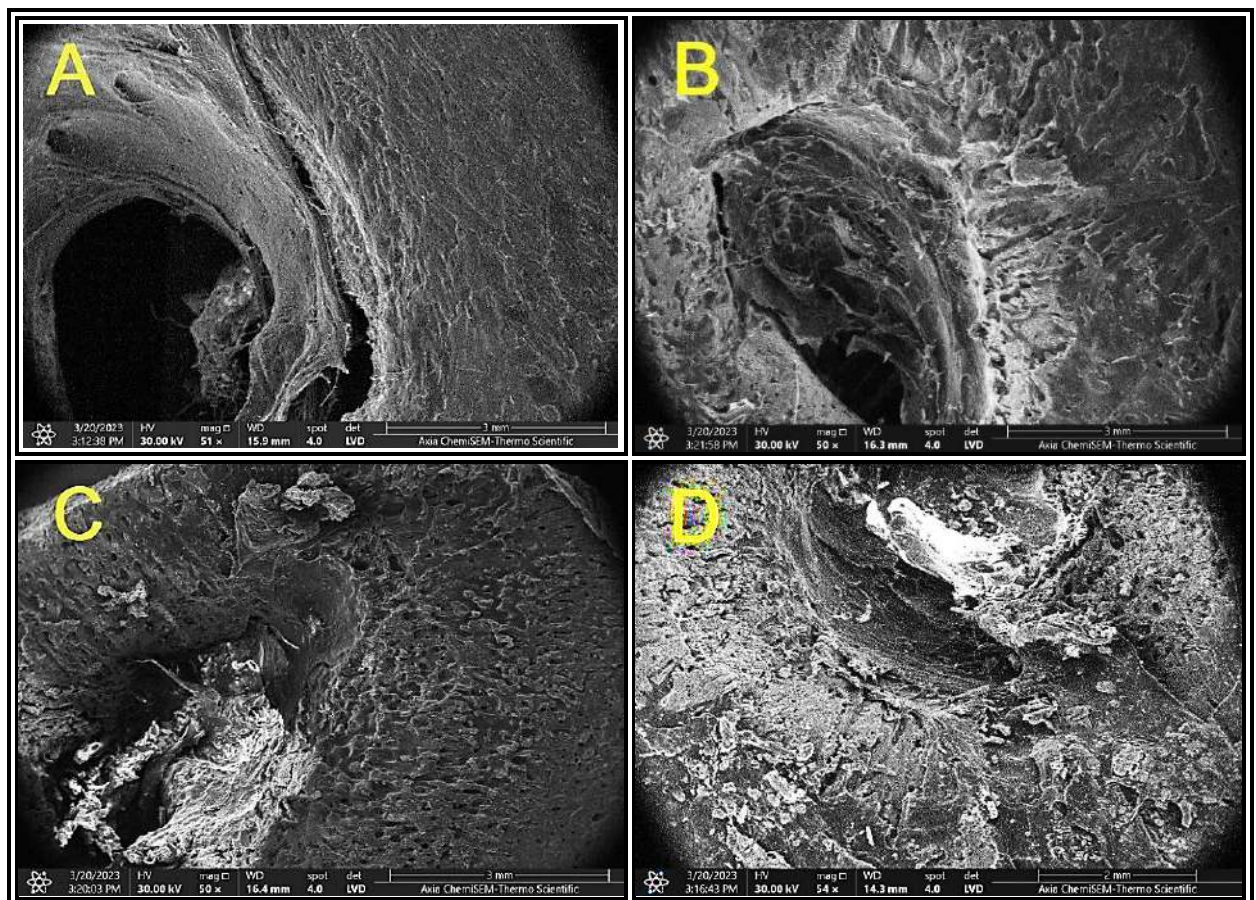


Figure 4-10: The FESEM images show the defective area of mandibular bone defects obtained at 30 days post-surgery, using magnification 50X. A, control group. B, second group. C, third group. D, fourth group.

#### **4-5: Clinical evaluations**

The experimental animals in all groups recovered well from the surgical procedures during the first week after surgery. the site of wounds in all animals was healed by the first intention within 10-15 days after the operation. Also, during the first three days post-surgery, all animals showed varying degrees of food and water intake ability with tenderness to the site of bone defect, especially in the first group. Then, the animals returned to the normal food intake without the appearance of any complications.

#### **4-6: Macroscopical evaluations**

The macroscopical appearance of the mandibular bone defect was evaluated before gently dissecting the bone samples for histopathological examinations. The macroscopical findings at seven days after surgery. In the first group, the bone defect appeared as a circular defect with well-defined defect margins and was filled with tiny tissue without a reduction in the size of the defect. In the second, third, and fourth groups, the bone defects appeared congested and slightly reduced in size with the presence of new soft tissue formation when applying pressure by a stainless-steel pointed needle. (Fig.4-11).

At 15 days after surgery, in the first group, the bone defect was filled with excessive tissue formation without reduction in its size. While in the second, third, and fourth groups, the bone defect revealed varying degrees of size reduction, with the presence of a small amount of semi-firm tissues that had variable consistency when applying pressure by a stainless-steel pointed needle within the defective area and the defective margins started becoming rounded and facing toward the center of the defect (Fig. 4-12).

At the 30 days after surgery. In the first group, there was a continuous presence of soft tissue formation that easily perforated by applying a

stainless-steel pointed needle, and the size of the defect likely appeared to be the same diameter as it appeared in seven and 15 days. In the second, third, and fourth groups, the size of bone defects decreased in size obviously, especially in the third and fourth groups. Also, there were varying degrees of hardness tissues within the center of the bone defect that appeared difficult to penetrate when applying a stainless-steel pointed needle, and the margins of the defects became more rounded and facing toward the center of the defect (Fig. 4-13).

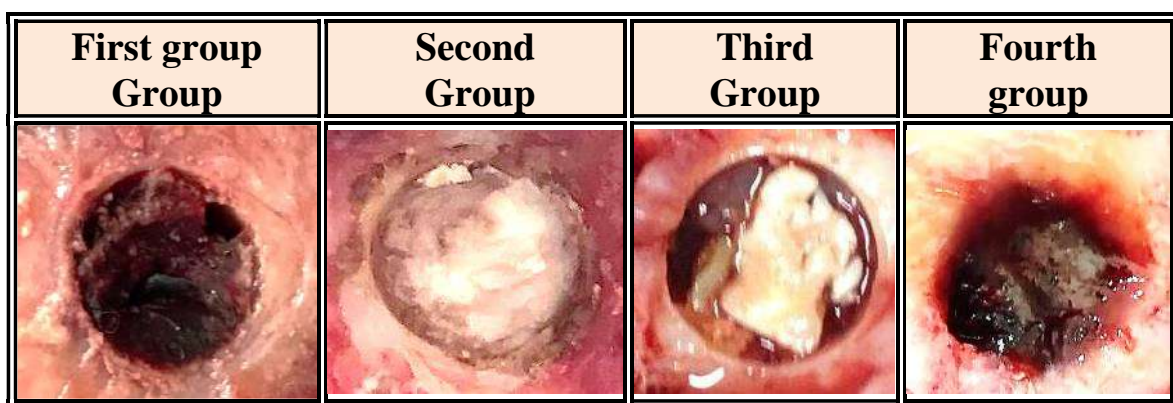


Figure 4-11: The macroscopical findings of the mandibular bone defect defects in different groups at seven days post-surgery.



Figure 4-12: The macroscopical findings of the mandibular bone defect defects in different groups at 15 days post-surgery.

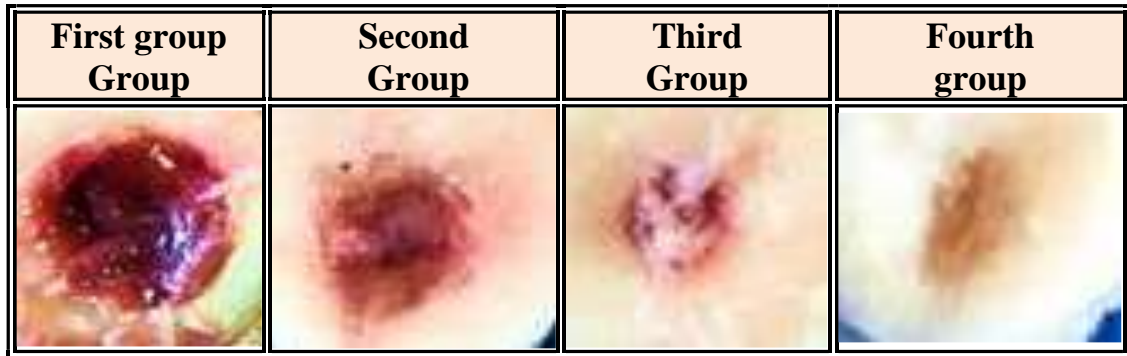


Figure 4-13: The macroscopical findings of the mandibular bone defect defects in different groups at 30 days post-surgery.

#### **4-7: Radiographical evaluations.**

##### **4-7-1: Radiography of the first group.**

The radiographic findings of the mandibular bone defect in the first group on day 15 post-surgery appeared to be a well-defined circular radiolucent bone defect with a relatively very slight increase in opacity, which exhibited in the center of the defective area that represented early little bone tissue formation, but without any trabecular bridging (Fig.4-14). Whereas at 30 days post-surgery, the defective area clearly outlined indicated a tiny radiopaque area related to the bone tissue formation that occurred in the center of the defect (Fig. 4-15). Finally, at 60 days post-surgery, the radiographical finding showed that the bone defect margin remained radiographically outlined. The defect was still open and radiolucent and showed a slightly radiopaque zone extended from the edges of the bone defect towards the center, which represents a new callus formation without a complete trabecular bridging (Fig. 4-16).



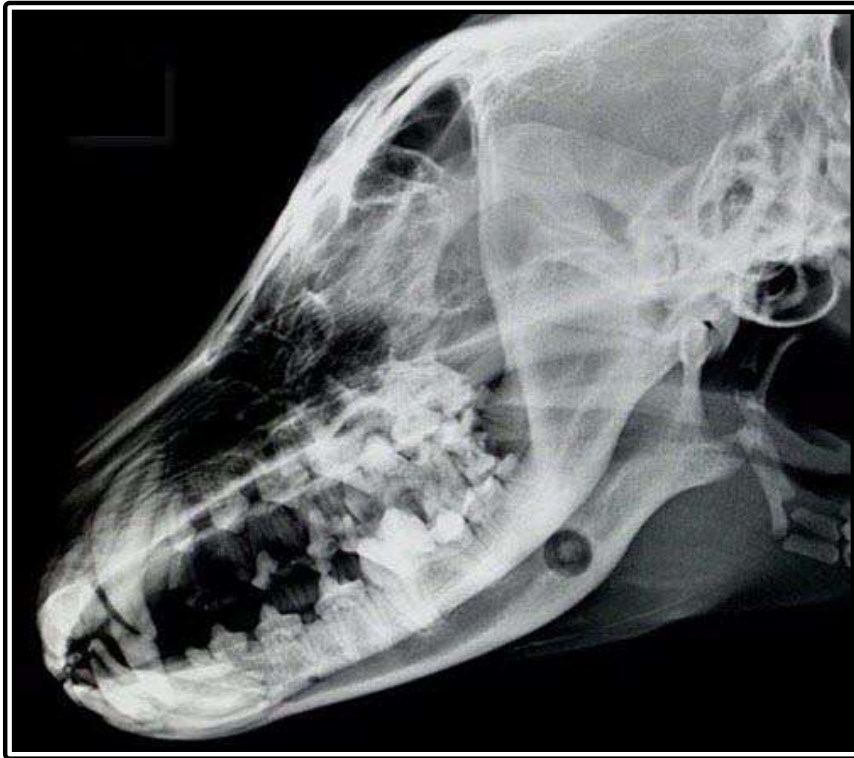


Figure 4-14: A lateral radiographical image of the first group at 15 days PS.



Figure 4-15: A lateral radiographical image of the first group at 30 days PS.



Figure 4-16: A lateral radiographical image of the first group at 60 days PS.

#### **4-7-2: Radiography of the second group.**

In the second group, at 15 days after the operation, the radiographic findings that the surrounding margins of the defective area of the mandibular bone clearly outline with a slightly blurry area in the center of the defect indicated the new bone tissue formation representing early callus formation. However, it is still radiolucent (Fig. 4-17). At 30 days post-surgery, the defect bone defect of the mandibular bone appeared to reduce in size as well as regression in its radiolucency, and its margins appeared irregularly outlined, with relatively increased density observed throughout the defect, representing a developing callus (Fig.4-18). At 60 days post-surgery, the defective site of the mandibular bone showed nearly a complete opacification of the bone defect, representing a maturing callus with increased opacity and slightly complete trabecular bridging (Fig. 4-19).

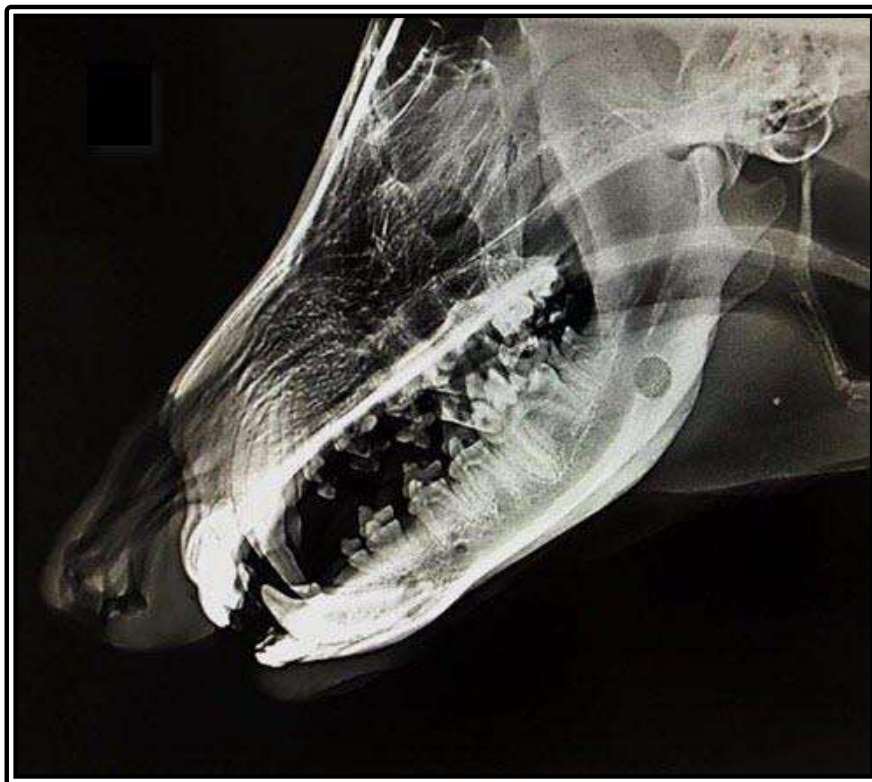


Figure 4-17: A lateral radiographical image of the second group at 15 days PS.



Figure 4-18: A lateral radiographical image of the second group at 30 days PS.



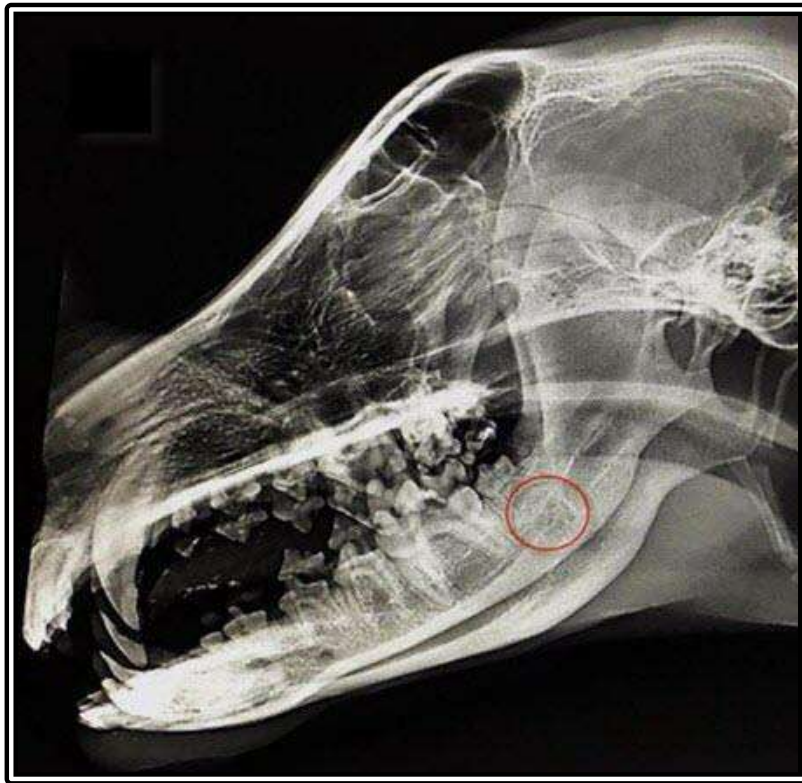


Figure 4-19: A lateral radiographical image of the second group at 60 days PS.

#### **4-7-3: Radiography of the third group.**

The radiographical finding in the third group at 15 days after the operation, the bone defect shows a well-defined, circular bone defect, and its margin is clearly outlined. The center of the defect becomes blurry in appearance, with a relative increase in the opacity seen throughout the defect, representing early callus formation (Fig. 4-20). At 30 days post-surgery, the defect bone defect of the mandibular bone reduced in size and exhibited a slightly definite circular defect size as compared with the control group. Also, a slight radiopaque area appeared throughout the center of the defect related to the progressive bone formation (Fig. 4-21). At 60 days after the operation, the radiographical findings showed a partially defined semicircular, slightly translucent bone defect area with a relative increase in opacity seen throughout the center of the defect, representing the maturing callus formation (Fig. 4-22).



Figure 4-20: A lateral radiographical image of the third group at 15 days PS.



Figure 4-21: A lateral radiographical image of the third group at 30 days PS.

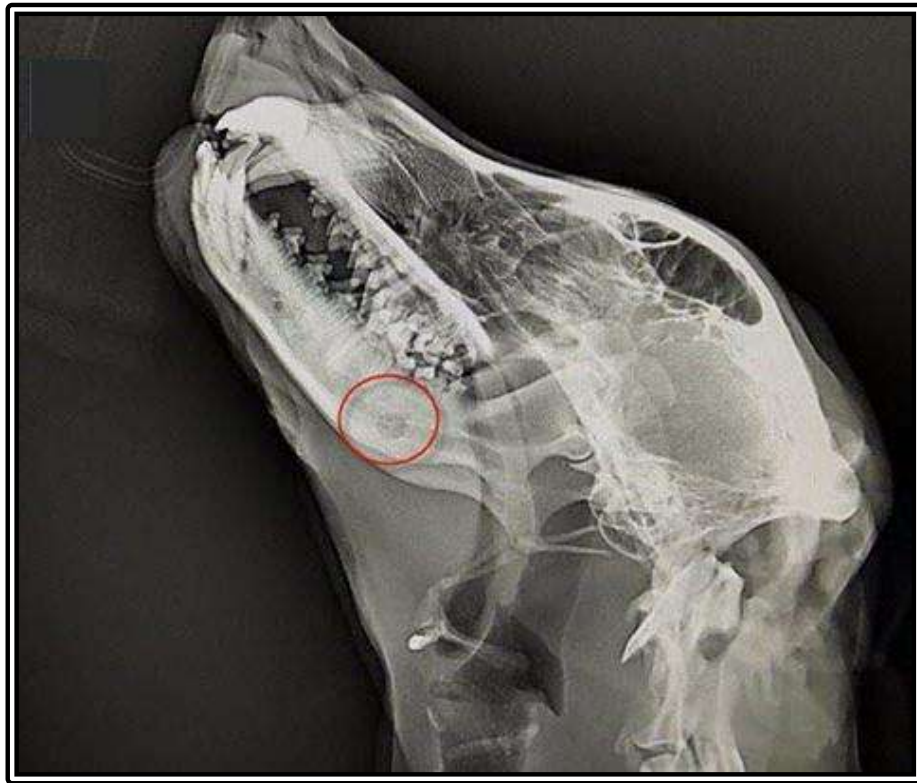


Figure 4-22: A lateral radiographical image of the third group at 60 days PS.

#### **4-7-4: Radiography of the fourth group.**

The radiographical finding of the fourth group at 15 days after the operation, the radiographical findings showed a considerable increase in opacity throughout the defect, which became blurry in appearance, representing a new callus formation (Fig.4-23). At 30 days post-surgery, the defect bone defect of the mandibular bone was reduced in size as compared with the control group and became semicircular. It looked like a small elongated and slightly increased opacity of the defect, an opacification seen throughout the defect that represents the early maturing callus (Fig.4-24). At 60 days post-surgery, the defective area disappearance (complete opacification) of the bone defect represents a mature callus formation and complete trabecular bridging (Fig. 4-25).





Figure 4-23: A lateral radiographical image of the fourth group at 15 days PS.



Figure 4-24: A lateral radiographical image of the fourth group at 30 days PS.

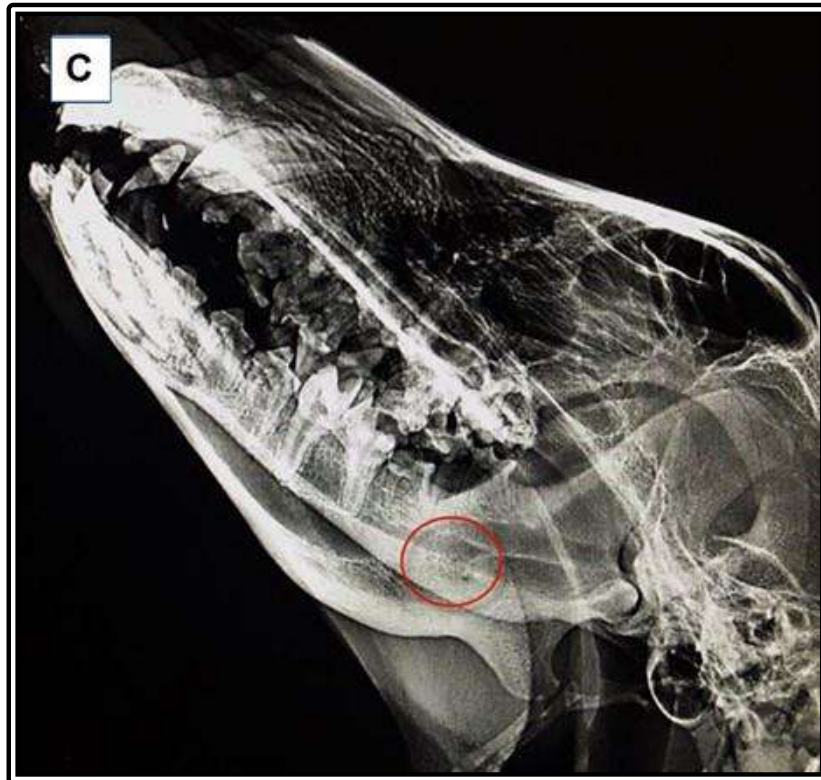


Figure 4-25: A lateral radiographical image of the fourth group at 60 days PS.

## **4-8: Histopathological evaluations**

### **4-8-1: Histopathological evaluation of the first group**

The histological section of the mandible bone in the control group at seven days Ps. showed the site of the defect hole was composed of blood clots, surrounded by a large area of granulation tissue, which clearly separated from the edge of the normal mandible bone (Fig.4-26). At 15 days after surgery, the histological section showed the site of a hole with hemorrhagic clot, with highly granulation tissue formation and new woven bone with newly formed blood vessels (Fig. 4-27). At 30 days after surgery, the histological sections of the mandible bone showed the site of a bone hole greatly filled with mature connective tissue that was rich in vascularity, and also the presence of a small area of newly formed woven bone that surrounded the edge of the mandible bone (Fig. 4-28).



#### **4-8-2: Histopathological evaluation of the second group**

The histological section of the mandible bone of the second group at seven days after surgery showed the site of a hole appeared surrounded by newly formed connective tissue, with a new woven bone formation that contained a large number of osteoblast cells (Fig. 4-29). At 15 days after surgery, the histological section of the mandible bone showed the site of a hole partially occluded by highly mature connective tissue and new woven bone formation (Fig. 4-30). At 30 days after surgery, the histological sections of the mandible bone showed the site of a hole occluded by highly mature connective tissue with high vasculature and well-developed new woven bone formation (Fig. 4-31).

#### **4-8-3: Histopathological evaluation of the third group**

The histological section of the mandible bone in the third group at seven days showed the site of a hole surrounded by highly mature connective tissue, highly new woven bone formation, with high vasculature at the edge of the mandible bone (Fig. 4-32). At 15 days after surgery, the histological sections of the mandible bone showed the site of a hole partially occluded by highly mature connective tissue, and the new woven bone formation continued from the margins of the defect towards the center, with the edge of the mandible bone (Fig. 4-33). At 30 days after surgery, the histological section of the mandible bone of showed the site of the hole was occluded by highly mature connective tissue with high vasculature, and well-developed new trabecular bone formation, surrounded by large numbers of osteoblasts cells with deeply embedded osteocytes (Fig. 4-34).

#### **4-8-4: Histopathological evaluation of the fourth group**

The histological section of the mandible bone of the fourth group at seven days after surgery showed the site of the hole, with remaining PRF

surrounded by highly mature connective tissue and new woven bone formation at the edge of the mandible bone (Fig. 4-35). At 15 days after surgery, the histological section of the mandible bone showed the site of the hole with the remaining PRF, occluded by mature connective tissue immature bone formation, and adult bone (Fig. 4-36). At 30 days after surgery, the histological section of the mandible bone showed the site of the hole, occluded by immature bone formation (black arrow) and well-developed mature bone (Fig. 4-37).

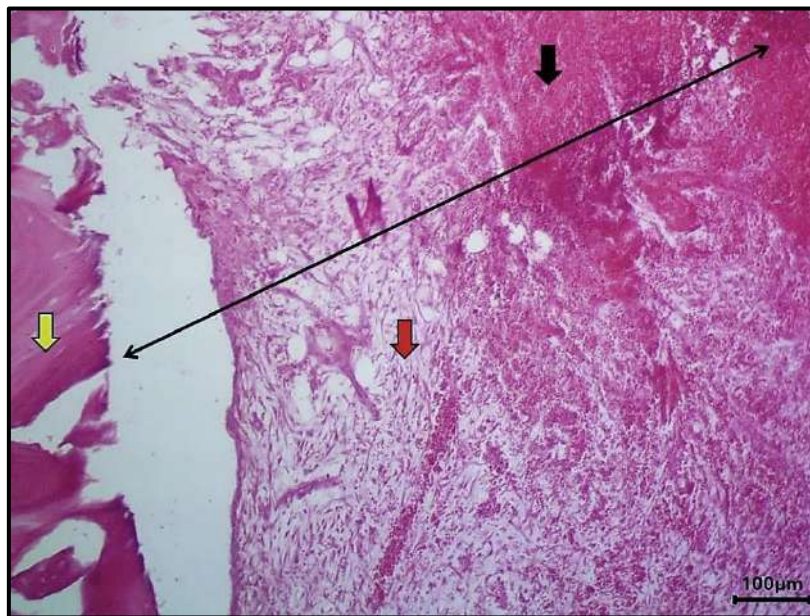


Figure 4-26: Histological section of the mandible bone of the first group (7 days) showing the site of the hole (↔) with severe hemorrhage or blood clot (black arrow), surrounding by granulation tissue (red arrow) and the edge of the mandible bone (yellow arrow). H&E stain, 100X.

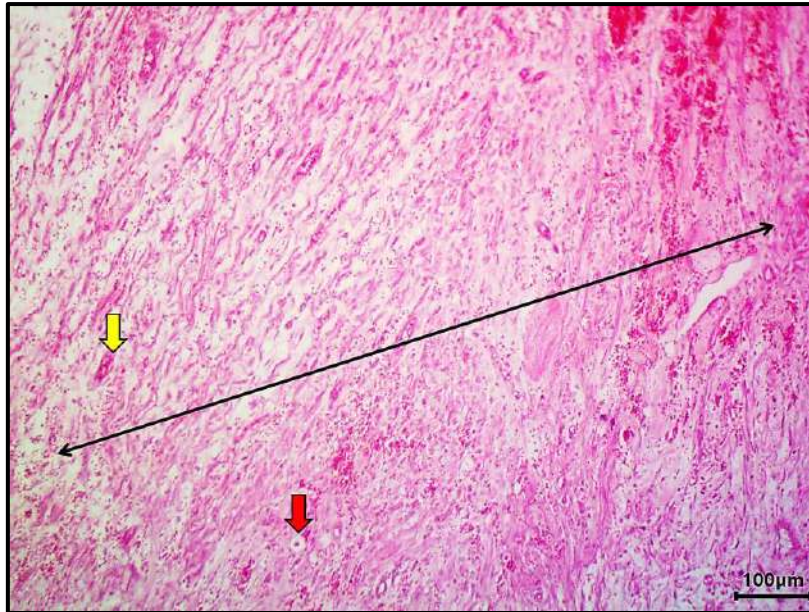


Figure 4-27: Histological section of the mandible bone of the first group (15 days) showing the site of the hole (↔) occluded with hemorrhagic clot (black arrow), highly granulation tissue with high connective tissue (red arrow), and vasculature or new blood vessels (yellow arrow). H&E stain, 100X.

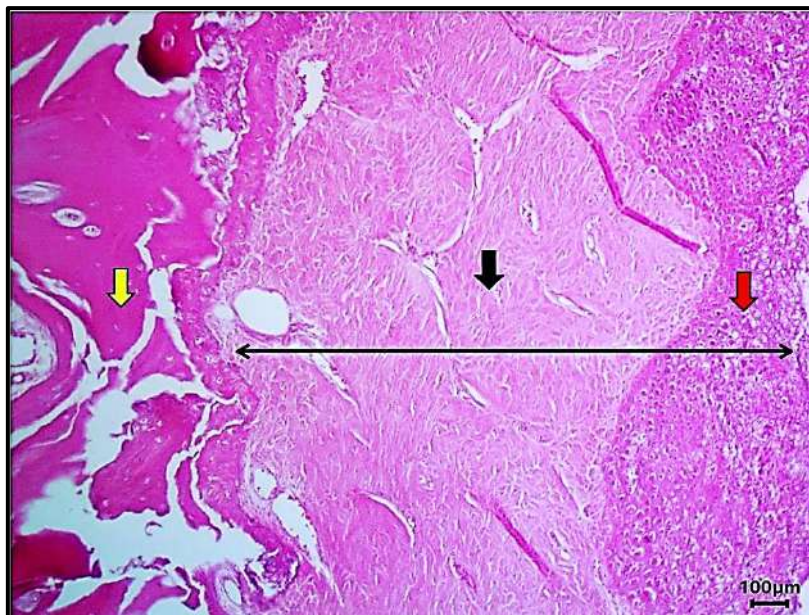


Figure 4-28: Histological section of the mandible bone of the first group (30 days) showing the site of the hole (↔) with highly mature connective tissue (black arrow) and new woven bone formation (red arrow), with the edge of the mandible bone (yellow arrow). H&E stain, 100X.



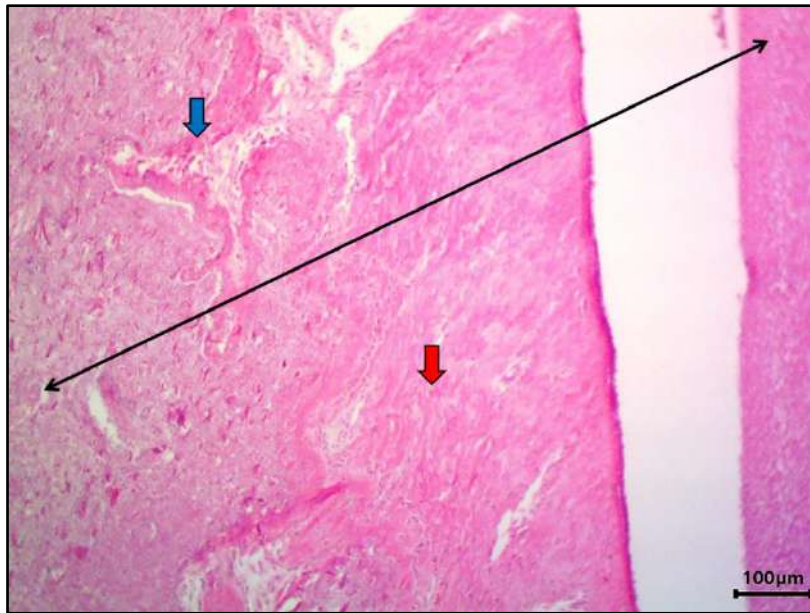


Figure 4-29: Histological section of the mandible bone of the second group (7 days) showing the site of the hole (↔), surrounded by highly mature connective tissue (red arrow), new woven bone formation with osteoblasts (blue arrow). H&E stain, 100X.

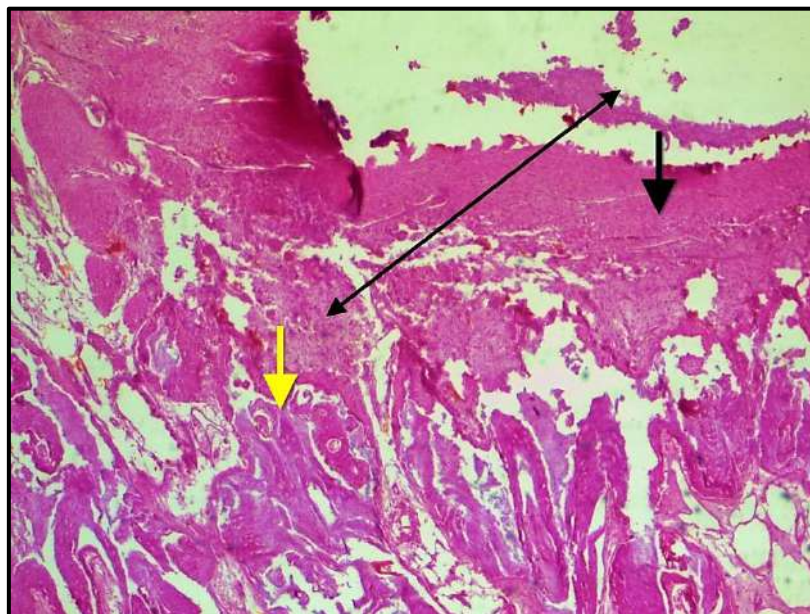


Figure 4-30: Histological section of the mandible bone of the second group (15 days) showing the site of the hole (↔) with highly mature connective tissue (black arrow) and new woven bone formation (yellow arrow). H&E stain, 100X.

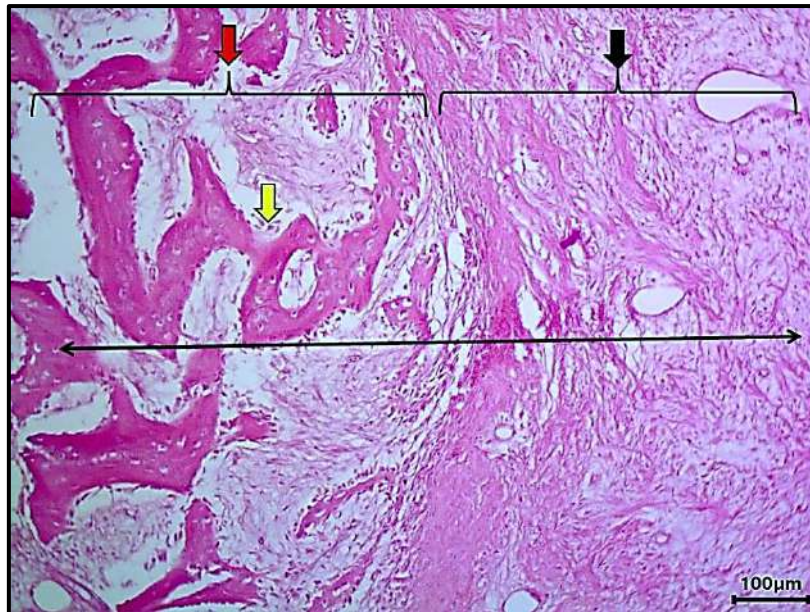


Figure 4-31: Histological section of the mandible bone of the second group (30 days) showing the site of the hole (↔) with by highly mature connective tissue with high vasculature (black arrow) and well-developed new woven bone formation (red arrow) with high osteoblasts numbers (yellow arrow). H&E stain, 100X.

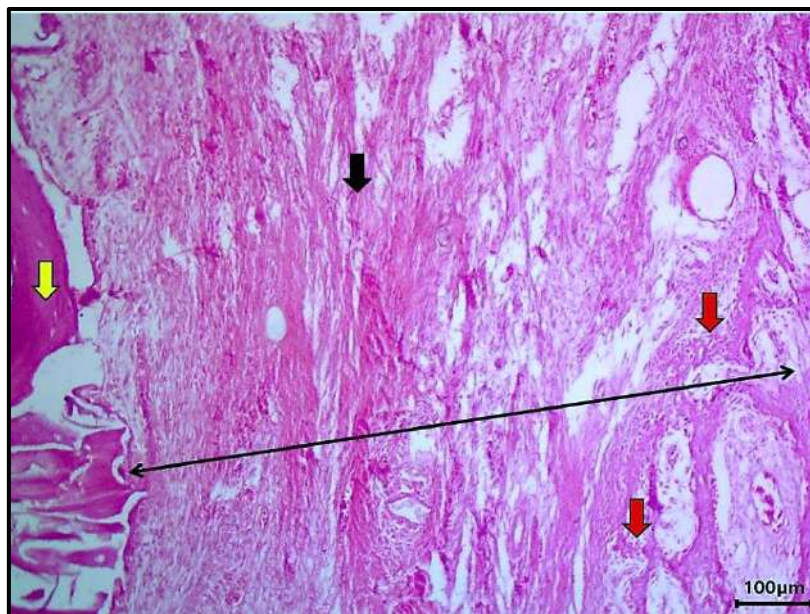


Figure 4-32: Histological section of the mandible bone of the third group (7 days) showing the site of the hole (↔) surrounded by highly mature connective tissue (black arrow), highly new woven bone formation (red arrow), and the edge of the mandible bone (yellow arrow). H&E stain, 100X.



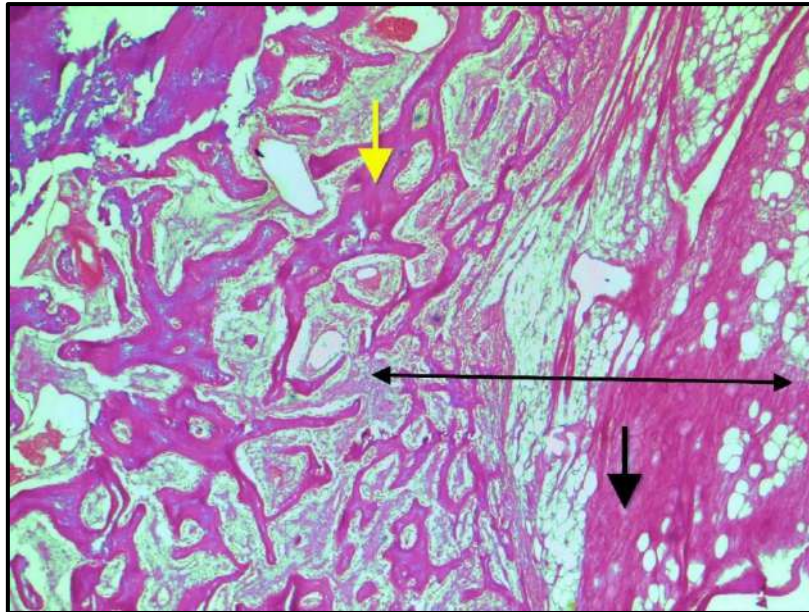


Figure 4-33: Histological section of the mandible bone of the third group (15 days) showing the site of the hole (↔) occluded by highly mature connective tissue (black arrow) and well-developed new woven bone formation (yellow arrow). H&E stain, 100X.

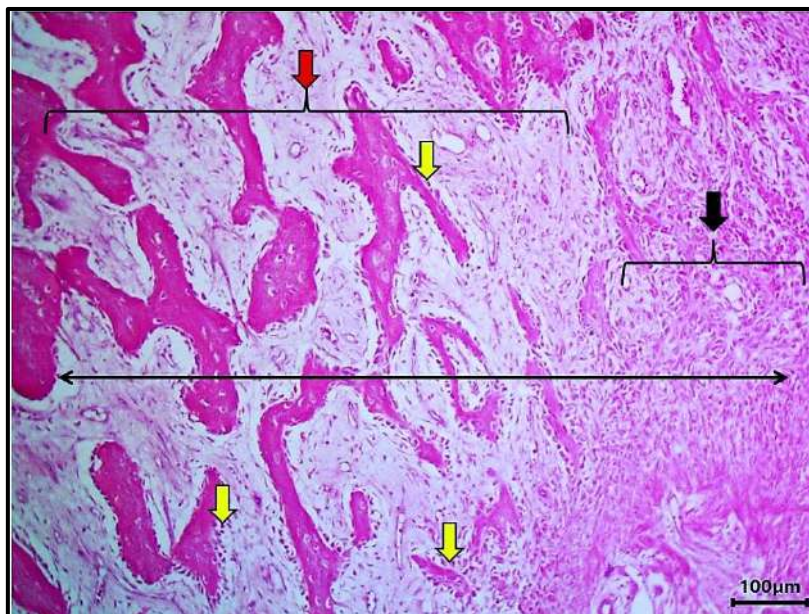


Figure 4-34: Histological section of the mandible bone of the third group (30 days) showing the site of the hole (↔) occluded by mature connective tissue (black arrow) and very well-developed new woven bone formation (red arrow), with high osteoblasts numbers (yellow arrow). H&E stain, 100X.

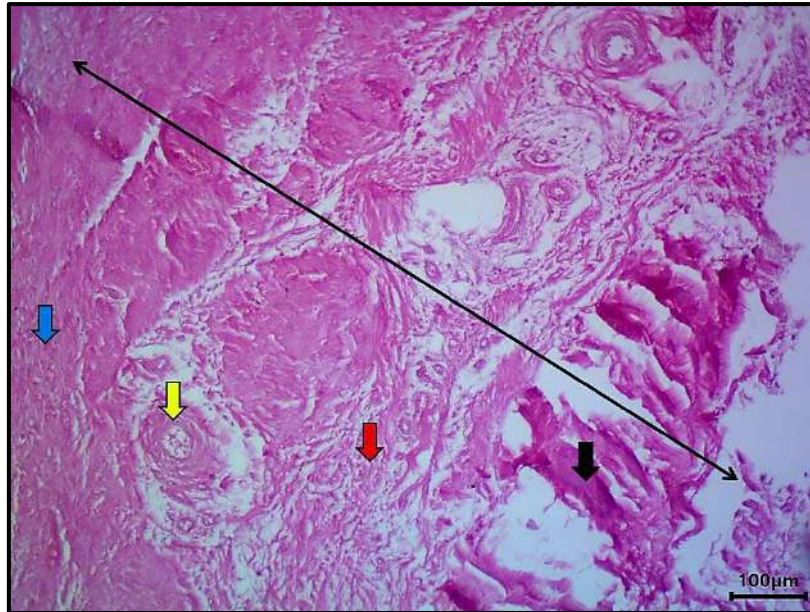


Figure 4-35: Histological section of the mandible bone of the fourth group (7 days) showing the site of the hole (↔) with remaining PRF (black arrow) surrounding by highly mature connective tissue (red arrow), new woven bone formation (blue arrow) with high vasculature (yellow arrow). H&E stain, 100X.

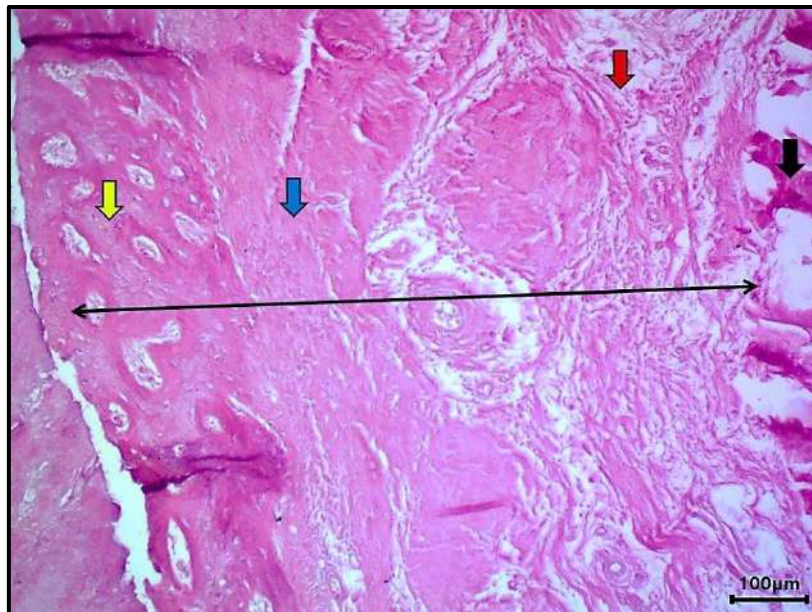


Figure 4-36: Histological section of the mandible bone of the fourth group (15 days) showing the site of the hole (↔) with the remaining PRF (black arrow), occluded by mature connective tissue (red arrow) immature bone formation (blue arrow), and mature bone (yellow arrow). H&E stain, 100X.



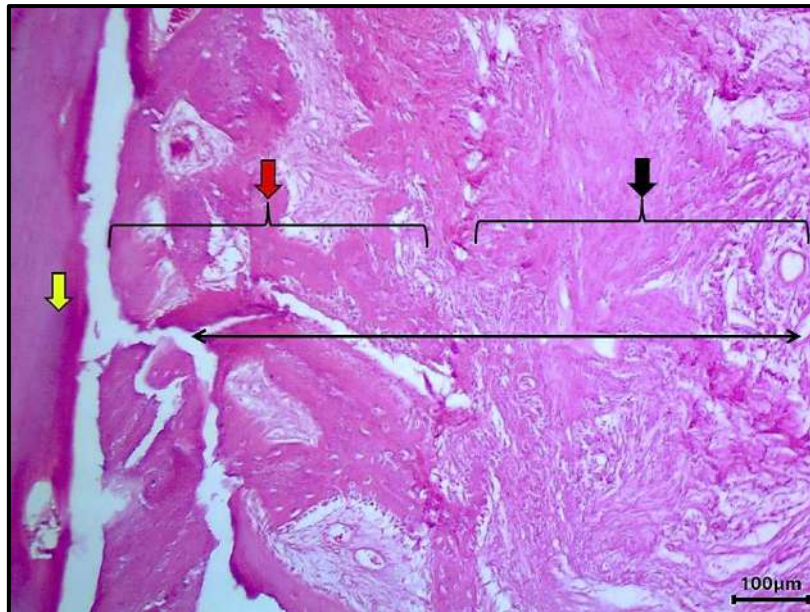


Figure 4-37: Histological section of the mandible bone of the fourth group (30 days) showing the site of the hole ( $\leftrightarrow$ ) occluded by immature bone formation (black arrow) and well-developed mature (lamellar) bone formation (red arrow), with the edge of the mandible bone (yellow arrow). H&E stain, 100X.



Table 4-3: The mean values of the histopathological score used Duncan's test.

N0.	Time Groups parameter names	Seven days after surgery				15 days after surgery				30 days after surgery			
		First group	Second group	Third group	Fourth group	First group	Second group	Third group	Fourth group	First group	Second group	Third group	Fourth group
1.	Osteoblast	0.25±0.13 B	0.25±0.13 B	0.75±0.13 B	1.83±0.29 A	0.58±0.14 C	1.75±0.21 B	2.08±0.22 AB	2.41±0.19 A	1.41±0.14 B	2.41±0.22 A	2.66±0.14 A	2.66±0.14 A
2.	Osteocytes	0.16±0.11 C	0.16±0.11 C	1.00±0.17 B	1.50±0.23 A	0.41±0.14 C	0.75±0.13 BC	1.00±0.17 AB	1.41±0.19 A	0.83±0.16 B	1.83±0.19 A	2.08±0.16 A	2.16±0.24 A
3.	Osteoclast	0.66±0.28 B	1.41±0.31 AB	1.83.00±0.29 A	1.91.00±0.25 A	1.66±0.22 AB	2.00±0.21 A	1.41±0.33 AB	1.08±0.28 B	1.58±0.22 A	1.08±0.19 AB	0.75±0.17 B	0.75±0.17 B
4.	Immature bone	1.91±0.08 A	1.85±0.14 B	1.00±0.0 C	1.33±0.14 B	1.75±0.13 A	0.66±0.14 B	0.75±0.13 B	0.41±0.14 B	0.58±0.19 B	0.83±0.20 B	1.33±0.14 A	1.66±0.14 A
5.	Mature bone	0.33±0.14 A	0.16±0.11 A	0.±25.13 A	0.50±0.15 A	0.41±0.19 B	0.25±0.13 B	1.41±0.19 A	1.50±0.15 A	0.33±0.14 C	2.08±0.19 B	2.41±0.14 AB	2.58±0.14 A
6.	Bone bridge	0.41±0.14 B	0.41±0.14 B	0.91±0.14 A	1.25±0.13 A	0.25±0.13 B	0.66±0.14 B	1.25±0.17 A	1.58±0.14 A	0.33±0.14 B	1.33±0.14 A	1.66±0.14 A	1.75±0.13 A
7.	Bone trabeculae	0.08±0.08 B	0.58±0.14 A	0.75±0.13 A	0.75±0.13 A	0.33±0.14 B	1.16±0.24 A	1.41±0.14 A	1.50±0.19 A	0.66±0.14 C	1.83±0.20 B	2.50±0.15 A	2.50±0.15 A
8.	Inflammation	0.00±0.00 C	0.16±0.11 BC	0.41±0.14 AB	0.66±0.14 A	0.41±0.14 B	0.66±0.14 AB	0.91±0.08 A	0.91±0.08 A	0.83±0.11 A	0.91±0.08 A	1.00±0 A	1.00±0 A
9.	Granulation tissue	0.50±0.15 AB	0.16±0.11 B	0.66±0.14 A	0.83±0.11 A	0.41±0.14 B	0.83±0.11 A	1.00±0.0 A	1.00±0.0 A	0.66±0.14 B	1.00±0.00 A	1.00±0 A	1.00±0 A
10.	New formation of blood vessels	1.22±0.013 C	1.50±0.15 BC	1.83±0.20 B	2.58±0.19 A	1.58±0.19 B	2.08±0.19 AB	2.25±0.21 A	2.50±0.26 A	1.33±0.25 B	2.16±0.27 A	2.08±0.22 A	2.75±0.25 A

\*Values are mean ±SE.

\*Different letters mean a significant difference of Duncan grouping ( $P \leq 0.05$ ) in the same row.

#### **4-9: Immunohistochemistry**

The IHC sections in the control group showed that the ALP expression activity appeared weakly expressed in both the cartilaginous and ossification zones. In contrast, the connective tissue zone, which located in the center of the defective area, did not exhibit any enzyme activity (negative expression) (Fig.4-38). In the second group, the ALP activity was mildly expressed in the ossification zone and showed a moderate expression in the cartilaginous zone which located in the center of the defective area. However, the distribution of ALP activity showed a progressive increase in ALP expression activity, being weakest in the ossification zone and higher in the cartilaginous zone (Fig.4-39). In the third group, the ALP activity was mildly expressed on the surface of the newly formed bone trabeculae. Also, no ALP activity could be detected in deeply embedded osteocytes, calcified bone matrix, or compact bone. While the ALP activity was moderately expressed in the cartilaginous zone (which is located in the center of the defective area) (Fig.4-40). In the fourth group, the ALP activity was highly expressed in the center of the defective area and moderately expressed in the surface of lamellar bone, on the newly embedded osteocytes of compact bone, and the Haversian canal respectively (Fig.4-41).

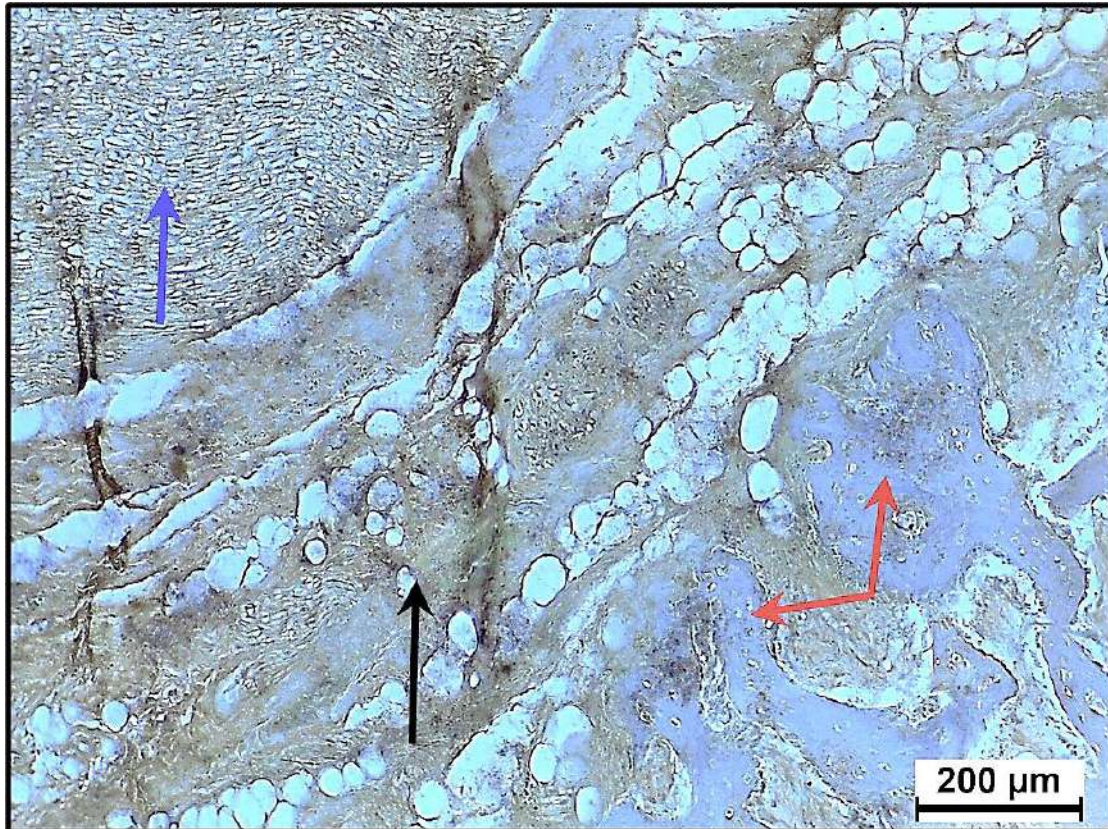


Figure 4-38: Immunohistochemical staining for expression of the ALP activity under the light microscope in the mandible bone defect area in the first group at 30 days PS appeared as (golden-brown) stain, indicating a weakly expressed in both the cartilaginous zone (black arrow) and the ossification zone (red arrow), while the connective tissue zone did not exhibit any enzyme activity (negative expression). Hematoxylin stain, scale bar: 200.



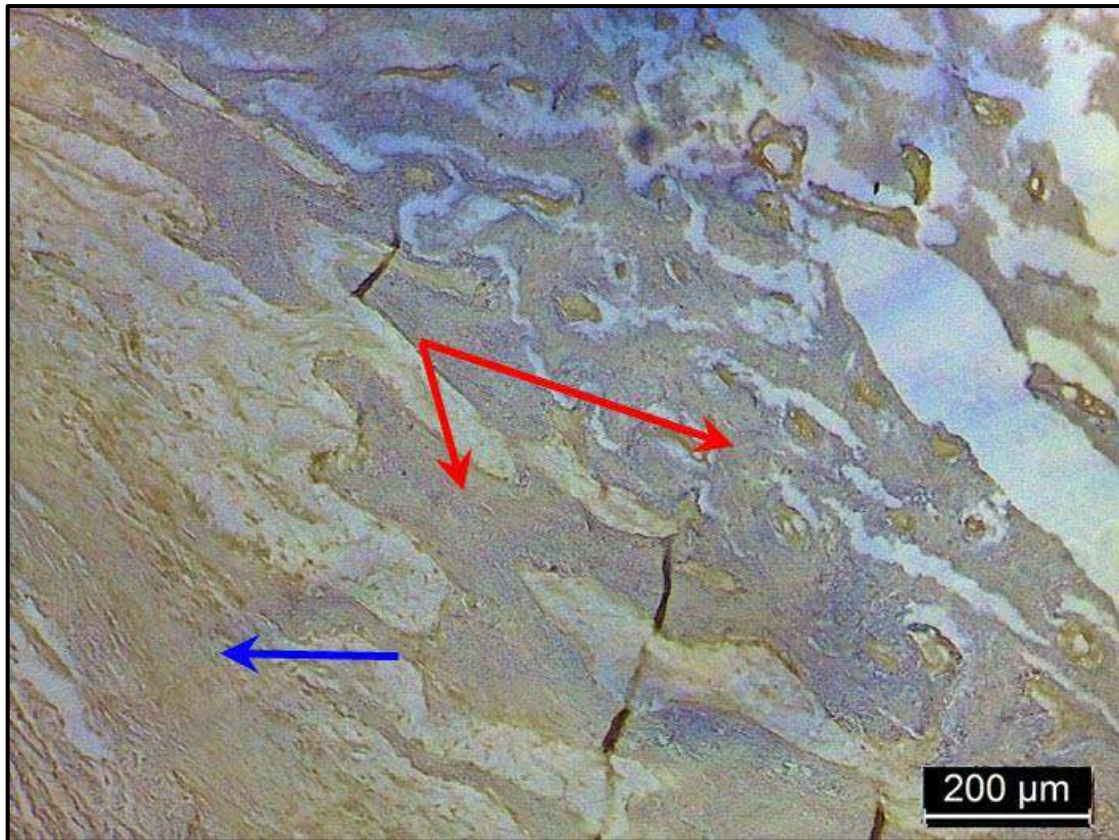


Figure 4-39: Immunohistochemical staining for expression of the ALP activity under the light microscope in the mandible bone defect area in the second group at 30 days PS appeared as (golden-brown) stain indicating a mildly expressed in the ossification zone (red arrow) and showed a moderate expression in both cartilaginous zone (blue arrow). Hematoxylin stain; scale bar:200.

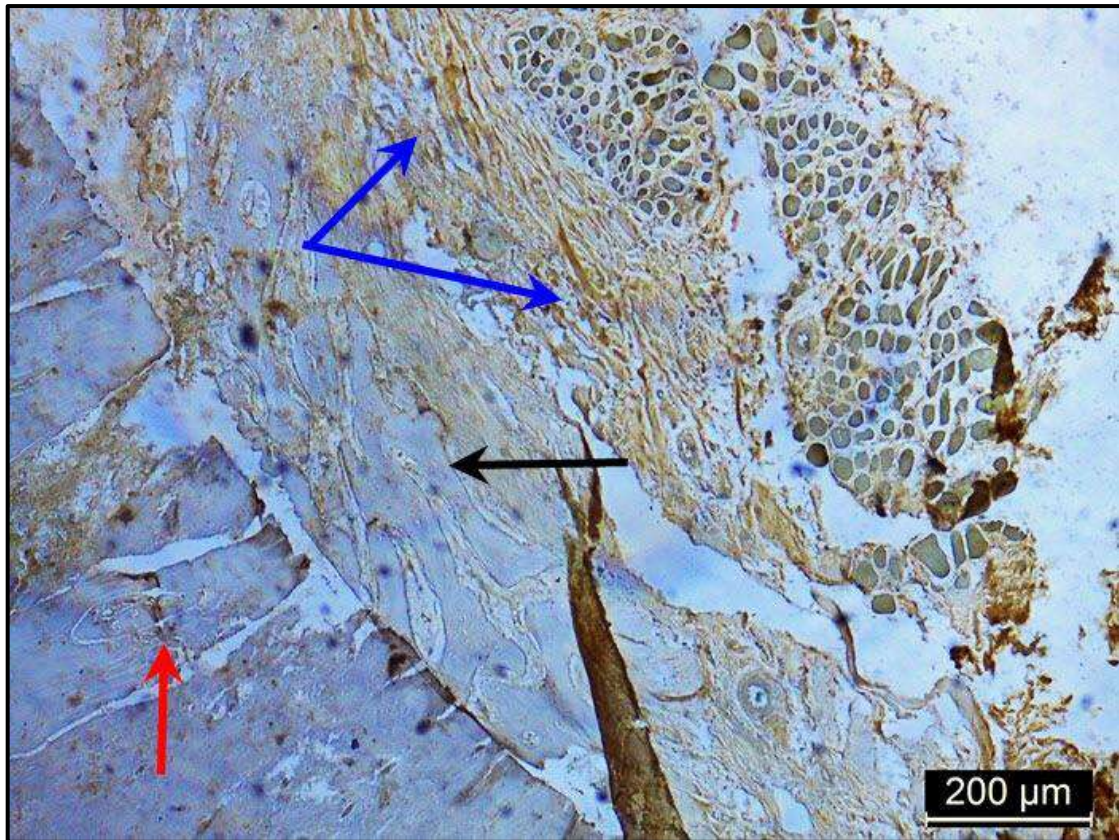


Figure 4-40: Immunohistochemical staining for expression of the ALP activity under the light microscope in the mandible bone defect area in the third group at 30 days PS appeared as (golden-brown) stain indicating moderately on the cartilaginous zone (blue arrow) and mildly expressed on the surface of newly formed bone trabeculae (black arrow) and the compact bone (red arrow) respectively. Hematoxylin stain; scale bar:200.



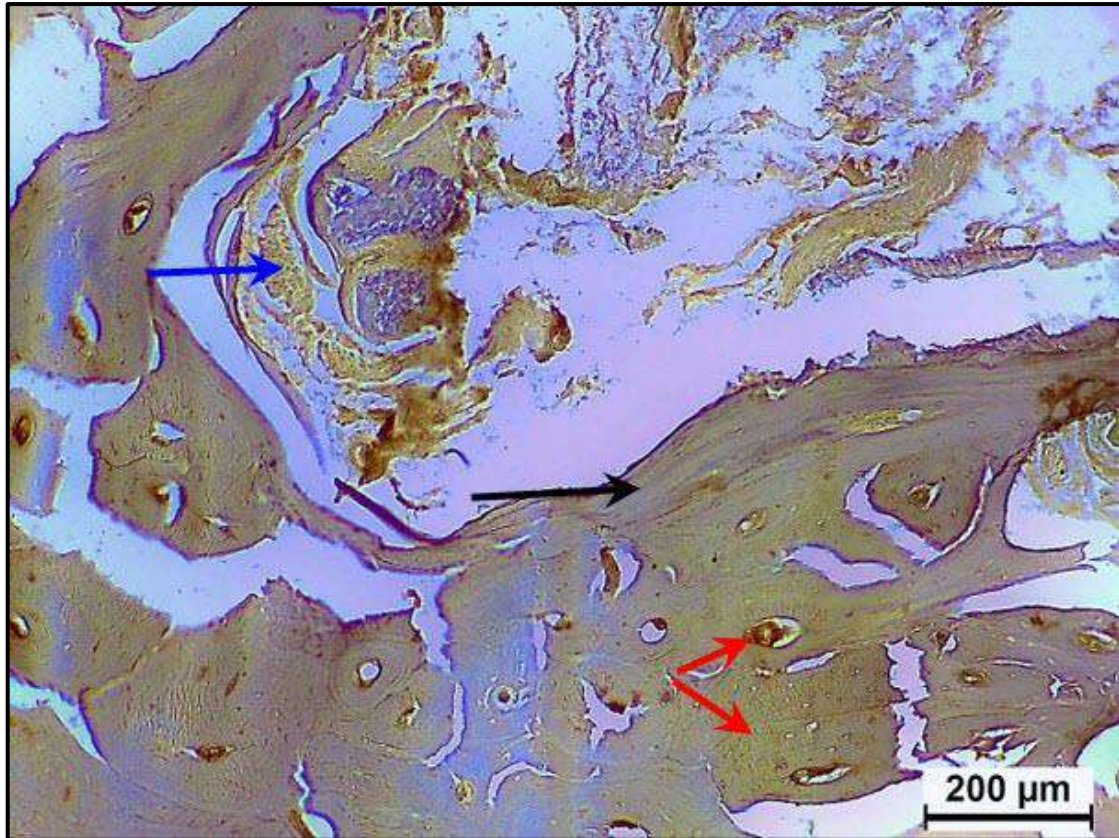


Figure 4-41: Immunohistochemical staining for expression of the ALP activity under the light microscope in the mandible bone defect area in the fourth group at 30 days PS appeared as (golden-brown) stain indicating a highly expressed in the center of the defective area (blue arrow), and moderately expressed on the surface of lamellar bone (black arrow), on the newly embedded osteocytes of the compact bone, and the Haversian canal respectively (red arrow). Hematoxylin stain; scale bar:200.

## Chapter five

### Discussion

#### **5-1: Induced the large size mandibular bone defect in dogs' models.**

Bone tissue can regenerate small losses to its structure, but surgical intervention is required in the case of large-size bone defects. The "large size bone defect" is defined as a defect that does not heal with the normal process of bone healing; it heals primarily with fibrous tissue formation (Piotrowski *et al.*, 2019). Various studies have reported different data on identifying large size defects in the mandible of dogs (King *et al.*, 2002; Arzi *et al.*, 2016). In vivo studies have been conducted to determine the size of the large bone defect in dog models and the surgical interventions that follow, including substitute biomaterials. Although some bone defect models have been developed in long or calvarial bones (Liu *et al.*, 2019). Our study found that a bone defect diameter of approximately 14 mm failed to heal bone defects spontaneously through the normal bone healing process, as seen in the evaluation of the control group. Unlike the treated groups, it recovered by creating fibrous tissue instead of forming new bone tissues.

Therefore, this study found that bone defects with a diameter of 14mm are considered large in size for dog models. Thus, our results disagree with the recent research, which clarifies that a 4 mm diameter is large in a dog model (Rashid *et al.*, 2021). The current study disagrees with the study that showed that 6 mm penetrating defects did not heal spontaneously in dog mandibles (Hjørtting-Hansen and Andreasen, 1971). Another study has found that the large size bone defect for mandibular bones in dogs is 10 mm (Chao *et al.*, 2021). Also, our current study

disagrees with recent research that used the standardized bone defect model in the mandibular bone because they failed to determine large size defects in dogs. They found spontaneous bone healing activity even at 4, 6, and 8 mm in size, respectively (Liu *et al.*, 2019).

## **5-2: Clinical evaluations**

During the present study, we established that the surgical wounds were healed with the first intention in all groups without signs of swelling, infection dehiscence, or wound exudation. Therefore, we suggest that the lateral surgical approach of the mandibular bone used in this study is considered surgically under aseptic conditions and suitable for rapid exposure to the lateral border of the mandibular bone with minimal soft tissue trauma. Therefore, we agree with the recent study that reported the lateral approach to the mandible in the dog was associated with less wound-related complications (Cinti *et al.*, 2021).

The typical clinical manifestations, indicated that the surgical technique and instruments used to induce a large size defect in the mandibular bone through continuous irrigation with saline solution were safe without adverse clinical reaction nor infectious complications or excessive soft tissue trauma. It appears that bone cooling is essential during surgical osteotomies or drilling procedures to prevent these problems, which is in line with our clinical results and the conclusions mentioned by (Anesi *et al.*, 2020). Also, thermal necrosis's adverse effects typically occur shortly after surgical procedures. Many orthopedic surgeons attempt to prevent the heating of bone during surgery because a high level of heat generation can kill bone cells and damage the surrounding bone tissue. Thus, heating is considered a real clinical problem in orthopedic surgeries. Recent research shows that cooling is highly effective in limiting temperature elevations and preventing thermal necrosis that typically



occurs shortly after surgical procedures (Mediouni *et al.*, 2019). Moreover, our clinical findings demonstrate that the drilling procedure can be successful when drilling parameters, such as the drill machine, tool used, force applied, angle, and speed, are carefully controlled, resulting in the induce of a large size defect in the mandibular bone of dogs without causing damage to the bone tissues.

Moreover, in the past, orthopedic surgeons added antibiotics to control bacterial infections. However, recent research has shown that calcium-based biomaterials and even autologous PRF have potential antibacterial effects (Feng *et al.*, 2020; Rupp *et al.*, 2022). The physicochemical properties of natural bone biomaterials influence can promote immune cells (e.g., macrophages) by regulating the expression of chemokines and inflammatory factors that are released by these cells that contribute to the differentiation of bone mesenchymal stem cells (BMSCs), leading to successful osteogenesis (Tang *et al.*, 2021). Thus, the natural bone substitute biomaterials interact with bone cells rather than induce immune rejection or foreign body reactions. That's why they are biocompatible. Therefore, our outcomes match with (Moshiri *et al.*, 2020), those who mentioned that biomaterials have superior cytocompatibility. Furthermore, biomaterials derived from either natural or synthetic sources that serve as bone substitutes, as an alternative to metallic bone implants, are utilized to repair large size bone deficiencies without adverse side effect (Pina *et al.*, 2018). Furthermore, these biomaterials can fill defects of any size or shape without requiring additional surgical procedures.

### **5-3: X-ray Diffraction (XRD)**

In this study, the XRD diffraction peaks of both oyster shell HA. and quail eggshell  $\text{Ca(OH)}_2$  show the main peaks with high purity that appeared as sharp and narrow diffraction peak patterns. These findings come in

contact with the previous studies had demonstrated the XRD pattern of the natural source oyster shell HA. and quail eggshell  $\text{Ca(OH)}_2$  powder obtained through calcination method at  $1200^\circ\text{C}$  (Pal *et al.*, 2017; Khan *et al.*, 2019). Nevertheless, in this study, the hydrothermal method used in the synthesis of biomaterials impacted the control of its particle size, chemical composition, and morphology. This process is often regarded as an eco-friendly option due to its low cost, ability to produce products with high crystallinity, and easily controllable chemical reactions (Earl *et al.*, 2006; Zhou and Lee, 2011; Sunil and Jagannatham, 2016). Therefore, the crystallinity of the fabricated bone substitutes is dependent on the method of fabrication, so the hydrothermal method can be obtained from the high stoichiometric compounds. Compared with the other fabricated methods, they produced a low crystallinity product (Sunil and Jagannatham, 2016).

Typically, when the calcination temperature is high. It produces a crystalline structure with higher phase purity and particles with uniform shapes and sizes in their final morphology (Fiume *et al.*, 2021). Thus, the appearance of the sharp narrow peaks of our XRD patterns in both the QESCH and third groups agrees with previous findings seen that the degree of sharpness of peaks increases gradually with increasing the calcinated temperature (Esmaeilkhani *et al.*, 2019). Therefore, the hydrothermal method is considered a successful and simple way to fabricate calcium-based biomaterials.

#### **5-4: Energy dispersive X-ray spectroscopy**

The EDS spectra of the bone substitute biomaterials analyzed in this study showed the presence of Ca, P, C, and O elements. These are the major elements found in calcium phosphate-based biomaterials, except carbon. The appearance of carbon in the EDS spectra of the fabricated bone substitute biomaterials is believed to be due to the absorption of  $\text{CO}_2$  by

the samples during atmospheric exposure. It occurred immediately after the synthetic process had finished, resulting in a partial carbonation of the samples. Our hypothesis is supported by the findings presented by (Chávez *et al.*, 2017), who concluded that once the container has been opened, the fabricated sample undergoes partial carbonation.

Many studies have suggested that these mineral elements can rapidly incorporate with the host tissues and enhance biocompatibility, new bone production, and regeneration through their physicochemical responses (Zhou and Lee, 2011; Shao *et al.*, 2015; Damia *et al.*, 2019). These minerals undergo ionic dissolution into calcium and hydroxyl ions, contribute to bone mineralization, and have antibacterial activity (Bhalla and Chockattu, 2021). In addition, these minerals mimic the mineral compositions of living bones and teeth and have the ability to form a chemical bonding with the bone tissues through the dissociation of calcium ( $\text{Ca}^{+2}$ ), phosphate ( $\text{PO}_4^{3-}$ ), and hydroxyl ( $\text{OH}^-$ ) ions that are present in the chemical structure of both HA and  $\text{Ca}(\text{OH})_2$ . Furthermore, many studies explain that these minerals act as a biomineral medium for multipotent stem cells, which support their differentiation into chondrocytes or osteoblasts, and subsequently responsible for the growth of bone, and also promote the formation of bone structures, facilitate the production, consolidation, and mineralization of fibrillar collagen (Cordonnier *et al.*, 2011; Ressler *et al.*, 2021; Gaidash *et al.*, 2022).

A recent study illustrated that the inorganic trace minerals observed in the EDS analysis were under-degraded and then dissociated into ions and ion groups after being implanted within the bone defects (Mu *et al.*, 2023). In this way, there were two mechanisms responsible for ionic dissolution. The physical process involves ions reacting with the surrounding bone tissue, causing materials to dissolve and form a bone-

like apatite layer on the biomaterial surface. Osteoblasts then deposit new bone on top of this layer, and the process continues until the material is entirely replaced by new living bone. This process is called bio integration of biomaterials via the deposition of this layer (Atiyah *et al.*, 2021). The second mechanism is the biological response, many studies illustrated that the biomaterial ions that directly interact with immune cells (e.g., neutrophils and macrophages) lead to the activation of cells and then release of inflammatory mediators, which gives rise to an increase in the expression and production of biological materials such as cytokines, growth factors and activate enzyme pathway. These materials then attract and encourage MSCs to differentiate into osteoblasts, which impact bone development and regeneration (Velard *et al.*, 2013; Wang *et al.*, 2016).

### **5-5: Field Emission Scanning Electron Microscopy (FESEM)**

Many studies have demonstrated that SEM is most suitable for imaging the surfaces of the bones. It has long been recognized that bone surface morphology can provide high-resolution bone surface images of both the hard and soft components of bones (Shah *et al.*, 2019). On the other hand, the FESEM can provide nanometer-level resolution of a sample's surface. Additionally, it is a valuable tool for scanning the entire surface of the bone and offering information over hundreds of micrometers. Also, understanding the shape and size of mineralized tissue, arrangements of minerals with collagenous matrix, and investigating the ultrastructural organization of bone tissue to provide information for future studies. The ultrastructure of the newly formed bone tissue includes the unit crystals, the crystal platelets, the mineralized matrix (osteoid), the collagen fibril, and the fibril bundles (if the fibrils have been organized in bundles) (Schwarcz *et al.*, 2017). The synthesis technique, processing parameters, and crystal structure of the materials dictated the surface morphology of

the manufactured powder samples. To improve the clinical results of bone tissue regeneration, it is essential to understand the surface morphology of biomaterials in order to design it to facilitate cell adhesions, proliferations, and differentiations (Zhou *et al.*, 2023).

Based on the FESEM images, the oyster shell HA in this investigation was found to be non-aggregating spherical particles ranging in size from 8 to 140 $\mu$ m. The spherical morphology of the oyster shell HA. Powder related to a synthesis method, which requires more time for aging through continuous rotation force by using the magnetic stirrer to reach the reaction PH 8, results in disaggregated particles and leads to the slow growth of homogeneously non-agglomerated spherical particles. Due to the quick reaction time that did not require pH correction or magnetic stirrer forces, the quail eggshell  $\text{Ca}(\text{OH})_2$  does not seem to have irregular agglomerated particles in the FESEM images (Zhou and Lee, 2011). Thus, the FESEM images of fabricated oyster shell HA., the Particles appeared more stoichiometric and regular in shape than fabricated quail eggshell  $\text{Ca}(\text{OH})_2$  particles. There was a strong relationship between particle size, particle morphology, and particle stoichiometry of fabricated inorganic biomaterials in response to bone healing (Atayde *et al.*, 2015).

On the other hand, the FESEM images in the fourth group showed that the surface morphology of the PRF gel appears homogenous without any porosity. This is related to the preparation procedure that used a high-speed centrifugation method, which allows a dense fibrin matrix to form (Dohan *et al.*, 2006a; Kosmidis *et al.*, 2023). Additionally, we used a PRF glass tube for the PRF preparation. This tube has been shown to rapidly activate blood coagulation during centrifugation time, thus forming a large volume of a solid PRF gel. Therefore, the large volume of PRF gel obtained is related to the PRF tubes, which contained a significant amount of silica

microparticles within the inner surface of these tubes, which allowed the rapid activation of the coagulation cascade. As a result, the fibrin matrix of the prepared PRF samples appeared homogenous and uniformly shaped like a smear in the FESEM images. As a result, this procedure is considered very simple, and it requires little time to achieve a solid fibrin matrix, which is suitable for use as an autologous injectable scaffold inside the bone defects. In addition, this procedure allows homogenous distribution patterns of the growth factors, mediators, and granulocyte cells, especially neutrophils, within the matrix during centrifugation protocol. Also, it increased the incorporation of cytokines within the fibrin matrix (Dohan *et al.*, 2006b; Wong *et al.*, 2020).

Recently, a new procedure for the preparation of PRF has been developed using low-speed centrifugation. In this procedure, the fibrin matrix shows a more porous structure that appears as a fiber bundle network (Ghanaati *et al.*, 2014). However, this process takes longer to obtain the PRF product, which could lead to protein denaturation of the sample. Thus, many studies have illustrated that the PRF gel is considered a natural bioscaffold and contains platelets, leukocytes, cytokines, growth factors, and fibrin matrix such as fibrinogen. It can promote cell migration and enhance cell adhesion, particularly for osteoblasts, when used as an injectable scaffold (Liu *et al.*, 2019; Caramês J *et al.*, 2022; Farshidfar *et al.*, 2022).

## **5-6: Field Emission Scanning Electron Microscopy (FESEM) at 30 days after surgery.**

At 30 days post-implantation, the examined FESEM images showed that the most bone tissue formation occurs in the second, third, and fourth groups respectively, compared to the control group. In the control group, they appeared to have excessive fibrous tissue formation around the bone

defect. Also, the FESEM images in the control group showed disorganized immature bone with no signs of compact or trabecular bone formation associated with excessive fibrous and vascular tissue ingrowth. Furthermore, the defect surface appears hematogenous without the appearance of a mineralized matrix or crystal plates or structures in or around the defective area of the bone, and the most prominent structures were the fibrous matrix. These results indicated that the mandibular defect in the control group failed to heal spontaneously on its own during the current experimental study. It has similarly been reported by (Elliott *et al.*, 2016), who mentioned that infected, larger-sized, or highly displaced bone contributes to failure to heal properly.

Furthermore, the FESEM images of the QESCH showed the growth of an unmineralized surface matrix surrounded by a thin layer of mineralized tissues, which indicated that calcium hydroxide possesses the ability to promote and enhance bone formation. These findings were supported by many researches that illustrated that high levels of calcium and hydroxyl ions released by calcium hydroxide can induce osteoblast proliferation, differentiation, and matrix mineralization through enhanced osteoblast cell adhesion and proliferation (Tan *et al.*, 2018; S. Wang *et al.*, 2018).

The  $\text{Ca(OH)}_2$  has a higher alkalinity than other compounds, and it works by causing the calcium and hydroxyl ions to dissociate when they come into touch with watery solution. Many researchers have shown that adding calcium hydroxide powder to the root canal can release hydroxyl ions and create a highly alkaline environment on the root surface. Thus, the most harmful bacteria cannot survive in alkaline conditions of slowly dissolving calcium hydroxide (Kahler *et al.*, 2018; Khosropanah *et al.*, 2018; Dako *et al.*, 2020; Paula-Silva *et al.*, 2021). Also, the alkaline pH

influences cellular processes, such as cell membrane metabolism, changes in the cell's shape, cell proliferation, and growth.

The high pH level provided by calcium hydroxide has bactericide effects, but on the other hand, it inhibits osteoclastic cell viability, migration, and differentiation and stimulates fibroblast cells, which can lead to fibrous tissue formation. Thus, an alkaline environment can decrease the rate of new bone formation (Guex *et al.*, 2021). Moreover, normal bone healing rates can be achieved, and tissue mineralization can be enhanced by adjusting the pH of the tissue environment to a non-alkaline environment. In addition, other researchers mentioned that the high pH level of calcium hydroxide causes superficial tissue necrosis with a mild inflammatory response and hard tissue formation (Eick *et al.*, 2014; Khosropanah *et al.*, 2018). However, the underlying mechanism of the calcium hydroxide induces bone mineralization is still unclear (Chen *et al.*, 2016; Y. Liu *et al.*, 2023).

The analysis of the FESEM images of the third group showed an increase in the mineralization surface, especially in the center of the defect, compared with the surface morphology of the control group. In addition, the surrounding surface of the defect shows the growth of the matrix, which is characterized by well-organized trabecular bone formation with the deposition of osteoid matrix. Our results agree with (Lins *et al.*, 2017), who showed that the size of HA larger than 75nm in diameter was well tolerated by body fluid and tissue for up to 42 days after implantation. These particles can accelerate the bone healing process. Upon observation of the FESEM images, it was noted that the bone matrix formed around the center of the bone defect area, consisting of well-defined lamellar bone. This result was supported by a previous study that showed that hydroxyapatite was in direct contact with the bone and included in the bone matrix (Lins



*et al.*, 2017). In addition, the appearance of organic bone matrix deposition indicates good cellular biocompatibility (Lei *et al.*, 2019). Furthermore, the surface of hydroxyapatite can facilitate the attachment, growth, and multiplication of osteoblastic cells, which enables the development of new bone through the creeping substitution from the surrounding bone tissues (Kaneko *et al.*, 2020).

In addition, hydroxyapatite is rich in  $\text{Ca}^{2+}$  and  $\text{PO}_4^{3-}$  ions, which are considered the most important ions for tissue mineralization. Therefore, our *in vivo* study intersected with an earlier *in vitro* study that discovered these elements could modulate bone metabolism, control the activity of osteoblasts and osteoclasts, promote the osteogenic differentiation of mesenchymal stem cells, and regulate cell adhesion, migration, and proliferation by activating calcium receptors. They could also stimulate the formation of new bone (Mocanu *et al.*, 2021).

However, in this work, the most mineralization surfaces in the bone substitute biomaterials groups appear in the fourth group. The FESEM images showed numerous mineralization crystals-like structures surrounded by osteoid in the center of the defect. On the other hand, the mineralized collagen fibrils are formed by the combination of collagen fibrils and bone mineral crystals. At this point, the crystals appear as platelets surrounding the bone defect area. Thus, we agree with the previous studies that indicated the formation of the crystal plates on the surface of the bone defect tissue is either intra or extra-fibrillar. When collagen fibrils have intrafibrillar crystals linked to their defective regions and extra-fibrillar crystals in the space around them, leading to the development of thick platelet surfaces (Rosen *et al.*, 2002; Georgiadis *et al.*, 2016; Buss *et al.*, 2022). Consequently, A protective layer of biological apatite is formed as bioactive chemicals break down slowly in live tissues.

When they reach the bone, they connect to it directly. Resorbable materials disintegrate without harming the bone, allowing new tissue to develop within (Ribeiro *et al.*, 2008).

The mineralization surface results in the fourth group are supported by the study, which concluded that PRF can promote osteoblastic maturation and calcification (Wang *et al.*, 2022). As a result, the formation of a large area of mineralization that appeared in the FESEM images indicates that the PRF has excellent biocompatibility, a superior biological response, and great potential for bone formation as compared with other treated groups (Farshidfar *et al.*, 2022). The outstanding biological response of the autologous PRF related to the rapid release of the growth factors during the early time of implantation within the tissues starts on the first day post-implantation (Fernández-Medina *et al.*, 2019). For this reason, our FESEM results show that the newly formed bone tissues in the fourth group appeared faster than in other treated groups.

These biological qualities aren't the only ones that have caught the attention of researchers lately, who have mentioned that the PRF gel also has anti-inflammatory, antibiofilm, and anti-microbial characteristics (Jasmine *et al.*, 2020; Zhang *et al.*, 2020). This is due to the abundance of cytokines, platelets, leukocytes, and stem cells in the PRF. Primarily utilized for maxillofacial and oral bone restoration, it has a reputation for being excellent in bone regeneration. Therefore, the use of PRF alone can promote newly formed bone tissue. Thus, our findings agree with the previous work, showing that the use of the PRF alone can enhance bone formation when used in the mandibular molar extracted socket area. It showed a significantly higher bone formation in beagle dogs (Neiva *et al.*, 2016). In general, the FESEM results of the newly grown bone tissue in all treatment groups were consistent with the previous research that noted the

biomaterials facilitate the directed ingrowth of bone-forming cells that migrate from the natural bone tissue surrounding the defect (Barbeck *et al.*, 2020).

## **5-7: Macroscopical evaluations**

In all treatment groups, we observed that the newly formed bone tissue filled the defect areas at the macroscopic level, but in the control group, we observed that the bone defects healed with fibrous tissue rather than bone tissue. Generally, more new bone tissue could be visually observed in the fourth group, which is filled with hard, firm tissues that fill the defective area, as compared with the second group and the third group, partially filled with hard tissue. These outcomes indicate that all biomaterials used in the present study enhance bone tissue formation in different clinical conditions. Therefore, our macroscopical findings agreed with previous observations that considered the use of bone substitute biomaterials stimulated osteoblast proliferation and can induce the formation of new bone with no immunological or inflammatory reaction to the biomaterial implanted in the large size bone defects (Manchón *et al.*, 2015; Oryan and Alidadi, 2018; Zhang *et al.*, 2019).

In particular, the surrounding mandibular bone tissues in all groups observed had no signs of osteonecrosis that resulted from the thermal effect, osteomyelitis due to infection, or even crack formation. These results indicated that the osteotomy technique used in the present study was a suitable and safe method for creating mandibular bone defects, resulting in the successful surgical procedure to induce the large size mandibular bone defects in dog models. Also, our results show no signs of immune reactions. At this point, we agree with a recent study that focused on the use of biomaterials for repairing and reconstruction of mandibular defects

bone to promote bone induction and healing without foreign body reactions or immune rejections (Zhang *et al.*, 2019).

### **5-8: Radiographical evaluations**

The radiographical findings in the control group of the present study indicated that the bone defect has incomplete ossification and healed with fibrous tissue. Also, the defect opacity was still radiolucent in the center and the peripheral area of the defect from the beginning of the current study until the end period study. The results indicated incomplete bone healing occurred. The results show that extracellular matrix deposition, granulation tissue proliferation, fibrocartilaginous tissue replacement, osteoid tissue development, ossification, maturation, and remodeling occurred as part of the secondary bone healing mechanism, our radiographical findings in the control group were in accordance with the current FESEM and macroscopical findings respectively. From a clinical point of view, these findings agree with the previous study, which reported that an increase in the radiographical density in the experimentally induced large-size bone defect may take longer (Mabrouk *et al.*, 2021).

The radiographical observation in the second group showed the healing process of the mandibular defect without osteomyelitis or excessive callus formation, suggesting that quail shell Calcium hydroxide has anti-bacterial effects related to a high PH value which is about ( 12.5-12.8) (Mohammadi and Dummer, 2011; Nirwana *et al.*, 2021), the higher pH level is considered to be unsuitable for a wide variety of microbes. The hydroxyl ions (OH<sup>-</sup>), which contribute to calcium hydroxide's alkaline pH and are powerful, reactive, and bioactive radicals, are essential to the compound's action mechanism. The cytoplasmic membrane, proteins, and DNA of bacteria are all susceptible to denaturation and destruction by

hydroxyl ions, which is why these ions can kill bacterial cells (Stojanović *et al.*, 2018).

According to the current radiographical evaluations through our research, we found that the mandibular defect in the second group filled faster compared with the control group through an increase in the defect density, which indicates that calcium hydroxide has good biocompatibility and can induce bone repair through the formation of newly mineralized bone tissue without immune reaction. These findings align with those mentioned by Liu *et al.* (2023), who demonstrated that calcium hydroxide's alkaline properties can neutralize the acidic environment in a bone defect area. This, in turn, promotes the proliferation and migration of osteogenic cells, ultimately stimulating bone tissue formation. Although, in the second group, the radiology of the mandibular bone defect did not wholly become radiopaque at 60 postoperative days, the significant decrease in the bone bridge formation may be related to the formation of a coagulative necrosis zone in the region of contact of this biomaterial with the bone tissue, may be due to the increase in alkalinity, which has similarly been reported by (Benetti *et al.*, 2019). Furthermore, a recent study mentioned that tissue irritation caused by a high alkaline Ph level of calcium hydroxide could stimulate fibroblast proliferation and lead to excessive fibrous tissue formation along the defect margin (Pribadi *et al.*, 2020).

In addition, the radiographical images also showed there were no bone resorption or any noticeable changes in bone osteomyelitis; these results were in agreement with the results mentioned by (Nelson-Filho *et al.*, 2002), whose radiographically studied the effect of calcium hydroxide on apical and Periapical tissues of dogs, and concluded that calcium hydroxide effectively detoxifies the bacterial endotoxin from the tissue ( Best *et al.*, 2021), also, these radiographical findings accordance with

current macroscopical results of this study, that showed formation of fibrous tissue around the bone defect as compared with oyster shell HA and fourth groups.

The radiographical observations of the third group revealed an increase in bone density and great bone formation (radiopaque images) at 60 days after surgery when compared with the second group, suggesting that HA has excellent bone conductive properties due to similar chemical and crystallographic structure with that of natural bone (Mahfuri *et al.*, 2022). In addition, Anitha *et al* (2017) discovered that hydroxyapatite is considered a resorbable filling material that contains no organic material and, hence, does not induce any allergic reaction (Anitha *et al.*, 2017). Another study suggested hydroxyapatite shows faster osteoconductive properties than other calcium phosphate-based biomaterials (Geus *et al.*, 2020). Furthermore, a study demonstrated that the body's extracellular fluid induces the disintegration of the hydroxyapatite granules, allowing the gradual growth of bone tissue into the defect without the interposition of fibrous tissue (Kwon *et al.*, 2013).

Additionally, there was a gradual rise in the density observed in the third group, starting from day 15 after the operation until the end of the current experiment. This suggests that new bone formation increased alongside the proliferation of osteoblasts, which was strongly influenced by the high concentrations of calcium, phosphate, and hydroxyl ions present in the chemical formula of hydroxyapatite. Subsequently, these ions are adsorbed on the host surface, and they can promote cell adhesion and directly affect osteogenesis. In agreement with this idea, a previous study showed that hydroxyapatite possesses a potential regenerative property in the cortical bone of the mandible in mature pigs (Vdoviaková *et al.*, 2023).

In the fourth group, the radiographical observations showed bone healing through a progressive rise in radiopacity until the end of this study, which showed nearly complete closure of the mandibular bone defect in this group. a study showed that many growth factors are released by the PRF gel, like PDGF, TGF-  $\beta$ , and VEGF. PDGF and TGF- $\beta$  support bone regeneration by promoting cell proliferation, cell differentiation, and motility (Revathy *et al.*, 2018). Another study suggested that the fibrin matrix of the PRF provides a scaffold to carry cells like platelets, leukocytes, and circulating stem cells into the matrix that are important to protect growth factors from proteolysis and assist in tissue regeneration (Bahammam and Attia, 2021). In this study, the fourth group showed a more radiopaque appearance in the mandibular defect 30 days after surgery. This indicated that the defect was filled with newly formed bone. At 60 days, the defect was completely closed and difficult to distinguish from the native bone compared to the other groups. These findings were in agreement with the previous study, which found an increase in the opacity of the tibial bone in dogs treated with PRF (El-shafey *et al.*, 2022).

### **5-9: Histopathological evaluations**

According to the histopathological perspective, the healing process of a bone fracture is as intricate as the cellular and molecular mechanisms involved in endochondral ossification and intramembranous bone formation (Xian *et al.*, 2004; He *et al.*, 2011). Histological investigation is the gold standard for the examination of bone development in bony defects. Nevertheless, there are some drawbacks to this method. For example, the histological sections only display a small portion of the cross-section. Therefore, it might not entirely depict the defect (Schortinghuis *et al.*, 2003). On the other hand, bone tissue healing is directly affected by the location and size of the bone lesion and mechanical stresses applied to the



injury. As a result, small lesions can heal on their own in a short amount of time, but larger defect sizes necessitate further surgical procedures to encourage the regeneration of bone tissue (Monfoulet *et al.*, 2010).

Several techniques for inducing bone fractures have been validated in animal studies. Therefore, many clinical studies suggested that the bone defect models must be experimentally easily accessible with low postoperative complications to thoroughly investigate the mechanisms of histopathological healing processes of the bone (Campbell *et al.*, 2003; Cui *et al.*, 2006). Thus, a study suggested that drill-hole bone defects are a relatively recent method used to investigate the histology of the bone healing process (Bromer *et al.*, 2022). According to many types of research, especially in dental, endodontic, and maxillofacial surgeries, bone necrosis surrounding the hole location is mainly caused by increased temperatures that result from the cutting process, which may affect the bone-healing process and lead to impaired response action of bone to implanted materials and even cause tissue necrosis or hemorrhage (Alam *et al.*, 2019; S. Li *et al.*, 2021).

Consequently, across all groups, our histological sections have revealed no clear indications of tissue necrosis or abnormal cellular activity (such as distraction of osteocytes) in the area of bone defect. This suggests that the drilling force caused neither heat production nor bone crack damage. Furthermore, osteocytes, considered the mechano-sensing cells of the bone matrix, are sensitive to mechanical strain around them. The typical appearance of osteocytes within the lacune in the native bone margin also indicated that mechanically loaded force was absent in the bone during the drilling technique (Alam *et al.*, 2019).

The histopathological scores showed a significant increase ( $P \leq 0.05$ ) in osteoblast, osteocytes, osteoclast formation, and bone trabeculae in the

fourth, third, and second groups compared to the control group at intervals of (7, 14, 30) days following surgery. Also, when comparing the fourth, third, and second groups with the control group, the histopathological score results revealed significant differences ( $p \leq 0.05$ ) at the beginning of immature and mature bone development at seven days post-surgery. In contrast to the second and third groups, the fourth group had much more bone maturation. These differences may related to the presence of growth factors within the PRF gel that differentiate the MSC into active osteoblasts and stimulate the production of further growth factors from surrounding blood vessels and can improve the osteogenesis process (Su *et al.*, 2018; Sadek *et al.*, 2023). Nevertheless, the PRF gel does not contain BMPse, which is considered the most important osteoinductive factor. Thus, we suggested that bone regeneration in the fourth group occurs through the osteoconductive properties of the PRF matrix's growth factors.

Furthermore, the presence of a large number of osteoblast cells around the newly formed woven bone tissue in both the third and fourth groups starts at the earlier period. Many recent studies indicated that the PRF matrix is rich in growth factors that have a direct effect on the proliferation of MSCs and then allow them to transform into osteoblasts, which in turn develop into osteocytes (Strauss *et al.*, 2020; de Lima Barbosa *et al.*, 2023). Hence, the current histopathological findings showed a high amount of mature bones formed in the last period of the present study. Accordingly, the histopathological results of the present investigation were consistent with the recent study that established the platelets and leucocytes, besides macrophages and cytokines present in the PRF matrix, have the potential effect of stimulating bone formation and contributing to the regeneration of mineralized tissue (Liu *et al.*, 2019). Also, this result agrees with the recent works that concluded that bone tissue improves with the use of PRF

gel when used in mandibular surgery (Castillo *et al.*, 2017; Sharma *et al.*, 2020).

Whereas, in the third group, the hydroxyapatite directly releases phosphate and calcium ions into the surrounding tissue, which can control osteoblast functions, causing a local ions supersaturation, increasing the number of binding sites for osteoblast cell receptors, and helping with the adsorption and retention of circulating osteogenic factors like BMPs, which are involved in osteogenesis. Accordingly, we agree with Polini and his colleague, who explained that calcium hydroxide ions provide a favorable environment with the ability to differentiate into osteoblasts and stimulate the osteogenesis process by gradually degrading the chemical dissolution of ions and finally replacing the newly formed bone tissue (Polini *et al.*, 2011). For this reason, we agree with recent studies that mention the process of bone formation begins with the implantation of apatite materials into the defect site. Over time, the apatite materials undergo degradation due to the chemical dissolution of ions and cell absorption. Eventually, the newly produced bone tissue takes its place (Schröter *et al.*, 2020). In addition, both in vitro and in vivo studies showed that hydroxyapatite suppressed osteoclastic bone resorption, increased proliferation and differentiation of osteoblasts, sped up bone remodeling in osteoporotic conditions, and improved osseointegration (Quan *et al.*, 2018). For instance, in the third group, the histopathological patterns showed more osteoconductive properties and less osteoinductive activity.

As a result, the current histopathological scores demonstrated that the bone was started bridged at seven days after surgery with a thin or loose woven bone in both the third and fourth groups. At the same time, there were no significant differences in the bone bridged formation in both QESCH and control groups. For this reason, we agree with the previous

study that observed the calcium hydroxide takes a longer time to activate osteoblasts, and the process begins with a gradual increase in tissue alkalinity to a PH of about (10.5), causing the osteoblasts to differentiate and grow (Kaskos, 2006). Also, many studies observed that the calcium hydroxide requires about (15-30) days after treatment to start calcification of the pulp root canals in experimental dogs (Holland *et al.*, 1982; Ammons, 2020). Researchers are wary of using calcium hydroxide on its own due to the strong alkaline environment and the severe cytotoxic effects of the pure powder of  $\text{Ca(OH)}_2$ . Consequently, some authors preferred to use calcium hydroxide combined with other materials to enhance rapid osteogenic activity. Li et al. (2018) suggested using the calcium hydroxide with ethyl cellulose encapsulated  $\text{Ca(OH)}_2$  to eliminate the cytotoxic effect of calcium hydroxide in the adjacent tissue and enhance fast osteogenic properties with prolonged antibacterial activity.

Moreover, many studies showed a strong correlation between fabricated biomaterial content, the size of particles size, and particle morphology (Figueiredo *et al.*, 2010; Coathup *et al.*, 2013; Ryabenkova *et al.*, 2017). Thus, the significant decreases in the amount of bone tissue and bone bridge formation in the QESCH compared with the third and fourth group may be related to the fabricated calcium hydroxide particles, which appeared in large, irregular morphology, which may affect the amount of bone formation. Our results are supported by the previous study that clarified that the large particles leave less space for the formation of new bone (Hruschka *et al.*, 2017).

Alternatively, the histopathological score showed no significant differences between different groups in the inflammatory response at 15 and 30 days after surgery, although it may have been present earlier in all groups. This indicated the surgical technique was under aseptic technique.

Besides, the selected site of the defect was suitable for evaluating the healing effect of experimentally large size bone defects. Thus, we agree with (Scelza *et al.*, 2016), who illustrated that the lowest inflammatory response maxillofacial surgery indicated that there is no potential source of irritation or cytotoxicity. The response to the inflammatory processes depends on the implant's surface, the implant's composition, and the manner of the bone defect (Velnar *et al.*, 2016). For this reason, when implanted, biomaterials integrate correctly with the surrounding tissue; however, the inflammatory process can resolve quickly (Xiao *et al.*, 2022). On the other hand, our histopathological section showed a prolonged inflammatory process in the control group related to the mechanical factor in which the mandibular bone defect was left empty without any filling materials, which immediately filled with hematoma rich in the inflammatory cells, and then gradually replaced with dense granulation tissue. Thus, we agree with the previous studies that illustrated that bone hematoma rich in Platelets, neutrophils, monocytes, and lymphocytes elevates the expression of the inflammatory mediators (Schmidt-Bleek *et al.*, 2014; Shiu *et al.*, 2018).

Furthermore, compared with the control group, the second, third, and fourth groups showed a marked significant difference in the distribution of newly formed bone tissue and blood vessels throughout the bone healing area, with an abundance of proliferating capillaries confined to the defect margin. These results were in agreement with many previous studies that showed that the blood vessels support newly formed trabecular bone formation during the bone defect process. Also, these researchers found that new blood vessels were highly located at the surface of trabecular bones during bone healing (Wang *et al.*, 2017). In addition, a study found

that impaired blood flow to the bone site can cause endochondral ossification to take longer or not happen at all (Lienau *et al.*, 2009).

During the 30 days after surgery, the histological sections demonstrated that the bone defect in the control group was caused by immature bone tissue formation, which was related to cartilaginous callus formation. While in the treated groups, the histological sections showed that the bone defect was filled with varying amounts of mature bone formation. Also, the histopathological results demonstrated that the regenerated process of the mandibular bone defect occurs with endochondral ossification. Therefore, the histopathological outcome was in agreement with a recent study that mentioned the large bone defect healing via endochondral ossification (Vasileva and Chaprazov, 2023). The histopathological sections of the control group showed fibrous tissue filling the defect, which separated it from the surrounding normal bone tissues. This layer remained until the end of the current study, while in the second, third, and fourth, it started to disappear at 15 days and entirely disappeared by the end of the present study.

## **5-10: Immunohistochemistry**

The immunohistochemical evaluations provide an additional level of evidence related to the early response of biomaterials following implantation. ALP is a marker enzyme produced by progenitor or maturing osteoblasts. Also, several osteoblasts lining the trabecular bone showed positive immunostaining for alkaline phosphatase on day 25 after the bone defect, and some cells lining the bone bridge expressed alkaline phosphatase (Xian *et al.*, 2004). There are many isoforms of bone ALP, all of which function as enzymes. The (B1x) isoform is typical of healthy bone. Isoforms B1 and B2 (Haarhaus *et al.*, 2009; Steinerova *et al.*, 2023). for example, exhibit varying degrees of enzymatic activity in various bone

tissues; for example, trabecular bone exhibits higher levels of B2 activity than cancellous bone, while the cortical bone exhibits higher levels of B1 activity (Magnusson and Farley, 2002). Thus, ALP was also detected around the remaining bone substitute particles, the surface of cartilage, and the surface of the newly formed bone (Cha *et al.*, 2021). Therefore, any positive expression that appeared on the surface of the bone indicated the osteogenic activity of ALP (Li *et al.*, 2018).

Conversely, ALP has also been shown to be expressed by other cells in the defect area of the bone, including granulocytes, especially in the secretory vesicles of osteoblast or on the plasma membrane of neutrophils, which is a product of the nonspecific bone ALP during an inflammatory process (Garattini and Gianni, 1996). Therefore, in the control group, during 30 days after surgery, the immunohistochemistry results showed a very weak ALP expression related to the presence of the granulocytes in the connective tissue. In the second group, the mild positive expression of ALP may be related to high calcium hydroxide PH in the bone tissue, inhibiting the ALP activity (Rajan *et al.*, 2008). While in the third group, we found a moderate positive expression of ALP activity. We agree with the previous result that suggested the ALP function may require large amounts of extracellular calcium and phosphate. Thus, the presence of hydroxyapatite can enhance ALP expression activities (Vimalraj, 2020); while other study suggested that the positive expression of ALP phosphatase in the bone defects area treated with calcium phosphate-based biomaterials were considered inductive materials for ALP activity (Walsh *et al.*, 2017).

On the other hand, the increase in the positive expression of ALP in the fourth group agrees with the previous study that demonstrated that the PRF gel can increase the expression of osteocalcin in osteoblasts and can



stimulate the osteoblast proliferation and finally increase the expression of ALP (Nugraha *et al.*, 2018), indicated that PRF can promote osteogenic proliferation and differentiation. Consequently, we agree with the previous work that clarified that the PRF gel possesses excellent biocompatibility without inducing any cell apoptosis or cell death (Wang *et al.*, 2018).

## **Conclusions**

1. Natural bone substitutes fabricated from recycled oyster shells and quail egg shells by using the hydrothermal method are easily available, economical, and environmentally friendly.
2. The different biomaterials, which include, fabricated calcium hydroxide powder of quail egg shells, fabricated hydroxyapatite powder of oyster shells, and platelets rich fibrin were showed the ability to repair the large mandibular bone defect.
3. The ability of FESEM images to clearly identify the osteoid matrix and the fibrous tissue deposited in the defective area.
4. According to the analysis of obtained results, the filling of mandibular bone defect with PRF gel was considered very better rather than fabricated calcium hydroxide powder of quail egg shells and fabricated hydroxyapatite powder of oyster shells.

## **Recommendations**

1. Investigate the efficacy of using PRF gel in conjunction with calcium hydroxide from quail eggs or hydroxyapatite from oysters in the form of gelatin sponges for the filling of bone deficiencies.
2. Add other bioactive materials to calcium hydroxide, such as concentrated growth factors, to improve its osteoconductive characteristics.
3. Add natural source fabricated biological polymer such as (collagen, cellulose, or hyaluronic acid) to the PRF gel to increase its consistency and provide its solidity when applied to the segmental bone defects.
4. Preparation of gelatin sponge loaded with PRF and coated with calcium hydroxide or hydroxyapatite as a scaffold for reconstruction of segmental bone defects.
5. Adding the potassium and phosphor minerals to calcium hydroxide powder to enhance its bone healing activities.

## References

- Abbasian, M.; Massoumi, B.; Mohammad-Rezaei, R.; Samadian, H., and Jaymand, M. (2019). Scaffolding polymeric biomaterials: Are naturally occurring biological macromolecules more appropriate for tissue engineering? *International journal of biological macromolecules*. 134: 673-694.
- Abdulghani, S., and Mitchell, G. R. (2019). Biomaterials for in situ tissue regeneration: A review. *Biomolecules*. 9(11): 750.
- Abdullaev Sh.Yu., Khalilov A.A., Yusupova D.Z., Zaynutdinov M.O., Dadaboyeva M.U. (2021). Complications in the treatment of mandibular fractures Literature review. in *Library*. 21(1): 684-691.
- Adams, D. R. (2004). *Canine anatomy: a systemic study*. Iowa State Press.
- Affshana, M. M., and Priya, J. (2015). Healing mechanism in bone fracture. *Journal of pharmaceutical sciences and research*. 7(7): 441.
- Akinbami, B. (2016). Reconstruction of continuity defects of the mandible with non-vascularized bone grafts. *Systematic literature review. Craniomaxillofacial Trauma & Reconstruction*. 9(3): 195-205.
- Akyol, S.; Ben Nissan, B.; Karacan, I.; Yetmez, M.; Gokce, H.; Suggett, D., and Oktar, F. (2019). Morphology, characterization, and conversion of the corals *Goniopora* spp. and *Porites cylindrica* to hydroxyapatite. *Journal of the Australian Ceramic Society*. 55 (20019): 893-901.
- Al-Hiyasat, A. S.; El-Farraj, H. S., and Alebrahim, M. A. (2021). The effect of calcium hydroxide on dentine composition and root fracture resistance of human teeth: An in vitro study. *European Journal of Oral Sciences*. 129(4): e12798.
- Al Maruf, D. A.; Parthasarathi, K.; Cheng, K.; Mukherjee, P.; McKenzie, D. R.; Crook, J. M., and Clark, J. R. (2023). Current and future

- perspectives on biomaterials for segmental mandibular defect repair. *International Journal of Polymeric Materials and Polymeric Biomaterials*. 72(9): 725-737.
- Alam, K.; Al-Ghaithi, A.; Piya, S., and Saleem, A. (2019). In-vitro experimental study of histopathology of bone in vibrational drilling. *Medical engineering & physics*. 67(2019): 78-87.
- Albrektsson, T., and Johansson, C. (2001). Osteoinduction, osteoconduction and osseointegration. *European spine journal*. 10(Suppl 2): S96-S101.
- Ali, S. H.; Almaatoq, M. M., and Mohamed, A. S. (2013). Classifications, surface characterization and standardization of nanobiomaterials. *International Journal of Engineering & Technology*. 2(3): 187.
- Alonzo, M.; Primo, F. A.; Kumar, S. A.; Mudloff, J. A.; Dominguez, E.; Fregoso, G., and Joddar, B. (2021). Bone tissue engineering techniques, advances, and scaffolds for treatment of bone defects. *Current opinion in biomedical engineering*. 17(2021): 100248.
- Ammons, C. L. (2020). *Outcome Assessment of Teeth with Necrotic Pulps and Apical Periodontitis Treated with Long-Term Calcium Hydroxide*. The University of North Carolina at Chapel Hill,
- André, S. B.; Tavares, P. M. H.; da Silva, M. P.; de Jesus, L. K.; Hadad, H.; Bizelli, V. F., and de Carvalho, P. S. P. (2022). Microscopic analysis of the repair of critical bone defects in rabbits calvaria after the use of particulated autogenous bone or particulate autogenous bone associated with inorganic biomaterial. *Research, Society and Development*. 11(5): e55211526709-e55211526709.
- Anesi, A.; Di Bartolomeo, M.; Pellacani, A.; Ferretti, M.; Cavani, F.; Salvatori, R., and Chiarini, L. (2020). Bone healing evaluation following different osteotomic techniques in animal models: A

- suitable method for clinical insights. *Applied Sciences*. 10(20): 7165.
- Anitha, C.; Senthilkumar, S.; Rajasekar, S.; Arun, R., and Srinivasan, S. (2017). Platelet rich fibrin and nanocrystalline hydroxyapatite: Hope for regeneration in aggressive periodontitis: A novel clinical approach. *International Journal of Applied Dental Sciences* 3(2017): 209-214.
- Arnett, T. R., and Orriss, I. R. (2018). Metabolic properties of the osteoclast. *Bone*. 115(2018): 25-30.
- Arzi, B.; Stover, S. M.; Garcia, T. C.; Leale, D. M., and Verstraete, F. J. (2016). Biomechanical evaluation of two plating configurations for critical-sized defects of the mandible in dogs. *American Journal of Veterinary Research*. 77(5): 445-451.
- Atayde, L. M.; Cortez, P. P.; Afonso, A.; Santos, M.; Mauricio, A. C., and Santos, J. D. (2015). Morphology effect of bioglass-reinforced hydroxyapatite (Bonelike((R)) ) on osteoregeneration. *J Biomed Mater Res B Appl Biomater*. 103(2): 292-304.
- Atiyah, A. G.; Al-Falahi, N. H. R., and Zarraq, G. A. (2021). Synthesis and Characterization of Porous  $\beta$ -Calcium Pyrophosphate Bone Scaffold Derived from Avian Eggshell. *Pakistan journal of zoology*.54(3):1001-1500.
- Ausenda, F.; Rasperini, G.; Acunzo, R.; Gorbunkova, A., and Pagni, G. (2019). New perspectives in the use of biomaterials for periodontal regeneration. *Materials*. 12(13): 2197.
- Bahammam, M. A., and Attia, M. S. (2021). Expression of vascular endothelial growth factor using platelet rich fibrin (PRF) and nanohydroxyapatite (nano-HA) in treatment of periodontal intra-bony defects-a randomized controlled trial. *Saudi journal of biological sciences*. 28(1): 870-878.

- Balanta-Melo, J.; Toro-Ibacache, V.; Kupczik, K., and Buvinic, S. (2019). Mandibular bone loss after masticatory muscles intervention with botulinum toxin: an approach from basic research to clinical findings. *Toxins*. 11(2): 84.
- Barbeck, M.; Alkildani, S., and Jung, O. (2023). Biology of Ceramic Bone Substitutes. In *Bioceramics, Biomimetic and Other Compatible Materials Features for Medical Applications*. Springer Nature.
- Barbeck, M.; Jung, O.; Smeets, R.; Gosau, M.; Schnettler, R.; Rider, P., . . . Korzinskas, T. (2020). Implantation of an injectable bone substitute material enables integration following the principles of guided bone regeneration. *in vivo*. 34(2): 557-568.
- Benetti, F.; de Azevedo Queiroz, Í. O.; Oliveira, P. H. C. d.; Conti, L. C.; Azuma, M. M.; Oliveira, S. H. P. d., and Cintra, L. T. A. (2019). Cytotoxicity and biocompatibility of a new bioceramic endodontic sealer containing calcium hydroxide. *Brazilian oral research*. 33(2019): e042-e042.
- Best, S.; Ammons, C. L.; Karunanayake, G. A.; Saemundsson, S. R., and Tawil, P. Z. (2021). Outcome assessment of teeth with necrotic pulps and apical periodontitis treated with long-term calcium hydroxide. *Journal of endodontics*. 47(1): 11-18.
- Best, S.; Porter, A.; Thian, E., and Huang, J. (2008). Bioceramics: Past, present and for the future. *Journal of the European Ceramic Society*. 28(7): 1319-1327.
- Best, S.; Ammons, C. L.; Karunanayake, G. A.; Saemundsson, S. R., and Tawil, P. Z. (2021). Outcome assessment of teeth with necrotic pulps and apical periodontitis treated with long-term calcium hydroxide. *Journal of endodontics*. 47(1): 11-18 .



- Bhalla, V. K., and Chockattu, S. J. (2021). Intracanal delivery of calcium hydroxide: a literature review. *Saudi Endodontic Journal*. 11(1): 1-6.
- Borciani, G.; Fischetti, T.; Ciapetti, G.; Montesissa, M.; Baldini, N., and Graziani, G. (2022). Marine biological waste as a source of hydroxyapatite for bone tissue engineering applications. *Ceramics International*. 49(2), 1572-1584.
- Brinker, W. O.; Piermattei, D. L., and Flo, G. L. (1983). *Handbook of small animal orthopedics and fracture treatment*. WB Saunders Co.
- Bromer, F. D.; Brent, M. B.; Thomsen, J. S., and Brüel, A. (2022). Drill-Hole Bone Defects in Animal Models of Bone Healing: Protocol for a Systematic Review. *JMIR Research Protocols*. 11(7): e34887.
- Brown, J. S.; Barry, C.; Ho, M., and Shaw, R. (2016). A new classification for mandibular defects after oncological resection. *The Lancet Oncology*. 17(1): e23-e30.
- Buchbender, M.; Neukam, F. W.; Lutz, R., and Schmitt, C. M. (2018). Treatment of enucleated odontogenic jaw cysts: a systematic review. *Oral surgery, oral medicine, oral pathology and oral radiology*. 125(5): 399-406.
- Buck, D. W., and Dumanian, G. A. (2012). Bone biology and physiology: Part I. The fundamentals. *Plastic and reconstructive surgery*. 129(6): 1314-1320.
- Burr, D. B. (2019). Bone morphology and organization. In *Basic and applied bone biology*. Elsevier.
- Buss, D. J.; Kröger, R.; McKee, M. D., and Reznikov, N. (2022). Hierarchical organization of bone in three dimensions: A twist of twists. *Journal of Structural Biology: X*. 6(2022): 100057.
- Calcei, J. G., and Rodeo, S. A. (2019). Orthobiologics for bone healing. *Clinics in sports medicine*. 38(1): 79-95.

- Campbell, T.; Wong, W., and Mackie, E. (2003). Establishment of a model of cortical bone repair in mice. *Calcified tissue international*. 73(2003): 49-55.
- Caramês, J. M. M.; Vieira, F. A.; Caramês, G. B.; Pinto, A. C.; Francisco, H. C. O., and Marques, D. N. d. S. (2022). Guided bone regeneration in the edentulous atrophic maxilla using Deproteinized Bovine Bone Mineral (DBBM) combined with platelet-rich fibrin (PRF) a prospective study. *Journal of Clinical Medicine*. 11(3): 894.
- Caruana, A.; Savina, D.; Macedo, J. P., and Soares, S. C. (2019). From platelet-rich plasma to advanced platelet-rich fibrin: biological achievements and clinical advances in modern surgery. *European journal of dentistry*. 13(02): 280-286.
- Castejón-González, A. C.; Stefanovski, D., and Reiter, A. M. (2022). Etiology, Clinical Presentation, and Outcome of Mandibular Fractures in Immature Dogs Treated with non-Invasive or Minimally Invasive Techniques. *Journal of Veterinary Dentistry*. 39(1): 78-88.
- Castillo, G. F. G.; Miranda, M. E. P.; Bojorque, J. A. B.; Barragán, K. I. N., and García, D. V. S. (2017). Gingival and bone tissue healing in lower third molar surgeries. Comparative study between use of platelet rich fibrin versus physiological healing. *Revista odontológica mexicana*. 21(2): 114-120.
- Cestari, F.; Agostinacchio, F.; Galotta, A.; Chemello, G.; Motta, A., and M. Sglavo, V. (2021). Nano-hydroxyapatite derived from biogenic and bioinspired calcium carbonates: synthesis and in vitro bioactivity. *Nanomaterials*. 11(2): 264.
- Cestari, F.; Chemello, G.; Galotta, A., and Sglavo, V. M. (2020). Low-temperature synthesis of nanometric apatite from biogenic sources. *Ceramics International*. 46(15): 23526-23533.

- Cha, J. K.; Pla, R.; Vignoletti, F.; Jung, U. W.; Sanz-Esporrin, J., and Sanz, M. (2021). Immunohistochemical characteristics of lateral bone augmentation using different biomaterials around chronic peri-implant dehiscence defects: an experimental in vivo study. *Clinical oral implants research*. 32(5): 569-580.
- Chaikina, M. V.; Bulina, N. V.; Vinokurova, O. B.; Prosanov, I. Y., and Dudina, D. V. (2019). Interaction of calcium phosphates with calcium oxide or calcium hydroxide during the “soft” mechanochemical synthesis of hydroxyapatite. *Ceramics International*. 45(14): 16927-16933.
- Chao, Y.-L.; Lin, L.-D.; Chang, H.-H., and Wang, T.-M. (2021). Preliminary evaluation of BMP-2-derived peptide in repairing a peri-implant critical size defect: A canine model. *Journal of the Formosan Medical Association*. 120(5): 1212-1220.
- Chávez Guerrero, L.; Garza-Cervantes, J.; Caballero-Hernández, D.; González-López, R.; Sepúlveda-Guzmán, S., and Cantú-Cárdenas, E. (2017). Synthesis and characterization of calcium hydroxide obtained from agave bagasse and investigation of its antibacterial activity. *Revista internacional de contaminación ambiental*. 33(2): 347-353.
- Chen, L.; Zheng, L.; Jiang, J.; Gui, J.; Zhang, L.; Huang, Y., and Fan, Y. (2016). Calcium hydroxide-induced proliferation, migration, osteogenic differentiation, and mineralization via the mitogen-activated protein kinase pathway in human dental pulp stem cells. *Journal of endodontics*. 42(9): 1355-1361.
- Chen, W.; Wu, Y.; Xie, Z.; Li, Y.; Tang, W., and Yu, J. (2022). Calcium hydroxide recycled from waste eggshell resources for the effective recovery of fluoride from wastewater. *RSC advances*. 12(43): 28264-28278.

- Cheng, C., and Shoback, D. (2019). Mechanisms underlying normal fracture healing and risk factors for delayed healing. *Current Osteoporosis Reports*. 17: 36-47.
- Chiroff, R. T.; White, E. W.; Weber, J. N., and Roy, D. M. (1975). Tissue ingrowth of replamineform implants. *Journal of biomedical materials research*. 9(4): 29-45.
- Chou, J.; Valenzuela, S.; Santos, J.; Bishop, D.; Milthorpe, B.; Green, D., and Ben-Nissan, B. (2014). Strontium-and magnesium-enriched biomimetic  $\beta$ -TCP microspheres with potential for bone tissue morphogenesis. *Journal of tissue engineering and regenerative medicine*. 8(10): 771-778.
- Coathup, M. J.; Cai, Q.; Campion, C.; Buckland, T., and Blunn, G. W. (2013). The effect of particle size on the osteointegration of injectable silicate-substituted calcium phosphate bone substitute materials. *Journal of Biomedical Materials Research Part B: Applied Biomaterials*. 101(6): 902-910.
- Cinti, F.; Rossanese, M.; Buracco, P.; Pisani, G.; Vallefucio, R.; Massari, F., and Cantatore, M. (2021). Complications between ventral and lateral approach for mandibular and sublingual sialoadenectomy in dogs with sialoceles. *Veterinary Surgery*. 50(3): 579-587.
- Cirstea, A. C.; Gheorghita, L.; Diaconu, O. A.; Bataiosu, M.; Georgescu, R. V., and Dascalu, I. (2020). Bioceramic-based root canal sealers: a review. *Rom J Oral Rehabil*. 12(3): 48-54.
- Cordonnier, T.; Sohier, J.; Rosset, P., and Layrolle, P. (2011). Biomimetic materials for bone tissue engineering—state of the art and future trends. *Advanced Engineering Materials*. 13(5): B135-B150.
- Cui, Q.; Xiao, Z.; Li, X.; Saleh, K. J., and Balian, G. (2006). Use of genetically engineered bone-marrow stem cells to treat femoral

- defects: an experimental study. *The Journal of Bone and Joint Surgery*. 88(suppl\_3): 167-172.
- Culla, A. C.; Vater, C.; Tian, X.; Bolte, J.; Ahlfeld, T.; Bretschneider, H., and Zwingenberger, S. (2022). Treatment of Critical Size Femoral Bone Defects with Biomimetic Hybrid Scaffolds of 3D Plotted Calcium Phosphate Cement and Mineralized Collagen Matrix. *International Journal of Molecular Sciences*. 23(6): 3400.
- Da Rosa, W.; Lima, V.; Moraes, R.; Piva, E., and Da Silva, A. (2019). Is a calcium hydroxide liner necessary in the treatment of deep caries lesions? A systematic review and meta-analysis. *International endodontic journal*. 52(5): 588-603.
- Dako, T.; Pop, M.; Fulop, J.; Kantor, J., and Monea, M. (2020). The use of calcium hydroxide as an intracanal medicament in the treatment of large periapical lesions. A review. *Acta Medica Transilvanica*. 25(2): 58-60.
- Damia, C.; Marchat, D.; Lemoine, C.; Douard, N.; Chaleix, V.; Sol, V., and Champion, E. (2019). Functionalization of phosphocalcic bioceramics for bone repair applications. *Materials Science and Engineering: C*. 95(2019): 343-354.
- DAVID, F. (1986). Definitions in biomaterials: proceedings of a consensus conference of the European Society for Biomaterials. In: London, Elsevier.
- De Lima Barbosa, R.; Stellet Lourenço, E.; de Azevedo dos Santos, J. V.; Rodrigues Santiago Rocha, N.; Mourão, C. F., and Alves, G. G. (2023). The Effects of Platelet-Rich Fibrin in the Behavior of Mineralizing Cells Related to Bone Tissue Regeneration—A Scoping Review of In Vitro Evidence. *Journal of functional biomaterials*. 14(10): 503.

- Dec, P.; Modrzejewski, A., and Pawlik, A. (2023). Existing and Novel Biomaterials for Bone Tissue Engineering. *International Journal of Molecular Sciences*. 24(1): 529.
- Dohan, D. M.; Choukroun, J.; Diss, A.; Dohan, S. L.; Dohan, A. J.; Mouhyi, J., and Gogly, B. (2006a). Platelet-rich fibrin (PRF): a second-generation platelet concentrate. Part I: technological concepts and evolution. *Oral Surgery, Oral Medicine, Oral Pathology, Oral Radiology, and Endodontology*. 101(3): e37-e44.
- Dohan, D. M.; Choukroun, J.; Diss, A.; Dohan, S. L.; Dohan, A. J.; Mouhyi, J., and Gogly, B. (2006b). Platelet-rich fibrin (PRF): a second-generation platelet concentrate. Part II: platelet-related biologic features. *Oral Surgery, Oral Medicine, Oral Pathology, Oral Radiology, and Endodontology*. 101(3): e45-e50.
- Doppalapudi, S.; Jain, A.; Khan, W., and Domb, A. J. (2014). Biodegradable polymers—an overview. *Polymers for Advanced Technologies*. 25(5): 427-435.
- Duchamp de Lageneste, O.; Julien, A.; Abou-Khalil, R.; Frangi, G.; Carvalho, C.; Cagnard, N., and Colnot, C. (2018). Periosteum contains skeletal stem cells with high bone regenerative potential controlled by Periostin. *Nature communications*. 9(1): 773.
- Dziadek, M.; Zagrajczuk, B.; Menaszek, E., and Cholewa-Kowalska, K. (2018). A new insight into in vitro behaviour of poly ( $\epsilon$ -caprolactone)/bioactive glass composites in biologically related fluids. *Journal of materials science*. 53(6): 3939-3958.
- Earl, J.; Wood, D., and Milne, S. (2006). *Hydrothermal synthesis of hydroxyapatite*. *Journal of Physics: Conference Series*.26(1):268.
- Eick, S.; Strugar, T.; Miron, R. J., and Sculean, A. (2014). In vitro-activity of oily calcium hydroxide suspension on microorganisms as well as

- on human alveolar osteoblasts and periodontal ligament fibroblasts. BMC oral health. 14(1): 1-10.
- Einhorn, T. A., and Gerstenfeld, L. C. (2015). Fracture healing: mechanisms and interventions. Nature Reviews Rheumatology. 11(1): 45-54.
- El-shafey, S. A.; El-Mezyen, A. E.-m. F.; Behery, A. S., and Abd El Raouf, M. (2022). Comparing efficacy of the platelet rich plasma and advanced platelet rich fibrin on tibial bone defect regeneration in dogs. Iraqi Journal of Veterinary Sciences. 36(4): 973-980.
- Elhamshary, A. A. S.; El Said, M. A.; Gabal, S., and Hassan, M. E. (2023). Value of Platelet Rich Fibrin as Surgical Adjuvant in Management of Mandibular Fracture. Benha Medical Journal. 40(special issue): 365-374.
- Elliott, D.; Newman, K.; Forward, D.; Hahn, D.; Ollivere, B.; Kojima, K., and Smith, R. (2016). A unified theory of bone healing and nonunion: BHN theory. The bone & joint journal. 98(7): 884-891.
- Esmailkhanian, A.; Sharifianjazi, F.; Abouchenari, A.; Rouhani, A.; Parvin, N., and Irani, M. (2019). Synthesis and characterization of natural nano-hydroxyapatite derived from turkey femur-bone waste. Applied biochemistry and biotechnology. 189(2019): 919-932.
- Evans, H. E., and De Lahunta, A. (2012). Miller's anatomy of the dog-E-Book. England. Elsevier health sciences.
- Faot, F.; Deprez, S.; Vandamme, K.; Camargos, G. V.; Pinto, N.; Wouters, J., and Duyck, J. (2017). The effect of L-PRF membranes on bone healing in rabbit tibiae bone defects: micro-CT and biomarker results. Scientific Reports. 7(1): 1-10.
- Farshidfar, N.; Amiri, M. A.; Jafarpour, D.; Hamedani, S.; Niknezhad, S. V., and Tayebi, L. (2022). The feasibility of injectable PRF (I-PRF) for bone tissue engineering and its application in oral and



- maxillofacial reconstruction: from bench to chairside. *Biomaterials Advances*. 134(2022): 112557.
- Farshidfar, N.; Jafarpour, D.; Firoozi, P.; Sahmeddini, S.; Hamedani, S.; de Souza, R. F., and Tayebi, L. (2022). The application of injectable platelet-rich fibrin in regenerative dentistry: A systematic scoping review of In vitro and In vivo studies. *Japanese Dental Science Review*. 58: 89-123.
- Feng, M.; Wang, Y.; Zhang, P.; Zhao, Q.; Yu, S.; Shen, K., and Zhang, Y. (2020). Antibacterial effects of platelet-rich fibrin produced by horizontal centrifugation. *International Journal of Oral Science*. 12(1): 32.
- Fernández-Medina, T.; Vaquette, C., and Ivanovski, S. (2019). Systematic comparison of the effect of four clinical-grade platelet rich hemoderivatives on osteoblast behaviour. *International Journal of Molecular Sciences*. 20(24): 6243.
- Fernandez de Grado, G.; Keller, L.; Idoux-Gillet, Y.; Wagner, Q.; Musset, A.-M.; Benkirane-Jessel, N., and Offner, D. (2018). Bone substitutes: a review of their characteristics, clinical use, and perspectives for large bone defects management. *Journal of tissue engineering*. 9(2018): 2041731418776819.
- Fiume, E.; Magnaterra, G.; Rahdar, A.; Verné, E., and Baino, F. (2021). Hydroxyapatite for biomedical applications: A short overview. *Ceramics*. 4(4): 542-563.
- Florencio-Silva, R.; Sasso, G. R. d. S.; Sasso-Cerri, E.; Simões, M. J., and Cerri, P. S. (2015). Biology of bone tissue: structure, function, and factors that influence bone cells. *BioMed Research International*. 2015.
- Fossum, T. W. (2018). *Small Animal Surgery E-Book*. England. Elsevier Health Sciences.

- Figueiredo, M.; Henriques, J.; Martins, G.; Guerra, F.; Judas, F., and Figueiredo, H. (2010). Physicochemical characterization of biomaterials commonly used in dentistry as bone substitutes—comparison with human bone. *Journal of Biomedical Materials Research Part B: Applied Biomaterials: An Official Journal of The Society for Biomaterials, The Japanese Society for Biomaterials, and The Australian Society for Biomaterials and the Korean Society for Biomaterials*. 92(2): 409-419.
- Furmanik, M., and Shanahan, C. M. (2018). ER stress regulates alkaline phosphatase gene expression in vascular smooth muscle cells via an ATF4-dependent mechanism. *BMC research notes*. 11(1): 1-8.
- Gaidash, A.; Blinova, M.; Aleksandrova, S.; Nashchekina, Y. A.; Krutko, V.; Musskaya, O., and Kulak, A. (2022). Morphogenesis of Osteoid Structures during Cultivation of Mesenchymal Stromal Cells on Fibrillary Collagen in the Presence of Silicoaluminophosphate. *Cell and Tissue Biology*. 16(1): 52-64.
- Gao, C.; Peng, S.; Feng, P., and Shuai, C. (2017). Bone biomaterials and interactions with stem cells. *Bone research*. 5(1): 1-33.
- Garattini, E., and Gianni, M. (1996). Leukocyte alkaline phosphatase a specific marker for the post-mitotic neutrophilic granulocyte: regulation in acute promyelocytic leukemia. *Leukemia & lymphoma*. 23(5-6): 493-503.
- Gautron, J.; Stapane, L.; Le Roy, N.; Nys, Y.; Rodriguez-Navarro, A., and Hincke, M. (2021). Avian eggshell biomineralization: an update on its structure, mineralogy and protein tool kit. *BMC Molecular and Cell Biology*. 22: 1-17.
- Georgiadis, M.; Müller, R., and Schneider, P. (2016). Techniques to assess bone ultrastructure organization: orientation and arrangement of

- mineralized collagen fibrils. *Journal of the Royal Society Interface*. 13(119): 20160088.
- Geus, J. L. d.; Antunes, S. R. M.; Alves, E. D. M.; Campagnoli, E. B.; Lara, É. d.; Santos, F. A. d., and Nakakogue, R. (2020). Histomorphometric and Radiographic Analysis of Biological Responses Following the Use of Pure Hydroxyapatite and Hydroxyapatite with Collagen. *Dental Oral Biology and Craniofacial Research*: 3(1):1-8.
- Ghanaati, S.; Booms, P.; Orlowska, A.; Kubesch, A.; Lorenz, J.; Rutkowski, J., and Choukroun, J. (2014). Advanced platelet-rich fibrin: a new concept for cell-based tissue engineering by means of inflammatory cells. *Journal of Oral Implantology*. 40(6): 679-689.
- Giannini, S.; Cielo, A.; Bonanome, L.; Rastelli, C.; Derla, C.; Corpaci, F., and Falisi, G. (2015). Comparison between PRP, PRGF and PRF: lights and shadows in three similar but different protocols. *Eur Rev Med Pharmacol Sci*. 19(6): 927-930.
- Ginebra, M.-P.; Espanol, M.; Maazouz, Y.; Bergez, V., and Pastorino, D. (2018). Bioceramics and bone healing. *EFORT open reviews*. 3(5): 173.
- Gollapudi, M.; Bajaj, P., and Oza, R. R. (2022). Injectable platelet-rich fibrin-a revolution in periodontal regeneration. *Cureus*. 14(8): e28647.
- Goloshchapov, D.; Kashkarov, V.; Rummyantseva, N.; Seredin, P.; Lenshin, A.; Agapov, B., and Domashevskaya, E. (2013). Synthesis of nanocrystalline hydroxyapatite by precipitation using hen's eggshell. *Ceramics International*. 39(4): 4539-4549.
- Green, D. W.; Ben-Nissan, B.; Yoon, K. S.; Milthorpe, B., and Jung, H.-S. (2017). Natural and synthetic coral biomineralization for human bone revitalization. *Trends in biotechnology*. 35(1): 43-54.

- Guex, A. G.; Poxson, D. J.; Simon, D. T.; Berggren, M.; Fortunato, G.; Rossi, R. M., and Rottmar, M. (2021). Controlling pH by electronic ion pumps to fight fibrosis. *Applied Materials Today*. 22(2021): 100936.
- Guzu, M., and Hennet, P. R. (2017). Mandibular body fracture repair with wire-reinforced interdental composite splint in small dogs. *Veterinary Surgery*. 46(8): 1068-1077.
- Haarhaus, M.; Fernström, A.; Magnusson, M., and Magnusson, P. (2009). Clinical significance of bone alkaline phosphatase isoforms, including the novel B1x isoform, in mild to moderate chronic kidney disease. *Nephrology Dialysis Transplantation*. 24(11): 3382-3389.
- Haines, N. M.; Lack, W. D.; Seymour, R. B., and Bosse, M. J. (2016). Defining the lower limit of a “critical bone defect” in open diaphyseal tibial fractures. *Journal of orthopaedic trauma*. 30(5): e158-e163.
- Hak, D. J.; Fitzpatrick, D.; Bishop, J. A.; Marsh, J. L.; Tilp, S.; Schnettler, R., and Alt, V. (2014). Delayed union and nonunions: epidemiology, clinical issues, and financial aspects. *Injury*. 45(2014): S3-S7.
- Härle, F., and Boudrieau, R. J. (2012). Maxillofacial bone healing. In *Oral and maxillofacial surgery in dogs and cats*. England. Elsevier.
- Hart, N. H.; Newton, R. U.; Tan, J.; Rantalainen, T.; Chivers, P.; Siafarikas, A., and Nimphius, S. (2020). Biological basis of bone strength: anatomy, physiology and measurement. *Journal of musculoskeletal & neuronal interactions*. 20(3): 347.
- Haugen, H. J.; Lyngstadaas, S. P.; Rossi, F., and Perale, G. (2019). Bone grafts: which is the ideal biomaterial? *Journal of clinical periodontology*. 46(2019): 92-102.

- Hawkins, J. J.; Torabinejad, M.; Li, Y., and Retamozo, B. (2015). Effect of three calcium hydroxide formulations on fracture resistance of dentin over time. *Dental Traumatology*. 31(5): 380-384.
- He, Y.-X.; Zhang, G.; Pan, X.-H.; Liu, Z.; Zheng, L.-z.; Chan, C.-W., and Wei, L. (2011). Impaired bone healing pattern in mice with ovariectomy-induced osteoporosis: A drill-hole defect model. *Bone*. 48(6): 1388-1400.
- Hellem, S., and Östrup, L. T. (1981). Normal and retrograde blood supply to the body of the mandible in the dog. II.: The role played by periosteal-medullary and symphyseal anastomoses. *International Journal of Oral Surgery*. 10(1): 31-42.
- Hermanson, J. W., and De Lahunta, A. (2018). *Miller and Evans' Anatomy of the Dog-E-Book*. Elsevier Health Sciences.
- Hench, L. L. (1991). Bioceramics: from concept to clinic. *Journal of the American Ceramic Society*. 74(7): 1487-1510.
- Henry, J. P., and Bordoni, B. (2022). Histology, osteoblasts. In *StatPearls [Internet]*: StatPearls Publishing.
- Hermanson, J. W., and De Lahunta, A. (2018). *Miller and Evans' Anatomy of the Dog-E-Book*. Elsevier Health Sciences.
- Hermanson, J. W., and DeLahunta, A. (2020). *Miller and Evans' anatomy of the dog*. Am Vet Med Assoc.
- Hjørting-Hansen, E., and Andreasen, J. (1971). Incomplete bone healing of experimental cavities in dog mandibles. *British Journal of Oral Surgery*. 9(1): 33-40.
- Holland, R.; Pinheiro, C. E.; de Mello, W.; Nery, M. J., and de Souza, V. (1982). Histochemical analysis of the dogs' dental pulp after pulp capping with calcium, barium, and strontium hydroxides. *Journal of endodontics*. 8(10): 444-447.

- Holmes, R. E. (1979). Bone regeneration within a coralline hydroxyapatite implant. *Plastic and reconstructive surgery*. 63(5): 626-633.
- Hruschka, V.; Tangl, S.; Ryabenkova, Y.; Heimel, P.; Barnewitz, D.; Möbus, G., Miller, C. (2017). Comparison of nanoparticulate hydroxyapatite pastes of different particle content and size in a novel scapula defect model. *Scientific Reports*. 7(1): 43425.
- Hsu, S.-m.; Raine, L., and Fanger, H. (1981). The use of antiavidin antibody and avidin-biotin-peroxidase complex in immunoperoxidase techniques. *American journal of clinical pathology*. 75(6): 816-821.
- Hsu, W. K.; Mishra, A.; Rodeo, S. R.; Fu, F.; Terry, M. A.; Randelli, P., . . . Kelly, F. B. (2013). Platelet-rich plasma in orthopaedic applications: evidence-based recommendations for treatment. *JAAOS-Journal of the American Academy of Orthopaedic Surgeons*. 21(12): 739-748.
- Huh, J.-Y.; Choi, B.-H.; Kim, B.-Y.; Lee, S.-H.; Zhu, S.-J., and Jung, J.-H. (2005). Critical size defect in the canine mandible. *Oral Surgery, Oral Medicine, Oral Pathology, Oral Radiology, and Endodontology*. 100(3): 296-301.
- Idumah, C. I. (2021). Progress in polymer nanocomposites for bone regeneration and engineering. *Polymers and Polymer Composites*. 29(5): 509-527.
- Ige, O. O.; Umoru, L. E., and Aribo, S. (2012). Natural products: a minefield of biomaterials. *International Scholarly Research Notices*. 2012(2012). 983062.
- Insuasti-Cruz, E.; Suárez-Jaramillo, V.; Mena Urresta, K. A.; Pila-Varela, K. O.; Fiallos-Ayala, X.; Dahoumane, S. A., and Alexis, F. (2022). Natural biomaterials from biodiversity for healthcare applications. *Advanced healthcare materials*. 11(1): 2101389.

- Islam, M. T.; Felfel, R. M.; Abou Neel, E. A.; Grant, D. M.; Ahmed, I., and Hossain, K. M. Z. (2017). Bioactive calcium phosphate-based glasses and ceramics and their biomedical applications: a review. *Journal of tissue engineering*. 8(2017): 2041731417719170.
- Ismail, R.; Laroybafih, M. B.; Fitriyana, D. F.; Nugroho, S.; Santoso, Y. I.; Hakim, A. J., Bayuseno, A. P. (2021). The effect of hydrothermal holding time on the characterization of hydroxyapatite synthesized from green mussel shells. *Journal of Advanced Research in Fluid Mechanics and Thermal Sciences*. 80(1): 84-93.
- Jasmine, S.; Thangavelu, A.; Janarthanan, K.; Krishnamoorthy, R., and Alshatwi, A. A. (2020). Antimicrobial and antibiofilm potential of injectable platelet rich fibrin—A second-generation platelet concentrate—Against biofilm producing oral staphylococcus isolates. *Saudi journal of biological sciences*. 27(1): 41-46.
- Jewer, D. D.; Boyd, J. B.; Manktelow, R. T.; Zuker, R. M.; Rosen, I. B.; Gullane, P., and Freeman, J. E. (1989). Orofacial and mandibular reconstruction with the iliac crest free flap: a review of 60 cases and a new method of classification. *Plastic and reconstructive surgery*. 84(3): 391-403.
- Jianpeampoolpol, B.; Phuminart, S., and Subbalekha, K. (2016). Platelet-rich fibrin formation was delayed in plastic tubes. *Br J Med Med Res*. 14(9): 1-9.
- Johnson, A. L.; Houlton, J. E., and Vannini, R. (2005). *AO principles of fracture management in the dog and cat*. Georg Thieme Verlag.
- Johnson, K. A. (2013). *Piermattei's Atlas of Surgical Approaches to the Bones and Joints of the Dog and Cat*. England. Elsevier Health Sciences.



- Kahler, S. L.; Shetty, S.; Andreasen, F. M., and Kahler, B. (2018). The effect of long-term dressing with calcium hydroxide on the fracture susceptibility of teeth. *Journal of endodontics*. 44(3): 464-469.
- Kalfas, I. H. (2001). Principles of bone healing. *Neurosurgical focus*. 10(4): 1-4.
- Kaneko, A.; Marukawa, E., and Harada, H. (2020). Hydroxyapatite nanoparticles as injectable bone substitute material in a vertical bone augmentation model. *in vivo*. 34(3): 1053-1061.
- Kaskos, H. (2006). The ability of Ca (OH) 2 to facilitate bone formation by measuring the alkaline phosphatase level (Experimental study). *Al-Rafidain Dental Journal*. 6(2): 130-135.
- Kattimani, V. S.; Kondaka, S., and Lingamaneni, K. P. (2016). Hydroxyapatite—Past, present, and future in bone regeneration. *Bone and Tissue Regeneration Insights*. 7(2016): BTRI. S36138.
- Kazimierczak, P., and Przekora, A. (2020). Osteoconductive and osteoinductive surface modifications of biomaterials for bone regeneration: A concise review. *Coatings*. 10(10): 971.
- Khan, S. R.; Jamil, S.; Rashid, H.; Ali, S.; Khan, S. A., and Janjua, M. R. S. A. (2019). Agar and egg shell derived calcium carbonate and calcium hydroxide nanoparticles: Synthesis, characterization and applications. *Chemical Physics Letters*. 732(2019): 136662.
- Khosropanah, H.; Lashkarizadeh, N.; Ayatollahi, M.; Kaviani, M., and Mostafavipour, Z. (2018). The impact of calcium hydroxide on the osteoinductive capacity of demineralized freeze-dried bone allograft: an in-vitro study. *Journal of Dentistry*. 19(1): 19.
- Khrunyk, Y.; Lach, S.; Petrenko, I., and Ehrlich, H. (2020). Progress in modern marine biomaterials research. *Marine drugs*. 18(12): 589.
- King, G. N.; Hermann, J. S.; Schoolfield, J. D.; Buser, D., and Cochran, D. L. (2002). Influence of the size of the microgap on crestal bone

- levels in non-submerged dental implants: A radiographic study in the canine mandible. *Journal of periodontology*. 73(10): 1111-1117.
- Klimek, K., and Ginalska, G. (2020). Proteins and peptides as important modifiers of the polymer scaffolds for tissue engineering applications-A review. *Polymers*. 12(4): 844.
- Knöfler, W.; Barth, T.; Graul, R., and Krampe, D. (2016). Retrospective analysis of 10,000 implants from insertion up to 20 years—analysis of implantations using augmentative procedures. *International journal of implant dentistry*. 2(2016): 1-10.
- Kosmidis, K.; Ehsan, K.; Pitzurra, L.; Loos, B., and Jansen, I. (2023). An in vitro study into three different PRF preparations for osteogenesis potential. *Journal of Periodontal Research*. 58(3): 483-492.
- Krishnakumar, S., and Senthilvelan, T. (2021). Polymer composites in dentistry and orthopedic applications-a review. *Materials Today: Proceedings*. 46(2021): 9707-9713.
- Kucko, N. W.; Herber, R.-P.; Leeuwenburgh, S. C., and Jansen, J. A. (2019). Calcium phosphate bioceramics and cements. In *Principles of Regenerative Medicine*. England. Elsevier.
- Kumar, K. R.; Genmorgan, K.; Rahman, S. A.; Rajan, M. A.; Kumar, T. A., and Prasad, V. S. (2016). Role of plasma-rich fibrin in oral surgery. *Journal of pharmacy & bioallied sciences*. 8(Suppl 1): S36.
- Kumar, V. V.; Jacob, P.; Ebenezer, S.; Kuriakose, M. A.; Kekatpure, V.; Baliarsing, A. S., and Wagner, W. (2016). Implant supported dental rehabilitation following segmental mandibular reconstruction-quality of life outcomes of a prospective randomized trial. *Journal of Cranio-Maxillofacial Surgery*. 44(7): 800-810.
- Kuwabara, A.; Uemura, M.; Toda, I.; Suwa, F., and Takemura, A. (2018). Microvascular architecture of the buccal periosteum of the

- mandibular body in the dog. *Journal of Osaka Dental University*. 52(2): 129-137.
- Kwon, B. J.; Kim, J.; Kim, Y. H.; Lee, M. H.; Baek, H. S.; Lee, D. H., .and Kwon, S. Y. (2013). Biological advantages of porous hydroxyapatite scaffold made by solid freeform fabrication for bone tissue regeneration. *Artificial Organs*. 37(7): 663-670.
- Lam, M. T., and Wu, J. C. (2012). Biomaterial applications in cardiovascular tissue repair and regeneration. *Expert review of cardiovascular therapy*. 10(8): 1039-1049.
- LeGeros, R. (1988). Calcium phosphate materials in restorative dentistry: a review. *Advances in dental research*. 2(1): 164-180.
- Lei, B.; Guo, B.; Rambhia, K. J., and Ma, P. X. (2019). Hybrid polymer biomaterials for bone tissue regeneration. *Frontiers of medicine*. 13(2019): 189-201.
- Lei, X.; Gao, J.; Xing, F.; Zhang, Y.; Ma, Y., and Zhang, G. (2019). Comparative evaluation of the physicochemical properties of nano-hydroxyapatite/collagen and natural bone ceramic/collagen scaffolds and their osteogenesis-promoting effect on MC3T3-E1 cells. *Regenerative Biomaterials*. 6(6): 361-371.
- Li, H.; Zhao, Y.; Li, W.; Yang, J., and Wu, H. (2016). Critical role of neutrophil alkaline phosphatase in the antimicrobial function of neutrophils. *Life sciences*. 157(2016): 152-157.
- Li, S.; Shu, L.; Kizaki, T.; Bai, W.; Terashima, M., and Sugita, N. (2021). Cortical bone drilling: a time series experimental analysis of thermal characteristics. *Journal of Manufacturing Processes*. 64(2021): 606-619.
- Li, Y.; Wang, J.; Wang, Y.; Du, W., and Wang, S. (2018). Transplantation of copper-doped calcium polyphosphate scaffolds combined with copper (II) preconditioned bone marrow mesenchymal stem cells for

- bone defect repair. *Journal of biomaterials applications*. 32(6): 738-753.
- Lienau, J.; Schmidt-Bleek, K.; Peters, A.; Haschke, F.; Duda, G. N.; Perka, C., and Schell, H. (2009). Differential regulation of blood vessel formation between standard and delayed bone healing. *Journal of orthopaedic research*. 27(9): 1133-1140.
- Lim, H.-K.; Choi, Y.-J.; Choi, W.-C.; Song, I.-S., and Lee, U.-L. (2022). Reconstruction of maxillofacial bone defects using patient-specific long-lasting titanium implants. *Scientific Reports*. 12(1): 1-12.
- Lin, X.; Patil, S.; Gao, Y.-G., and Qian, A. (2020). The bone extracellular matrix in bone formation and regeneration. *Frontiers in pharmacology*. 11(2020): 757.
- Lins, L. E. F.; de Santana, E. J. B.; Falcão, A. F. P.; Martins, P. P. M.; Calmon, T. R. V., and Sarmiento, V. A. (2017). The influence of hydroxyapatite on bone healing in titanium implants as shown by scanning electron microscopy. *Journal of Morphological Sciences*. 20(1): 0-0.
- Liu, G.; Guo, Y.; Zhang, L.; Wang, X.; Liu, R.; Huang, P., and Chen, Z. (2019). A standardized rat burr hole defect model to study maxillofacial bone regeneration. *Acta biomaterialia*. 86(2019): 450-464.
- Liu, W.; Du, B.; Tan, S.; Wang, Q.; Li, Y., and Zhou, L. (2020). Vertical guided bone regeneration in the rabbit calvarium using porous nanohydroxyapatite block grafts coated with rhVEGF165 and cortical perforation. *International journal of nanomedicine*. 10(2020): 10059-10073.
- Liu, X.; Bao, C.; Xu, H. H.; Pan, J.; Hu, J.; Wang, P., and Luo, E. (2016). Osteoprotegerin gene-modified BMSCs with hydroxyapatite scaffold for treating critical-sized mandibular defects in

- ovariectomized osteoporotic rats. *Acta biomaterialia*. 42(2016): 378-388.
- Liu, X.; Miao, Y.; Liang, H.; Diao, J.; Hao, L.; Shi, Z., and Wang, Y. (2022). 3D-printed bioactive ceramic scaffolds with biomimetic micro/nano-HAp surfaces mediated cell fate and promoted bone augmentation of the bone–implant interface in vivo. *Bioactive materials*. 12(2022): 120-132.
- Liu, Y.; Liu, N.; Na, J.; Li, C.; Yue, G.; Fan, Y., and Zheng, L. (2023). Wnt/ $\beta$ -catenin plays a dual function in calcium hydroxide induced proliferation, migration, osteogenic differentiation and mineralization in vitro human dental pulp stem cells. *International endodontic journal*. 56(1): 92-102.
- Liu, Y.; Sun, X.; Yu, J.; Wang, J.; Zhai, P.; Chen, S., and Zhou, Y. (2019). Platelet-rich fibrin as a bone graft material in oral and maxillofacial bone regeneration: classification and summary for better application. *BioMed Research International*. 2019(1):1-16.
- Lopes, C. d. C. A.; Limirio, P. H. J. O.; Novais, V. R., and Dechichi, P. (2018). Fourier transform infrared spectroscopy (FTIR) application chemical characterization of enamel, dentin and bone. *Applied Spectroscopy Reviews*. 53(9): 747-769.
- Lucaciu, O.; Gheban, D.; Sorițau, O.; Băciuț, M.; Câmpian, R. S., and Băciuț, G. (2015). Comparative assessment of bone regeneration by histometry and a histological scoring system/Evaluarea comparativă a regenerării osoase utilizând histometria și un scor de vindecare histologică. *Revista Romana de Medicina de Laborator*. 23(1): 31-45.
- Luo, Y., and Amromanoh, O. (2021). Bone Organic-Inorganic Phase Ratio Is a Fundamental Determinant of Bone Material Quality. *Applied Bionics and Biomechanics*. 2021(1):1-7.

- Dohan, M.; Bielecki, D.; Jimbo, T.; Barbe, R.; Del, G.; Corso, M.; Inchingolo, F.; and Sammartino, G. (2012). Do the fibrin architecture and leukocyte content influence the growth factor release of platelet concentrates? An evidence-based answer comparing a pure platelet-rich plasma (P-PRP) gel and a leukocyte- and platelet-rich fibrin (L-PRF). *Current pharmaceutical biotechnology*. 13(7): 1145-1152.
- Mabrouk, M.; Taha, S. K.; Abdel Hamid, M. A.; Kenawy, S. H.; Hassan, E. A., and El-Bassyouni, G. T. (2021). Radiological evaluations of low cost wollastonite nano-ceramics graft doped with iron oxide in the treatment of induced defects in canine mandible. *Journal of Biomedical Materials Research Part B: Applied Biomaterials*. 109(7): 1029-1044.
- Magnusson, P., and Farley, J. (2002). Differences in sialic acid residues among bone alkaline phosphatase isoforms: a physical, biochemical, and immunological characterization. *Calcified tissue international*. 71: 508-518.
- Mahfuri Sr, A.; Shehada, A.; Darwich, K.; Saima, R.; Mahfuri, A., and Sayma, R. (2022). Radiological Comparative Study Between Conventional and Nano Hydroxyapatite With Platelet-Rich Fibrin (PRF) Membranes for Their Effects on Alveolar Bone Density. *Cureus*. 14(12): e32381.
- Malhotra, S.; Hegde, M. N., and Shetty, C. (2014). Bioceramic technology in endodontics. *British Journal of Medicine and Medical Research*. 4(12): 2446.
- Manchón, A.; Alkhraisat, M.; Rueda-Rodriguez, C.; Torres, J.; Prados-Frutos, J.; Ewald, A., and López-Cabarcos, E. (2015). Silicon calcium phosphate ceramic as novel biomaterial to simulate the bone

- regenerative properties of autologous bone. *Journal of Biomedical Materials Research Part A*. 103(2): 479-488.
- Marsell, R., and Einhorn, T. A. (2010). Emerging bone healing therapies. *Journal of orthopaedic trauma*. 24(2010): S4-S8.
- Marsell, R., and Einhorn, T. A. (2011). The biology of fracture healing. *Injury*. 42(6): 551-555.
- Mediouni, M.; Kucklick, T.; Poncet, S.; Madiouni, R.; Abouaomar, A.; Madry, H., and Arora, M. (2019). An overview of thermal necrosis: present and future. *Current medical research and opinion*. 2019(1): 1555-1562.
- Meeson, R.; Moazen, M.; Sanghani-Kerai, A.; Osagie-Clouard, L.; Coathup, M., and Blunn, G. (2019). The influence of gap size on the development of fracture union with a micro external fixator. *Journal of the Mechanical Behavior of Biomedical Materials*. 99(2019): 161-168.
- Migliorini, F.; La Padula, G.; Torsiello, E.; Spiezia, F.; Oliva, F., and Maffulli, N. (2021). Strategies for large bone defect reconstruction after trauma, infections or tumour excision: a comprehensive review of the literature. *European journal of medical research*. 26(2021): 1-10.
- Mills, A. (2013). Small animal dental procedures: anesthesia and the dental patient. *Veterinary Technician*. 34(1): unpaginated.
- Miron, R. J.; Kawase, T.; Dham, A.; Zhang, Y.; Fujioka-Kobayashi, M., and Sculean, A. (2021). A technical note on contamination from PRF tubes containing silica and silicone. *BMC oral health*. 21(1): 1-11.
- Miron, R. J.; Xu, H.; Chai, J.; Wang, J.; Zheng, S.; Feng, M., and Mourão, C. F. d. A. B. (2020). Comparison of platelet-rich fibrin (PRF) produced using 3 commercially available centrifuges at both high (~



- 700 g) and low (~ 200 g) relative centrifugation forces. Clinical oral investigations. 24(2020): 1171-1182.
- Mocanu, A.; Cadar, O.; Frangopol, P. T.; Petean, I.; Tomoaia, G.; Paltinean, G.-A., and Tomoaia-Cotisel, M. (2021). Ion release from hydroxyapatite and substituted hydroxyapatites in different immersion liquids: in vitro. Royal society. 8(2021): 201785.
- Mohammadi, Z., and Dummer, P. M. H. (2011). Properties and applications of calcium hydroxide in endodontics and dental traumatology. International endodontic journal. 44(8): 697-730.
- Mohammed, F.; Alkattan, L.; Shareef, A., and Ismail, H. K. (2022). The role of adding hyaluronic acid in the grafting process for the repair of an experimentally induced tibial defect in dogs' model. Iraqi J Vet Sci. 36(3): 555-561.
- Monfoulet, L.; Rabier, B.; Chassande, O., and Fricain, J.-C. (2010). Drilled hole defects in mouse femur as models of intramembranous cortical and cancellous bone regeneration. Calcified tissue international. 86(2010): 72-81.
- Moshiri, A.; Maroof, N. T., and Sharifi, A. M. (2020). Role of organic and ceramic biomaterials on bone healing and regeneration: An experimental study with significant value in translational tissue engineering and regenerative medicine. Iranian Journal of Basic Medical Sciences. 23(11): 1426.
- Moukbil, Y.; Isindag, B.; Gayir, V.; Ozbek, B.; Haskoylu, M. E.; Oner, E. T., and Gunduz, O. (2020). 3D printed bioactive composite scaffolds for bone tissue engineering. Bioprinting. 17(2020): e00064.
- Moura, G. R. S.; Reis, R. d. S.; Mendonça, M. d. O.; Salgado, H. R.; Abreu, K. d. S.; Madella, G. d. S., and Lima, M. B. d. (2020). Substitution of limestone for eggshell powder in the diet of Japanese laying

- quails. *Revista Brasileira de Saúde e Produção Animal*. *Revista Brasileira de Saúde e Produção Animal*.21(2020).
- Mu, Y.; Du, Z.; Xiao, L.; Gao, W.; Crawford, R., and Xiao, Y. (2023). The localized ionic microenvironment in bone modelling/remodelling: A potential guide for the design of biomaterials for bone tissue engineering. *Journal of functional biomaterials*. 14(2): 56.
- Muthutantri, A. I. (2009). Novel processing of porous bioceramic structures. UCL (University College London),
- Naik, B.; Karunakar, P.; Jayadev, M., and Marshal, V. R. (2013). Role of Platelet rich fibrin in wound healing: A critical review. *Journal of conservative dentistry: JCD*. 16(4): 284.
- Nardo, T.; Carmagnola, I.; Ruini, F.; Caddeo, S.; Calzone, S.; Chiono, V., and Ciardelli, G. (2017). Synthetic biomaterial for regenerative medicine applications. In *Kidney Transplantation, Bioengineering and Regeneration*. England. Elsevier.
- Naredla, M.; Osmani, R. A.; Meenakshi, S.; Gupta, M. S., and Gowda, D. V. (2022). Potential applications of coral sand in bone healing and drug delivery. *Journal of Drug Delivery Science and Technology*: 69(2022).103150.
- Neiva, R. F.; Gil, L. F.; Tovar, N.; Janal, M. N.; Marao, H. F.; Bonfante, E. A., and Coelho, P. G. (2016). The synergistic effect of leukocyte platelet-rich fibrin and micrometer/nanometer surface texturing on bone healing around immediately placed implants: an experimental study in dogs. *BioMed Research International*. 2016:9.
- Nelson-Filho, P.; Leonardo, M. R.; Silva, L. A. B., and Assed, S. (2002). Radiographic evaluation of the effect of endotoxin (LPS) plus calcium hydroxide on apical and periapical tissues of dogs. *Journal of endodontics*. 28(10): 694-696.

- Nirwana, I.; Munadziroh, E.; Yogiartono, R. M.; Thiyaagu, C.; Ying, C. S., and Dinaryanti, A. (2021). Cytotoxicity and proliferation evaluation on fibroblast after combining calcium hydroxide and ellagic acid. *Journal of advanced pharmaceutical technology & research*. 12(1): 27.
- Nugraha, A. P.; Narmada, I. B.; Ernawati, D. S.; Dinaryanti, A.; Hendrianto, E.; Riawan, W., and Rantam, F. A. (2018). Bone alkaline phosphatase and osteocalcin expression of rat's Gingival mesenchymal stem cells cultured in platelet-rich fibrin for bone remodeling (in vitro study). *European journal of dentistry*. 12(04): 566-573.
- Opris, H.; Dinu, C.; Baciut, M.; Baciut, G.; Mitre, I.; Crisan, B., and Bran, S. (2020). The influence of eggshell on bone regeneration in preclinical In vivo studies. *Biology*. 9(12): 476.
- Oryan, A., and Alidadi, S. (2018). Reconstruction of radial bone defect in rat by calcium silicate biomaterials. *Life sciences*. 201(2018): 45-53.
- Pal, A.; Paul, S.; Choudhury, A. R.; Balla, V. K.; Das, M., and Sinha, A. (2017). Synthesis of hydroxyapatite from Lates calcarifer fish bone for biomedical applications. *Materials Letters*. 203(2017): 89-92.
- Panda, S.; Satpathy, A.; Chandra Das, A.; Kumar, M.; Mishra, L.; Gupta, S., and Del Fabbro, M. (2020). Additive Effect of Platelet Rich Fibrin with Coronally Advanced Flap Procedure in Root Coverage of Miller's Class I and II Recession Defects-A PRISMA Compliant Systematic Review and Meta-Analysis. *Materials*. 13(19): 4314.
- Paré, A.; Bossard, A.; Laure, B.; Weiss, P.; Gauthier, O., and Corre, P. (2019). Reconstruction of segmental mandibular defects: current procedures and perspectives. *Laryngoscope Investigative Otolaryngology*. 4(6): 587-596.

- Parvizi, J., and Kim, G. K. (2010). Chapter 94 - Fracture Healing. In J. Parvizi and G. K. Kim (Eds.), *High Yield Orthopaedics*. Philadelphia. W.B. Saunders.
- Paula-Silva, F. W. G.; Arnez, M. F. M.; de Campos Chaves Lamarque, G.; Petille, R.; Ribeiro-Santos, F. R.; de Sena, M. F., and da Silva, L. A. B. (2021). Osteoclast formation, inflammation, and matrix metalloproteinase-9 are downregulated in bone repair following root canal treatment in dogs teeth. *Clinical oral investigations*.1(2021): 1-9.
- Peltier, L. F. (1961). The use of plaster of Paris to fill defects in bone. *Clin Orthop*. 21(1961): 1-31.
- Pina, S.; Rebelo, R.; Correlo, V. M.; Oliveira, J. M., and Reis, R. L. (2018). Bioceramics for Osteochondral Tissue Engineering and Regeneration. *Adv Exp Med Biol*. 1058(2018): 53-75.
- Pinto, N. R.; Ubilla, M.; Zamora, Y.; Del Rio, V.; Dohan Ehrenfest, D. M., and Quirynen, M. (2018). Leucocyte-and platelet-rich fibrin (L-PRF) as a regenerative medicine strategy for the treatment of refractory leg ulcers: a prospective cohort study. *Platelets*. 29(5): 468-475.
- Piotrowski, S. L.; Wilson, L.; Dharmaraj, N.; Hamze, A.; Clark, A.; Taylor, R., and Young, S. (2019). Development and characterization of a rabbit model of compromised maxillofacial wound healing. *Tissue Engineering Part C: Methods*. 25(3): 160-167.
- Polini, A.; Pisignano, D.; Parodi, M.; Quarto, R., and Scaglione, S. (2011). Osteoinduction of human mesenchymal stem cells by bioactive composite scaffolds without supplemental osteogenic growth factors. *PloS one*. 6(10): e26211.

- Prakasam, M.; Locs, J.; Salma-Ancane, K.; Loca, D.; Largeau, A., and Berzina-Cimdina, L. (2017). Biodegradable materials and metallic implants-a review. *Journal of functional biomaterials*. 8(4): 44.
- Prathap, S.; Rajesh, K.; Thomas, N. G., and Prathap, M. (2022). Synthesis and Extraction of Hydroxyapatite Grafts from Animal Sources. *Journal of Dental Science Research Reviews & Reports*. 2022(4): 139.
- Pribadi, N.; Widjiastuti, I., and Nadia, A. (2020). Effect of calcium hydroxide-propolis combination on the number of fibroblast cells and angiogenesis in Wistar rats pulp. *Conservative Dentistry Journa*. 10(1): 14-18.
- Puspitasari, P.; Chairil, M.; Sukarni, S., and Supriyanto, N. S. W. (2021). Physical properties and compressibility of quail eggshell nanopowder with heat treatment temperature variations. *Materials Research Express*. 8(5): 055008.
- Quan, H.; He, Y.; Sun, J.; Yang, W.; Luo, W.; Dou, C., and Yang, X. (2018). Chemical self-assembly of multifunctional hydroxyapatite with a coral-like nanostructure for osteoporotic bone reconstruction. *ACS applied materials & interfaces*. 10(30): 25547-25560.
- Rajan, S.; Awang, H.; Devi, S.; Pooi, A., and Hassan, H. (2008). Alkaline phosphatase activity assessment of two endodontic materials: a preliminary study. *Annals of Dentistry University of Malaya*. 15(1): 5-10.
- Raji, R.; Elangomannan, S.; Subramani, R.; Louis, K.; Periasamy, M., and Dhanaraj, G. (2022). Calotropis Gigantea Fiber— A Biogenic Reinforcement Material for Europium Substituted Hydroxyapatite/Poly (3, 4-propylenedioxythiophene) Matrix: A Novel Ternary Composite for Biomedical Applications. *ACS omega*. 7(7): 6024-6034.

- Rashid, U.; Sandhu, M. A.; Yaqoob, M., and Yousaf, A. (2021). Critical bone gap repair using autologous adipose derived canine mesenchymal stem cell graft. *Pak Vet J.* 41(4): 513-518.
- Ratner, B. D.; Hoffman, A. S.; Schoen, F. J.; Lemons, J. E.; Wagner, W. R.; Sakiyama-Elbert, S. E., and Yaszemski, M. J. (2020). *Introduction to biomaterials science: an evolving, multidisciplinary endeavor.* USA. Academic Press Cambridge.
- Ravi, S., and Chaikof, E. L. (2010). Biomaterials for vascular tissue engineering. *Regenerative medicine.* 5(1): 107-120.
- Reece, W. O., and Rowe, E. W. (2017). *Functional anatomy and physiology of domestic animals.* France. John Wiley & Sons.
- Ressler, A.; Ivanković, T.; Polak, B.; Ivanišević, I.; Kovačić, M.; Urlić, I., Ivanković, H. (2022). A multifunctional strontium/silver-co-substituted hydroxyapatite derived from biogenic source as antibacterial biomaterial. *Ceramics International.* 48(13): 18361-18373.
- Ressler, A.; Žužić, A.; Ivanišević, I.; Kamboj, N., and Ivanković, H. (2021). Ionic substituted hydroxyapatite for bone regeneration applications: A review. *Open Ceramics.* 6(2021): 100122.
- Revathy, N. S.; Kannan, R.; Karthik, R.; Kumar, M. S.; Munshi, M., and Vijay, R. (2018). Comparative study on alveolar bone healing in postextraction socket versus healing aided with autologous platelet-rich fibrin following surgical removal of bilateral mandibular impacted third molar tooth: A radiographic evaluation. *National journal of maxillofacial surgery.* 9(2): 140.
- Rey-Vinolas, S.; Engel, E., and Mateos-Timoneda, M. (2019). Polymers for bone repair. In *Bone Repair Biomaterials* (pp. 179-197): Elsevier.

- Ribeiro, C.; Bressiani, J. C., and Bressiani, A. H. A. (2008). Characterization of the calcium phosphate porous ceramic obtained by foam consolidation using albumin. *Key Engineering Materials*. 361: 971-974.
- Riquelme, M. A.; Cardenas, E. R., and Jiang, J. X. (2020). Osteocytes and bone metastasis. *Frontiers in endocrinology*. 11(2020): 567844.
- Risselada, M. (2020). *Atlas of Surgical Approaches to Soft Tissue and Oncologic Diseases in the Dog and Cat*. John Wiley & Sons.
- Roberts, T. T., and Rosenbaum, A. J. (2012). Bone grafts, bone substitutes and orthobiologics: the bridge between basic science and clinical advancements in fracture healing. *Organogenesis*. 8(4): 114-124.
- Robison, R. (1923). The possible significance of hexosephosphoric esters in ossification. *Biochemical Journal*. 17(2): 286.
- Rocha, J.; Lemos, A.; Agathopoulos, S.; Valério, P.; Kannan, S.; Oktar, F., and Ferreira, J. (2005). Scaffolds for bone restoration from cuttlefish. *Bone*. 37(6): 850-857.
- Rosen, V. B.; Hobbs, L., and Spector, M. (2002). The ultrastructure of anorganic bovine bone and selected synthetic hydroxyapatites used as bone graft substitute materials. *Biomaterials*. 23(3): 921-928.
- Rudy, R., and Boudrieau, R. (1992). *Maxillofacial and mandibular fractures*. Paper presented at the Seminars in Veterinary Medicine and Surgery (small Animal).
- Rupp, M.; Klute, L.; Baertl, S.; Walter, N.; Mannala, G. K.; Frank, L., and Kerschbaum, M. (2022). The clinical use of bone graft substitutes in orthopedic surgery in Germany-A 10-years survey from 2008 to 2018 of 1,090,167 surgical interventions. *Journal of Biomedical Materials Research Part B: Applied Biomaterials*. 110(2): 350-357.
- Ryabenkova, Y.; Pinnock, A.; Quadros, P.; Goodchild, R.; Möbus, G.; Crawford, A., Miller, C. (2017). The relationship between particle

- morphology and rheological properties in injectable nano-hydroxyapatite bone graft substitutes. *Materials Science and Engineering: C*. 75: 1083-1090.
- Sadek, A. A.; Abd-Elkareem, M.; Abdelhamid, H. N.; Moustafa, S., and Hussein, K. (2023). Repair of critical-sized bone defects in rabbit femurs using graphitic carbon nitride (g-C<sub>3</sub>N<sub>4</sub>) and graphene oxide (GO) nanomaterials. *Scientific Reports*. 13(1): 5404.
- Safadi, F. F.; Barbe, M. F.; Abdelmagid, S. M.; Rico, M. C.; Aswad, R. A.; Litvin, J., and Popoff, S. N. (2009). Bone structure, development and bone biology. *Bone pathology*. 2009: 1-50.
- Samavedi, S.; Poindexter, L. K.; Van Dyke, M., and Goldstein, A. S. (2014). Synthetic biomaterials for regenerative medicine applications. In *Regenerative medicine applications in organ transplantation*. England. Elsevier.
- Sarkar, K.; Xue, Y., and Sant, S. (2017). Host response to synthetic versus natural biomaterials. The immune response to implanted materials and devices: the impact of the immune system on the success of an implant. France. Springer nature, 81-105.
- Scelza, M. Z.; Campos, C.; Scelza, P.; Adeodato, C.; Barbosa, I. B.; de Noronha, F., and Alves, G. G. (2016). Evaluation of Inflammatory Response to Endodontic Sealers in a Bone Defect Animal Model. *The journal of contemporary dental practice*. 17(7): 536-541.
- Schemitsch, E. H. (2017). Size matters: defining critical in bone defect size! *Journal of orthopaedic trauma*. 31: S20-S22.
- Schmidt-Bleek, K.; Schell, H.; Lienau, J.; Schulz, N.; Hoff, P.; Pfaff, M., and Buttgerit, F. (2014). Initial immune reaction and angiogenesis in bone healing. *Journal of tissue engineering and regenerative medicine*. 8(2): 120-130.



- Schortinghuis, J.; Ruben, J. L.; Meijer, H. J.; Bronckers, A. L.; Raghoobar, G. M., and Stegenga, B. (2003). Microradiography to evaluate bone growth into a rat mandibular defect. *Archives of oral biology*. 48(2): 155-160.
- Schröter, L.; Kaiser, F.; Stein, S.; Gbureck, U., and Ignatius, A. (2020). Biological and mechanical performance and degradation characteristics of calcium phosphate cements in large animals and humans. *Acta biomaterialia*. 117(2020): 1-20.
- Schwarcz, H. P.; Abueidda, D., and Jasiuk, I. (2017). The ultrastructure of bone and its relevance to mechanical properties. *Frontiers in Physics*. 5(2017): 39.
- Sekar, V.; Chidambaranathan, A. S., and Balasubramaniam, M. (2021). Role of Surface Geometry of Dental Implants on Osseointegration-Revisited. *Annals of Dental Specialty*. 9(4): 57.
- Sela, J. J., and Bab, I. A. (2012). *Principles of bone regeneration*. Springer Science & Business Media. London. Springer Nature.
- Shadjou, N., and Hasanzadeh, M. (2015). Bone tissue engineering using silica-based mesoporous nanobiomaterials: Recent progress. *Materials Science and Engineering*. 55(2015): 401-409.
- Shaffer, C. D., and App, G. R. (1971). The use of plaster of paris in treating infrabony periodontal defects in humans. *Journal of periodontology*. 42(11): 685-690.
- Shah, F. A.; Ruscsák, K., and Palmquist, A. (2019). 50 years of scanning electron microscopy of bone-a comprehensive overview of the important discoveries made and insights gained into bone material properties in health, disease, and taphonomy. *Bone research*. 7(1): 15.
- Shamsoddin, E.; Houshmand, B., and Golabgiran, M. (2019). Biomaterial selection for bone augmentation in implant dentistry: A systematic

- review. *Journal of advanced pharmaceutical technology & research*. 10(2): 46.
- Shang, F.; Yu, Y.; Liu, S.; Ming, L.; Zhang, Y.; Zhou, Z., and Jin, Y. (2021). Advancing application of mesenchymal stem cell-based bone tissue regeneration. *Bioactive materials*. 6(3): 666-683.
- Shao, R.; Quan, R.; Zhang, L.; Wei, X.; Yang, D., and Xie, S. (2015). Porous hydroxyapatite bioceramics in bone tissue engineering: current uses and perspectives. *Journal of the Ceramic Society of Japan*. 123(1433): 17-20.
- Sharifianjazi, F.; Esmailkhanian, A.; Moradi, M.; Pakseresht, A.; Asl, M. S.; Karimi-Maleh, H., and Varma, R. S. (2021). Biocompatibility and mechanical properties of pigeon bone waste extracted natural nano-hydroxyapatite for bone tissue engineering. *Materials Science and Engineering*. 264(2021): 114950.
- Sharma, A.; Ingole, S.; Deshpande, M.; Ranadive, P.; Sharma, S.; Kazi, N., and Rajurkar, S. (2020). Influence of platelet-rich fibrin on wound healing and bone regeneration after tooth extraction: A clinical and radiographic study. *Journal of oral biology and craniofacial research*. 10(4): 385-390.
- Sharma, U.; Pal, D., and Prasad, R. (2014). Alkaline phosphatase: an overview. *Indian journal of clinical biochemistry*. 29(2014): 269-278.
- Sheen, J. R., and Garla, V. V. (2022). Fracture healing overview. United Kingdom. StatPearls Publishing.
- Shiu, H. T.; Leung, P. C., and Ko, C. H. (2018). The roles of cellular and molecular components of a hematoma at early stage of bone healing. *Journal of tissue engineering and regenerative medicine*. 12(4): e1911-e1925.

- Simonpieri, A.; Del Corso, M.; Vervelle, A.; Jimbo, R.; Inchingolo, F.; Sammartino, G., and M Dohan Ehrenfest, D. (2012). Current knowledge and perspectives for the use of platelet-rich plasma (PRP) and platelet-rich fibrin (PRF) in oral and maxillofacial surgery part 2: Bone graft, implant and reconstructive surgery. *Current pharmaceutical biotechnology*. 13(7): 1231-1256.
- Singh, B. (2018). Dyce, Sack, and Wensing's textbook of veterinary anatomy. Missouri. Saunders St. Louis.
- Smith, L. (1963). Ceramic-plastic material as a bone substitute. *Archives of Surgery*. 87(4): 653-661.
- Soares, L. F. F.; Carrera, T. M. I.; de Oliveira Alves, R.; Marcantonio, C. C.; Cirelli, J. A.; de Oliveira, G. J. P. L., and Pigossi, S. C. (2023). Platelet-rich fibrin (PRF) membrane isolated and injectable-PRF-mixed particulate bovine bone graft in rattibiae non-critical defects healing. preprint copy.
- Steinerova, M.; Nedomova, S.; Slama, P., and Pavlik, A. (2023). Importance of selected proteins of compact bone tissue in poultry. (2032): e10083.
- Sterner, R. M.; Kremer, K. N.; Dudakovic, A.; Westendorf, J. J.; Van Wijnen, A. J., and Hedin, K. E. (2018). Tissue-Nonspecific Alkaline Phosphatase Is Required for MC3T3 Osteoblast-Mediated Protection of Acute Myeloid Leukemia Cells from Apoptosis. *The Journal of Immunology*. 201(3): 1086-1096.
- Stojanović, N.; Krunic, J.; Mladenović, I.; Stojanović, Z.; Apostolska, S., and Živković, S. (2018). Influence of different forms of calcium hydroxide and chlorhexidine intracanal medicaments on the outcome of endodontic treatment of teeth with chronic apical periodontitis. *Srpski arhiv za celokupno lekarstvo*. 146(3-4): 143-148.

- Strauss, F.-J.; Nasirzade, J.; Kargarpour, Z.; Stähli, A., and Gruber, R. (2020). Effect of platelet-rich fibrin on cell proliferation, migration, differentiation, inflammation, and osteoclastogenesis: a systematic review of in vitro studies. *Clinical oral investigations*. 24(2020): 569-584.
- Su, P.; Tian, Y.; Yang, C.; Ma, X.; Wang, X.; Pei, J., and Qian, A. (2018). Mesenchymal stem cell migration during bone formation and bone diseases therapy. *International Journal of Molecular Sciences*. 19(8): 2343.
- Sun, R.-X.; Lv, Y.; Niu, Y.-R.; Zhao, X.-H.; Cao, D.-S.; Tang, J., and Chen, K.-Z. (2017). Physicochemical and biological properties of bovine-derived porous hydroxyapatite/collagen composite and its hydroxyapatite powders. *Ceramics International*. 43(18): 16792-16798.
- Sunil, B. R., and Jagannatham, M. (2016). Producing hydroxyapatite from fish bones by heat treatment. *Materials Letters*. 185: 411-414.
- Syafaat, F. Y., and Yusuf, Y. (2018). Effect of Ca: P concentration and calcination temperature on hydroxyapatite (HAp) powders from quail eggshell (*Coturnix Coturnix*). *International Journal of Nanoelectronics and Materials*. 11(2018): 51-58.
- Tan, J.; Wang, D.; Cao, H.; Qiao, Y.; Zhu, H., and Liu, X. (2018). Effect of local alkaline microenvironment on the behaviors of bacteria and osteogenic cells. *ACS applied materials & interfaces*. 10(49): 42018-42029.
- Tang, G.; Liu, Z.; Liu, Y.; Yu, J.; Wang, X.; Tan, Z., and Ye, X. (2021). Recent trends in the development of bone regenerative biomaterials. *Frontiers in Cell and Developmental Biology*. 9(2021): 665813.
- Tatara, A. M.; Koons, G. L.; Watson, E.; Piepergerdes, T. C.; Shah, S. R.; Smith, B. T., and Demian, N. (2019). Biomaterials-aided mandibular

- reconstruction using in vivo bioreactors. *Proceedings of the National Academy of Sciences*. 116(14): 6954-6963.
- Terzopoulou, Z.; Zamboulis, A.; Koumentakou, I.; Michailidou, G.; Noordam, M. J., and Bikiaris, D. N. (2022). Biocompatible synthetic polymers for tissue engineering purposes. *Biomacromolecules*. 23(5): 1841-1863.
- Tulli, H. M.; Carlson, C. S.; Jayo, M. J.; Fisher, L. W.; Tracy, R. P., and Mann, K. G. (1992). Immunohistochemical method for the simultaneous demonstration of three proteins in EDTA decalcified paraffin embedded bone sections. *Journal of Histotechnology*. 15(2): 93-97.
- Tzelepi, V.; Tsamandas, A. C.; Zolota, V., and Scopa, C. D. (2009). Bone anatomy, physiology and function. *Bone Metastases: A translational and clinical approach*. (2009): 3-30.
- Udduttula, A.; Zhang, J. V., and Ren, P.-G. (2019). *Bioinert Ceramics for Biomedical Applications*. Hoboken, NJ, USA. Wiley.
- Ullah, S., and Chen, X. (2020). Fabrication, applications and challenges of natural biomaterials in tissue engineering. *Applied Materials Today*. 20(2020): 100656.
- Vasileva, R., and Chaprazov, T. (2023). Bone Healing of Critical-Sized Femoral Defects in Rats Treated with Erythropoietin Alone or in Combination with Xenograft. *Veterinary Sciences*. 10(3): 196.
- Vatankhah, M.; Khosravi, K.; Zargar, N.; Shirvani, A.; Nekoofar, M. H., and Dianat, O. (2022). Antibacterial efficacy of antibiotic pastes versus calcium hydroxide intracanal dressing: A systematic review and meta-analysis of ex vivo studies. *Journal of Conservative Dentistry*. 25(5): 463.
- Vdoviaková, K.; Jenca, A.; Jenca Jr, A.; Danko, J.; Kresáková, L.; Simaiová, V., . . . Vrzgula, M. (2023). Regenerative Potential of

- Hydroxyapatite-Based Ceramic Biomaterial on Mandibular Cortical Bone: An In Vivo Study. *Biomedicines*. 11(3): 877.
- Velard, F.; Braux, J.; Amedee, J., and Laquerriere, P. (2013). Inflammatory cell response to calcium phosphate biomaterial particles: an overview. *Acta biomaterialia*. 9(2): 4956-4963.
- Velnar, T.; Bunc, G.; Klobucar, R., and Gradisnik, L. (2016). Biomaterials and host versus graft response: a short review. *Bosnian journal of basic medical sciences*. 16(2): 82.
- Vimalraj, S. (2020). Alkaline phosphatase: Structure, expression and its function in bone mineralization. *Gene*. 754(2020): 144855.
- Voss, K.; Langley-Hobbs, S. J.; Grundmann, S., and Montavon, P. M. (2009). 26 - Mandible and maxilla. In P. M. Montavon, K. Voss, and S. J. Langley-Hobbs (Eds.), *Feline Orthopedic Surgery and Musculoskeletal Disease*. Edinburgh: W.B. Saunders.
- Walsh, W. R.; Oliver, R. A.; Christou, C.; Lovric, V.; Walsh, E. R.; Prado, G. R., and Haider, T. (2017). Critical size bone defect healing using collagen–calcium phosphate bone graft materials. *PloS one*. 12(1): e0168883.
- Wang, J.; Gao, Y.; Cheng, P.; Li, D.; Jiang, H.; Ji, C., and Song, Y. (2017). CD31hiEmcnhi vessels support new trabecular bone formation at the frontier growth area in the bone defect repair process. *Scientific Reports*. 7(1): 4990.
- Wang, J.; Sun, Y.; Liu, Y.; Yu, J.; Sun, X.; Wang, L., and Zhou, Y. (2022). Effects of platelet-rich fibrin on osteogenic differentiation of Schneiderian membrane derived mesenchymal stem cells and bone formation in maxillary sinus. *Cell Communication and Signaling*. 20(1): 88.
- Wang, M.; Yu, Y.; Dai, K.; Ma, Z.; Liu, Y.; Wang, J., and Liu, C. (2016). Improved osteogenesis and angiogenesis of magnesium-doped

- calcium phosphate cement via macrophage immunomodulation. *Biomaterials science*. 4(11): 1574-1583.
- Wang, S.; Noda, K.; Yang, Y.; Shen, Z.; Chen, Z., and Ogata, Y. (2018). Calcium hydroxide regulates transcription of the bone sialoprotein gene via a calcium-sensing receptor in osteoblast-like ROS 17/2.8 cells. *European Journal of Oral Sciences*. 126(1): 13-23.
- Wang, W., and Yeung, K. W. (2017). Bone grafts and biomaterials substitutes for bone defect repair: A review. *Bioactive materials*. 2(4): 224-247.
- Wang, J.; Gao, Y.; Cheng, P.; Li, D.; Jiang, H.; Ji, C., Song, Y. (2017). CD31hiEmcnhi vessels support new trabecular bone formation at the frontier growth area in the bone defect repair process. *Scientific Reports*. 7(1): 4990.
- Wang, X. (2013). Overview on biocompatibilities of implantable biomaterials. *Advances in Biomaterials Science and Biomedical Applications in Biomedicine*, Lazinica, Corroatia, PP. 111-155.
- Wang, X.; Zhang, Y.; Choukroun, J.; Ghanaati, S., and Miron, R. J. (2018). Effects of an injectable platelet-rich fibrin on osteoblast behavior and bone tissue formation in comparison to platelet-rich plasma. *Platelets*. 29(1): 48-55.
- Wilson, J. (2002). Blood supply to developing, mature and healing bone. *Bone in clinical orthopedics*: 23-115.
- Winkler, T.; Sass, F.; Duda, G., and Schmidt-Bleek, K. (2018). A review of biomaterials in bone defect healing, remaining shortcomings and future opportunities for bone tissue engineering: The unsolved challenge. *Bone & joint research*. 7(3): 232-243.
- Wong, C.-C.; Huang, Y.-M.; Chen, C.-H.; Lin, F.-H.; Yeh, Y.-Y., and Bai, M.-Y. (2020). Cytokine and growth factor delivery from implanted

- platelet-rich fibrin enhances rabbit Achilles tendon healing. *International Journal of Molecular Sciences*. 21(9): 3221.
- Xian, C. J.; Zhou, F. H.; McCarty, R. C., and Foster, B. K. (2004). Intramembranous ossification mechanism for bone bridge formation at the growth plate cartilage injury site. *Journal of orthopaedic research*. 22(2): 417-426.
- Xiao, L.; Ma, Y.; Crawford, R.; Mendhi, J.; Zhang, Y.; Lu, H., and Wang, X. (2022). The interplay between hemostasis and immune response in biomaterial development for osteogenesis. *Materials Today*. 54(2022): 202-224.
- Yamaguchi, S.; Aizawa, H.; Sato, A.; Tsujino, T.; Isobe, K.; Kitamura, Y., and Kawase, T. (2020). Concentrated growth factor matrices prepared using silica-coated plastic tubes are distinguishable from those prepared using glass tubes in platelet distribution: application of a novel near-infrared imaging-based, quantitative technique. *Frontiers in Bioengineering and Biotechnology*. 8(2020): 600.
- Yang, C.; Gao, X.; Younis, M. R.; Blum, N. T.; Lei, S.; Zhang, D., Lin, J. (2021). Non-invasive monitoring of in vivo bone regeneration based on alkaline phosphatase-responsive scaffolds. *Chemical Engineering Journal*. 408: 127959.
- Yao, Z.; Chen, T.; Li, H.; Xia, M.; Ye, Y., and Zheng, H. (2013). Mechanical and thermal properties of polypropylene (PP) composites filled with modified shell waste. *Journal of hazardous materials*. 262(2013): 212-217.
- Ye, B.; Wu, B.; Su, Y.; Sun, T., and Guo, X. (2022). Recent Advances in the Application of Natural and Synthetic Polymer-Based Scaffolds in Musculoskeletal Regeneration. *Polymers*. 14(21): 4566.



- Yoon, G.-L.; Kim, B.-T.; Kim, B.-O., and Han, S.-H. (2003). Chemical–mechanical characteristics of crushed oyster-shell. *Waste Management*. 23(9): 825-834.
- Zedan, I. A.; Alkattan, L. M., and Aliraqi, O. M. (2022). An evaluation of Aloe vera leaves gel with polypropylene mesh to repair of ventro-lateral abdominal hernia in rams. *Iraqi Journal of Veterinary Sciences*. 36(2022): 19-25.
- Zedan, I. A.; Alkattan, L., and Al-Mahmood, S. S. (2023). Histopathological and immunohistochemical assessment of the using platelets rich fibrin to reinforce ventral hernioplasty in the sheep model. *Iraqi Journal of Veterinary Sciences*. 37(4): 821 829.
- Zhang, J.; Yin, C.; Zhao, Q.; Zhao, Z.; Wang, J.; Miron, R. J., and Zhang, Y. (2020). Anti-inflammation effects of injectable platelet-rich fibrin via macrophages and dendritic cells. *Journal of Biomedical Materials Research Part A*. 108(1): 61-68.
- Zhang, Q.; Wu, W.; Qian, C.; Xiao, W.; Zhu, H.; Guo, J., and Cui, W. (2019). Advanced biomaterials for repairing and reconstruction of mandibular defects. *Materials Science and Engineering*. 103(2019): 109858.
- Zhang, X., and Williams, D. (2019). Definitions of biomaterials for the twenty-first century. England. Elsevier.
- Zhou, H., and Lee, J. (2011). Nanoscale hydroxyapatite particles for bone tissue engineering. *Acta biomaterialia*. 7(7): 2769-2781.
- Zhou, J.; Xiong, S.; Liu, M.; Yang, H.; Wei, P.; Yi, F., and Liu, Y. (2023). Study on the influence of scaffold morphology and structure on osteogenic performance. *Frontiers in Bioengineering and Biotechnology*. 11: 1127162.

## الخلاصة

هدفت الدراسة إلى إعادة تكوين عيوب عظم الفك السفلي الكبيرة المستحدثة جراحياً باستخدام أنواع مختلفة من المواد الحيوية في نموذج الكلاب. شملت هذه الدراسة ثمانية وأربعين كلباً محلياً ذكراً سليماً بوزن ( $0.5 \pm 20$ ) كغم وعمر ( $0.6 \pm 2$ ) سنة. تم تقسيم جميع الحيوانات بالتساوي إلى أربع مجموعات. تم إنشاء عيب عظمي فكي سفلي دائري قطره (14) ملم في عظم الفك السفلي لجميع الحيوانات. في المجموعة الأولى (مجموعة السيطرة)، تم ترك الخلل دون أي علاج. في المجموعة الثانية (مجموعة QESCH)، تم ملئ العيب العظمي بمسحوق هيدروكسيد الكالسيوم المصنّع من قشور بيض السمك. في المجموعة الثالثة (مجموعة OSHA)، تم ملئ العيب العظمي بمسحوق الهيدروكسي ابتايت المصنّع من أصداف المحار. في المجموعة الرابعة (مجموعة PRF)، تم ملئ العيب العظمي بهلام الفيبرين الغني بالصفائح الدموية الذاتية. اعتماداً على التقييمات اللاحقة للعمليات الجراحية مثل العلامات السريرية والمجهر العياني والمجهر الإلكتروني الماسح بالانبعاث الميداني (FESEM) والإشعاعي والنسجي والكيميائي المناعي في فترات مختلفة من الدراسة لتقييم النتائج التي تم الحصول عليها.

وأظهر التقييم السريري أن جميع الحيوانات تعافت بشكل جيد بعد العمليات الجراحية دون أي مضاعفات. ومع ذلك، أظهرت جميع الحيوانات في المجموعات المعالجة علامات طبيعية للأكل والمضغ والنباح خلال الأسبوع الأول بعد العمليات الجراحية. بينما أظهرت حيوانات المجموعة الأولى درجات متفاوتة من القدرة على تناول الطعام بشكل طبيعي خلال نفس الفترات. عيانياً، في جميع المجموعات، تم شفاء موقع الجروح الجراحية بشكل طبيعي. بالإضافة إلى ذلك، أظهرت النتائج العيانية في المجموعات المعالجة خلال جميع فترات الدراسة انخفاضاً تدريجياً في حجم عيب عظم الفك السفلي من خلال تكوين نسيج ضام جديد، خاصة في المجموعة الرابعة. وعلى النقيض من مجموعة السيطرة، كان عيب عظم الفك السفلي لا يزال مفتوحاً نسبياً في نهاية هذه الدراسة.

كشفت النتائج الإشعاعية لعيب عظم الفك السفلي في مجموعة السيطرة عن تكوين قليل للأنسجة العظمية مع وجود جسر تربقي أقل أو غائب حيث ظل العيب العظمي مفتوحاً وشفافاً للأشعة في اليوم 60 بعد العملية. بينما في المجموعات المعالجة أظهر الفحص الشعاعي اختفاء تدريجي في حجم عيب عظم الفك السفلي من خلال تكوين أنسجة عظمية جديدة وجسر تربقي حيث ظهر العيب العظمي معتماً للأشعة واختفى نسبياً وفي نهاية الدراسة انحصر في المجموعة

ب

الرابعة أيضا. بالإضافة إلى ذلك، كشف المجهر الإلكتروني الماسح بالانبعاث الميداني عن إغلاق عيب عظم الفك السفلي نسبياً مع وجود نسيج ضام جديد في المجموعة المعالجة، خاصة في المجموعة الرابعة، على العكس من المجموعة الأولى، حيث ظل العيب فيها مفتوحاً.

أظهرت المقاطع النسجية المرضية بعد معالجة عيب عظم الفك السفلي بمواد حيوية مختلفة في جميع حيوانات التجارب درجات مختلفة من تكوين العظام والأنسجة الحبيبية الجديدة. بالإضافة إلى تكوين الأوعية الدموية وتسلل الخلايا الالتهابية. وبشكل عام أظهرت النتائج النسيجية المرضية في المجموعات المعالجة زيادة معنوية بنسب متفاوتة في تكاثر الخلايا العظمية وتكوين الخلايا العظمية مع الأولوية للمجموعة الرابعة عند مستوى ( $P \leq 0.05$ ) مقارنة بالمجموعة الأولى خلال فترات الدراسة بعد العمليات الجراحية. وعلاوة على ذلك، أظهرت النتائج الكيميائية المناعية في المجموعة الأولى ضعف التعبير عن لأنزيم الفوسفات القلوي (ALP) في كل من مناطق الغضروف والتعظم. في المجموعة الثانية، ظهر تعبير ALP بشكل خفيف في منطقة التعظم وباعتدال في المنطقة الغضروفية. في المجموعة الثالثة، ظهر تعبير ALP بشكل معتدل في سطح التريبك العظمي المشكل حديثاً ومعتدل في المنطقة الغضروفية. في المجموعة الرابعة، ظهر تعبير ALP بشكل كبير في وسط المنطقة العيب العظمي وتم التعبير عنه بشكل معتدل في سطح العظم الصفائحي المشكل حديثاً.

في الختام، فإن ملئ عيوب عظم الفك السفلي بمسحوق هيدروكسيد الكالسيوم المصنع من قشور بيض السمك، ومسحوق الهيدروكسي ابتايت المصنع من أصداف المحار، والفيريون الغني بالصفائح الدموية أدى إلى تحسين عملية الشفاء من عيب العظام. وعززت الانغلاق عليه خاصة في المجموعة الرابعة مقارنة بالمجموعة الأولى.

# تأثير أنواع مختلفة من المواد البيولوجية على التئام الأذى المستحدث جراحيا لعظم الفك في الكلاب

أطروحة تقدم بها  
علي غازي عطيه زراك

إلى  
مجلس كلية الطب البيطري في جامعة الموصل  
وهي جزء من متطلبات نيل شهادة الدكتوراه فلسفة  
في اختصاص الطب البيطري / الجراحة البيطرية

بإشراف  
الإستاذ الدكتور

ليث محمود داود القطان



جامعة الموصل  
كلية الطب البيطري

## تأثير أنواع مختلفة من المواد البيولوجية على التئام الأذى المستحدث جراحيا لعظم الفك في الكلاب

علي غازي عطيه زراك

أطروحة دكتوراه  
الطب البيطري / الجراحة البيطرية

بإشراف  
الإستاذ الدكتور

ليث محمود داود القطان